Magnetization of $HgBa_2CuO_{4+\delta}$ with $0.03 \leq \delta \leq 0.4$

Q. Xiong, S. Afonso, Y. Q. Tang, F. T. Chan, and G. Salamo
Physics Department/High Density Electronics Center, University of Arkansas, Fayetteville, Arkansas 72701

Y. Y. Xue and C. W. Chu
Physics Department and Texas Center for Superconductivity, University of Houston, Houston, Texas 77204

$HgBa_2CuO_{4+\delta}$ (Hg1201) samples with $0.03 \leq \delta \leq 0.4$ have been obtained. The magnetization of the powdered Hg1201 samples was determined using a Quantum Design SQUID magnetometer. It was observed that while the magnetization of Hg1201 increased with δ in the underdoped region, the magnetization decreased with δ in the overdoped region. These results suggest an increase of n_s/m^* with oxidation in the underdoped region and a decrease in the overdoped region, similar to that reported in underdoped HTSs and overdoped Tl2201 and Tl1201. © *1996 American Institute of Physics.* [S0021-8979(96)03108-6]

I. INTRODUCTION

Soon after the discovery of high-temperature superconductivity (HTS), it was realized that the existence of CuO_2 layers in HTSs is very crucial and the charge carriers in the CuO_2 layers control the physical properties in both the superconducting state and the normal state. T_c is one of the properties that the charge carriers in the CuO_2 layers have a marked effect upon. On the one hand, it was found that there are three different regimes in the relationship of T_c to the number of charge carriers n in the CuO_2 layers (where n is determined from valence balance or thermoelectric).[1–3] The underdoped region is where the superconducting phase appears near the insulating magnetic phase. T_c increases with increased n in this region. The optimal doping region is where T_c approaches the highest values within the given series. Next, comes the overdoped region. In this region, T_c decreases with further increases in n. On the other hand, based on muon spin-rotation (μSR) measurements,[4–6] it was found that T_c vs n_s/m^* forms a double-valued relation in Tl2201 (where n_s is the superconducting condensate density, m^* is the effective mass). This means that as n increases, n_s/m^* increases in the underdoped region, and decreases in the overdoped region. Until now, most studies have concentrated on the underdoped and optimal region, probably because underdoped and optimally doped samples are fairly easy to synthesize for most HTS systems. On the contrary, the overdoped region has been observed in only a few systems. The $HgBa_2CuO_{4+\delta}$ compound (Hg1201) has been shown to be scientifically significant,[7] because it has the highest T_c among all HTS materials that have one CuO_2 plane, and has the widest doping range that can be achieved by changing oxygen content alone.[8] Thus it is a good candidate for studies on charge carrier and doping related properties in the overdoped region.

In this article, we report a study of T_c vs n_s/m^* done by measuring the magnetization volume fluctuation of Hg1201 when oxygen content is varied from 0.03 to 0.4, covering the entire range from $T_c = 0$ K (underdoping region) to $T_c = 20$ K (overdoping region). We observed that the magnetization of Hg1201 increases with δ in the underdoped region and decreases with δ in the overdoped region. The results suggest that a double-valued relation of T_c to n_s/m^* also exists in the Hg1201 compound.

II. EXPERIMENT

All samples were synthesized by a two-step method, i.e., by first forming a precursor of (Ba, Cu) oxides, then reacting HgO with the precursor inside an evacuated quartz tube. Precursor with an initial composition of Ba_2CuO_y was prepared by a solid-state reaction. High-purity powders of BaO (99.95%) were thoroughly mixed in appropriate proportions. The mixed powders were calcined in an alumina crucible at 930 °C for 24 h under a mixed gas of Ar:O=4:1. Three intermediate regrindings were carried out during this period. The composite Hg source used was a prereacted Hg1:2:0:1 pellet made by compacting the thoroughly mixed HgO (99.998%) and pulverized precursor powder. A reactant pellet was sealed in an evacuated quartz tube of fixed volume, together with an extra Ba_2CuO_y precursor pellet. Details were given in Ref. 9. A stainless-steel tube was used to contain the quartz tube as a safety precaution. The whole assembly was then heated to 800–830 °C for 8 h before slow cooling to room temperature. Samples with different oxygen content were obtained by heating as-synthesized samples at different temperatures and oxygen partial pressures for appropriate periods of time.[9] To reach the underdoped region, the sample was heated in a vacuum of $\sim 2 \times 10^{-6}$ Torr at a temperature between 200 and 450 °C for 20–100 h. For the overdoped samples, the as-synthesized compound was heated in a 1–500 bar O atmosphere between 240 and 400 °C for 10–300 h. Phase characterization was performed by x-ray powder diffraction on a Rigaku DMAX/BIII diffractometer. The magnetization was measured using a Quantum Design SQUID magnetometer. The oxygen content δ of the samples were measured by thermogravimetric analysis[8] and calibrated using neutron powder diffraction.[10]

III. RESULTS AND DISCUSSION

Figure 1 shows the x-ray diffraction pattern of one of our as-synthesized samples, which indicated that the Hg1201 sample was nearly single phase. Figure 2 shows the normal state susceptibility as a function of the temperature. The data fits the Curie law, $\chi = \chi_0 + C/T$, very well with $\chi_0 = 1.04 \times 10^{-6}$ emu/g and $C = 2.45 \times 10^{-4}$ emu/g. The magnetization in various magnetic fields H has also been measured. As shown in the inset of Fig. 2, the magnetization

 0021-8979/96/79(8)/6580/3/$10.00

IN SITU THIN FILM STRESS MEASUREMENT USING HIGH STABILITY PORTABLE HOLOGRAPHIC INTERFEROMETER

George Dovgalenko, Shahid Hague, Anatoly Kniazkov, Yuri Onischenko,
Greg Salamo, H. Naseem
University of Arkansas, Fayetteville, AR, 72701, USA

ABSTRACT

A stress in thin film SiO_2 was detected using high stability portable holographic interferometer. A stress relaxation phenomenon in this film thickness of 0.5 μm on Si wafer has been observed. This phenomenon does not exist in film with thickness of 1 μm. The advantages of the proposed measured technique and results are discussed.
Key words: interferometry, stress instability, relaxation, thin film, portability.

1. INTRODUCTION

Stress in thin film after deposition on hot substrate causes damage to the film because of the difference in the thermal expansion coefficients of the film and wafer. Traditionally the standard dual wavelength laser deflection device Tencor FLX 2320A is used. This device needs recalibration in time, is expensive, not portable, operates in quasi-real time.
The challenge of thin film fabrication technology is stress measurement [1] using a portable, economical real-time technique. We demonstrate a prototype of interferometer which satisfies condition listed above.

2. EXPERIMENT

A prototype of the device for stress testing of thin film is presented in Fig. 1. Using a single-beam construction [2] of interferometer and a reversible thermoplastic camera which is fixed on a rigid frame, we can eliminate a vibroprotection system. Under this condition it is possible to create high stable real-time interferometer for testing long time stress relaxation processes.The diffracted efficiency of thermoplastic film is15 % using 2 mW

0-8194-2168-5/96/$6.00

ELSEVIER

Physica C 267 (1996) 355–360

PHYSICA C

Fabrication of biaxially aligned $YBa_2Cu_3O_{7-x}$ thin films on glass substrates

K.Y. Chen [a,*], G.J. Salamo [a], S. Afonso [a], X.L. Xu [a], Y.Q. Tang [a], Q. Xiong [a], F.T. Chan [a], L.W. Schaper [b]

[a] *Department of Physics, High Density Electronics Center, University of Arkansas, Fayetteville, AR 72701, USA*
[b] *Department of Electrical Engineering, High Density Electronics Center, University of Arkansas, Fayetteville, AR 72701, USA*

Received 22 April 1996

Abstract

Biaxially aligned $YBa_2Cu_3O_{7-x}$ thin films have been fabricated on glass substrates with an in-plane aligned yttria-stabilized zirconia (YSZ) buffer layer. Ion-beam assisted pulsed laser deposition was used to prepare the YSZ buffer layers on amorphous glass substrates. The YSZ films deposited at room temperature exhibited (001) orientation, whereas at temperatures higher than 300°C, YSZ grew with high degree of (111) orientation. Both the (001) and (111) YSZ films were biaxially aligned. $YBa_2Cu_3O_{7-x}$ films deposited using pulsed laser deposition on biaxially aligned (001) YSZ on glass were highly *c*-axis oriented and strongly *a–b* plane aligned. A critical temperature T_{c0} ($R = 0$) of 87.1 K was routinely achieved and J_c was in the range of $\sim 10^4$ A/cm^2. The limitation in J_c was found to be due to microcracks in the YBCO film caused by the tensile stress resulting from the thermal expansion mismatch between the glass and YBCO. The results suggest that glass with a better thermal expansion match to YBCO would lead to higher J_c values.

Keywords: Multilayers; Thermal expansion; Thin films; YSZ structure

1. Introduction

Fabricating $YBa_2Cu_3O_{7-x}$ (YBCO) films on non-single-crystal substrates has been a challenge since the successful deposition of epitaxial YBCO films on single crystal substrates [1]. One reason for the intense interest is that some polycrystalline and amorphous materials have more appropriate physical properties for device applications than that of single crystal substrates used in YBCO film growth. For example, the low dielectric constant and low loss tangent of some non-single-crystal materials are attractive for substrates or insulating layers in superconducting multi-chip modules. Substrate cost is another significant factor in favor of non-single-crystal materials. In recent years, biaxially aligned YBCO films have been successfully deposited on polycrystalline metal alloy substrates, through the use of a yttria-stabilized zirconia (YSZ) buffer layer, which is deposited by an ion beam assisted deposition (IBAD) technique [2–6]. A J_c value of 1×10^6 A/cm^2 has been achieved at 75 K for a YBCO film on Ni based alloy [6], demonstrating that growing high quality YBCO films on polycrystalline substrates is possible.

The success with polycrystalline metal alloy substrates has prompted an even more intense interest in

* Corresponding author. Fax: +1 501 575 4580.

PII S0921-4534(96)00386-3

Proceedings of the 10th Anniversary HTS Workshop on Physics, Materials and Applications, p 167-70, 1996

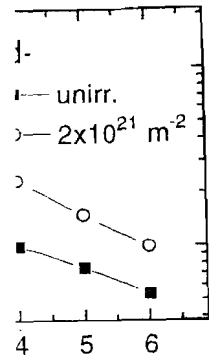

)

t-processed Nd-123 (Hllc) at 77 K.

ere clearly not yet optimized in their

neasurements on neutron irradiated Bi-
expectations, according to which the
dignment of grain colonies, the results
g *within* the grains, once the low-field
tors between 2 and 4 were found at 77
surface after low fluence irradiation.
in the Ag-tube, this kind of experiment

701 (1995)

FABRICATION OF HIGHLY TEXTURED SUPERCONDUCTING THIN FILMS ON POLYCRYSTALLINE SUBSTRATES USING ION BEAM ASSISTED DEPOSITION

[1]Q. Xiong, [1]S. Afonso, [1]F. T. Chan, [1]K.Y. Chen, [1]G.J. Salamo, [2]G.Florence, J. Cooksey, S. Scott, [2]S. Ang, [2]W.D. Brown and [2]L. Schaper.
[1]Physics Department, [2]Electrical Engineering Department / High Density Electronics Center, University of Arkansas, Fayetteville, AR 72701

ABSTRACT

$Tl_2Ba_2CaCu_2O_y$(Tl2212) thin films on ceramic Al_2O_3 substrates with J_c(77K) of about 10^5 A/cm^2 and high quality YBCO/YSZ/SiO_2/YSZ/YBCO/$LaAlO_3$ multilayers with J_c(77K) of about $6\cdot10^5$ A/cm^2, the top YBCO layer have been successful deposited for the first time. These Mirror-like, highly c-axis oriented films were grown on highly textured YSZ buffer layers, which were deposited through Ion Beam-Assisted Laser Ablation. The zero resistance temperature is 95-108K for the Tl2212 films, and 85-90K for the multilayer YBCO films. The results suggest that using cheap non-single crystal substrates to fabricate good HTS films is possible.

I. Introduction

Since the discovery of high temperature superconductors(HTS), many possible applications of HTS thin films have been design and demonstrated, from very useful fault current limiters to the electronic interconnects on multichip module (MCM) substrates. All of these applications would benefit from the use of HTS thin films. One of the major problems for the application of HTS's is that HTS's can carry only a limited amount of current without resistance. This problem is related to their two dimensional layered structure. According to earlier studies[1-2], if the layers do not line up properly the critical current density will decrease dramatically in the misaligned region. One way to overcome this problem is to grow micron-thin layers of the material on well organized substrates, epitaxially. The process has the effect of lining up the superconducting layers more accurately. HTS thin films grown on single crystal substrates of $LaAlO_3$ or $SrTiO_3$ have good lattice match between the HTS and substrate, and have critical current densities of about ~10^6 A/cm^2 which is large enough for most HTS thin film applications. While this effort is impressive, it is far from useful, since the films so developed are much too expensive because the single crystal substrates are very expensive and available only in relatively small sizes. Moreover, for some electronic applications such as HTS multi-chip modules(MCM's),

QTuD 10:30 am Hyatt A

Spatial Solitons II

Barry Luther-Davies, *Australian National University, Presider*

QTuD1 (Invited) 10:30 am

Physics of dark solitons

Yuri S. Kivshar, *Optical Sciences Centre, Australian National University, ACT 0200 Canberra, Australia*

The main objective of this talk is to give a simple introduction into the physics and properties of "dark" solitons and related localized modes, which occur in different problems of nonlinear optics. Unlike conventional (bright) solitons, dark solitons are spatially localized modes (or pulses) that exist on a background wave with nonvanishing asymptoics, the latter being usually modulationally stable. In the other words, a 2D dark soliton is a phase-kink that connects two plane waves with the same amplitudes but different phases. In practice, such solitons are created of a background beam (or pulse) of finite extent but much longer than the soliton itself.

From the physical point of view dark solitons can be viewed as the reflectionless modes of the optical waveguide they induce whereas bright spatial solitons are the bound modes.[1] In the case of two transverse degrees of freedom such solitons may be observed as dark soliton stripes or grids[2] with the properties similar to those of 2D dark solitons. Dark solitons of circular symmetry (optical vortex solitons)[3] have been predicted and shown to be stable, and they have been already observed experimentally in self-defocusing materials. On the other hand, dark soliton stripes are unstable to transverse long-wavelength modulations.

Along with the topics which were previously reviewed in the literature (see, e.g., the review paper,[4] the present talk also mentions very recent results including polarization domain walls, optical vortex solitons, ring dark solitons,[5] dark solitons in media with $\chi^{(2)}$ nonlinear susceptibility, etc.

In particular, in dispersive materials with quadratic nonlinearities dark solitons may exist only for the opposite dispersion of the fundamental and second harmonics. For a small phase mismatch of the wavevectors of two harmonics such solitons are shown to possess nonmonotonous (oscillating) tails, which make the interaction between the neighboring solitons nontrivial: For example, such solitons may form stable bound states of two (or more) dark solitons.

A link between a variety of optical problems and corresponding problems of the theory of a weakly compressible fluid and nonideal Bose gas will be mentioned as well.

1. A. W. Snyder, D. J. Mitchell, and B. Luther-Davies, J. Opt. Soc. Am B **10**, 2341 (1993).
2. G. A. Swartzlander, Jr., D. R. Andersen, J. J. Regan, H. Yin, and A. E. Kaplan, Phys. Rev. Lett. **66**, 1583 (1991).
3. A. W. Snyder, L. Poladian, and D. J. Mitchell, Opt. Lett. **17**, 789 (1992); G. A. Swartzlander, Jr. and C. T. Law, Phys. Rev. Lett. **69**, 2503 (1992).
4. Yu. S. Kivshar, IEEE J. Quantum Electron. **29**, 250–264 (1993).
5. Yu. S. Kivshar and X. Yang, Phys. Rev. E **50**, R40 (1994).

QTuD2 (Invited) 11:00 am

Photorefractive dark solitons as waveguides

Matthew E. Morin, Galen C. Duree, Jr., Gregory J. Salamo, Mordechai Segev,* Bruno Crosignani,** Paolo Di Porto,** Amnon Yariv,† Edward J. Sharp,‡ Ratnakar R. Neurgaonkar,§ Department of Physics, University of Arkansas, Fayetteville, Arkansas 72701

Recently, we reported on the prediction[1,2] and observation[3] of a new type of spatial soliton. For this new spatial soliton, compensation for diffraction is accomplished through the photorefractive effect. In this case, a Gaussian beam incident on a photorefractive crystal is trapped at a diameter of about 30 μm and propagates through the crystal while maintaining its spatial shape and defying the rules of diffraction. We have referred to our observation as a photorefractive bright soliton.

Physically, this phenomenon can be understood by picturing diffraction of a Gaussian beam as if each Fourier component of the beam propagates independently. Because each component has a different k-vector projection along the propagation direction, the relative phase between Fourier components changes as a function of propagation distance z. Consequently, the sum of the Fourier components produces a different waveform at each z along the propagation direction. Thus, diffraction can be compensated if a material-index distribution can produce a k-vector distribution in which a Fourier component has the same magnitude projection along the propagation direction, thus ensuring a constant-phase relationship between Fourier components. For photorefractive solitons, the induced index change needed to produce the proper k-vector distribution arises from the gratings formed between all pairs of Fourier components through two-beam photorefractive coupling.

Our observations of bright photorefractive solitons have led to more recent observations of dark planar and vortex photorefractive solitons.[4,5] Here we report on the experimental observation of the use of a dark planar soliton to act as a waveguide for a second laser beam, which is injected into the dark notch of the planar soliton. To produce the planar dark soliton, we used the output of an argon-ion laser (Fig. 1) with a thin glass slide inserted into half of the beam to produce a wave front at the SBN photorefractive crystal that had the proper π phase jump at its center. Figure 2 shows the waveform at the output crystal face with and without dark-soliton formation. The external field required to trap the dark soliton was −400 V/cm along the c axis of the crystal. The width (FWHM) of the dark notch was 33 μm at the entrance face of the crystal. At the exit face, the dark notch was 49 μm without the applied voltage. With the applied voltage, the dark soliton formed about halfway through the crystal, with a width of 10 μm. Once the planar dark soliton was formed, the argon beam was blocked and a He–Ne beam was focused and injected into the notch. As shown in Fig. 3, the He–Ne Gaussian beam diameter was 22 μm at the entrance face of the crystal. The He–Ne beam diameter at the exit face was 105 μm without the use of a dark planar soliton and was 18 μm with the use of the dark planar soliton. Alignment of the He–Ne beam was found

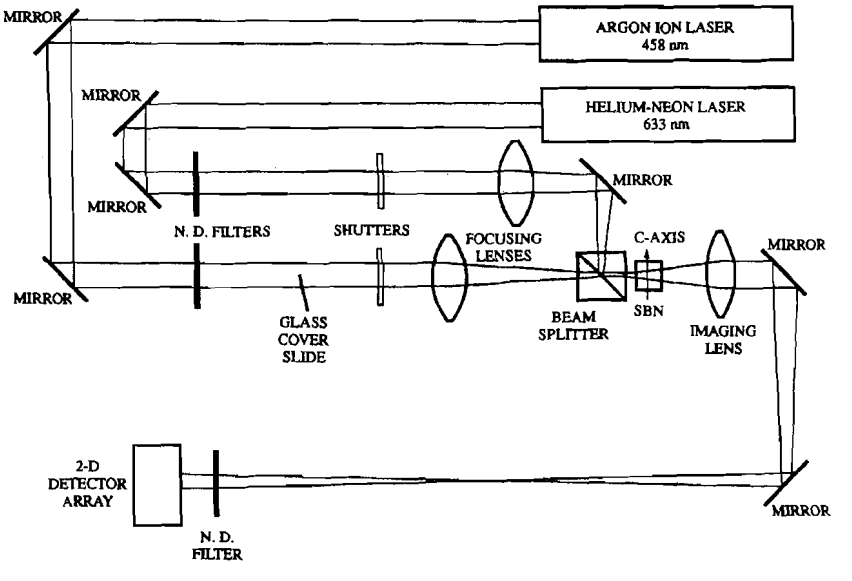

QTuD2 Fig. 1. Apparatus for observing dark photorefractive solitons as waveguides.

Dark Photorefractive Spatial Solitons and Photorefractive Vortex Solitons

Galen Duree,[1] Matthew Morin,[1] and Gregory Salamo,[1]
Mordechai Segev,[2] Bruno Crosignani,[3] Paolo Di Porto,[3] Edward Sharp,[4] and Amnon Yariv[5]
[1]*Physics Department, University of Arkansas, Fayetteville, Arkansas 72701*
[2]*Electrical Engineering Department and Advanced Center for Photonics and Optoelectronic Materials (POEM) and Princeton Material Institute (PMI), Princeton University, Princeton, New Jersey 08544*
[3]*Dipartimento di Fisica, Universitá dell'Aquila, L'Aquila, Italy*
[4]*Army Research Laboratory, Fort Belvoir, Virginia 22060*
[5]*California Institute of Technology, Pasadena, California 91125*
(Received 30 June 1994)

We report on the first experimental observations of dark, planar, spatial photorefractive solitons, and photorefractive vortex solitons that are trapped in a bulk (three-dimensional) photorefractive media. Both the dark and vortex solitons possess the "signatures" of the photorefractive solitons: they are independent of absolute intensity, can afford significant absorption, and are inherently asymmetric with respect to the transverse dimensions of trapping.

PACS numbers: 42.50.Rh

Spatial solitons in photorefractive (PR) materials [1] have been the object of growing interest during the last two years. Thus far, three different types of PR solitons have been investigated. The first type of PR soliton which has been studied stems from the nonlocal nature of the photorefractive effect, as manifested in the dependence of the perturbation in the refractive index on the transverse derivatives of the light intensity distribution [1,2]. This type of PR soliton [3–6] exists when an external voltage is applied to the PR material, after the index gratings have been formed, but before the external field is screened by the background conductivity. Solitons of this type are transient by nature and we refer to their time window of existence as quasi-steady-state. Their most distinct properties are (i) independence of the absolute light intensity [1–3] (for intensities much larger than the dark irradiance) and (ii) the capability of trapping in two transverse dimensions [3–5]. The second type of PR soliton, which we call the screening soliton [7], appears in the steady state after the external field is screened, nonuniformly, due to the transversely nonuniform intensity distribution. This effect is local and results in an index perturbation that is inversely proportional to the sum of the optical and dark irradiances. Its most distinct properties are (i) dependence on the ratio between the optical and dark irradiances and convergence to the narrowest size for large ratios and (ii) existence of bright solitons for a negative perturbation in the index while dark solitons require a positive perturbation in the index while dark solitons require a positive perturbation (this implies that the polarity of the applied field is *opposite* to the polarity required to generate PR solitons of the first type). The third type of PR soliton is present in materials that are both photorefractive and photovoltaic. These photovoltaic solitons [8] stem from photovoltaic currents that generate (in steady state) an index perturbation analogous to the nonlinearity in a saturable absorber (sometimes called a thresholding nonlinearity), which is a local effect as well. Their most distinct property is the dependence on the ratio between the optical and dark irradiances, the narrowest solitons being obtained when this ratio is between 1 and 2.

In this Letter we report on the first experimental observation of photorefractive dark solitons and vortex solitons, both belonging to the first (nonlocal) type.

Photorefractive solitons of the first type evolve when diffraction is exactly balanced by self-scattering (two-wave mixing) of the spatial (plane wave) components of the soliton beam [1,2]. Intuitively, self-trapping occurs when diffraction (which involves accumulation, by each plane wave component of a beam, of a phase that is linear in the propagation distance) is balanced by nonlinear phase coupling that leaves the complex amplitudes of the plane-wave components unchanged. Photorefractive gratings, however, typically give rise to amplitude coupling (energy-exchange interaction) due to a dominant diffusion transport mechanism for the redistribution of the photogenerated charge carriers. Inherently, this process cannot compensate for diffraction since it alters the amplitudes of the plane-wave components rather than balancing their phases. The presence of an external bias field, on the other hand, results in strong phase coupling and is, therefore, required for the formation of these PR solitons. Our recent observations of photorefractive bright solitons of the first type [3,4] revealed that, unlike the Kerr-like solitons, the PR solitons may be trapped in two transverse dimensions and maintain their stability. We also presented experimental results [5] addressing the two-dimensional problem and pointed out that the trapping is inherently asymmetric with respect to the two transverse dimensions. We have shown experimentally that the self-trapping effects in the direction parallel to the external electric field (x direction) exist regardless of the size of the beam in the other transverse di-

 0031-9007/95/74(11)/1978(4)$06.00

Waveguides formed by quasi-steady-state photorefractive spatial solitons

Matthew Morin, Galen Duree, and Gregory Salamo

Department of Physics, University of Arkansos, Fayetteville, Arkansas 72701

Mordechai Segev

Department of Electrical Engineering, Princeton University, Center for Photonics and Optoelectronic Materials and the Princeton Material Institute, Princeton University, Princeton, New Jersey 08544

Received May 18, 1995

We show that a quasi-steady-state photorefractive spatial soliton forms a waveguide structure in the bulk of a photorefractive material. Although the optically induced waveguide is formed by a very low-power (microwatts) soliton beam, it can guide a powerful (watt) beam of a longer wavelength at which the medium is nonphotosensitive. Furthermore, the waveguide survives, either in the dark or when guiding the longer-wavelength beam, for a long time after the soliton beam is turned off. We take advantage of the solitons' property of evolution from a relatively broad input beam into a narrow channel and show that the soliton induces a tapered waveguide (an optical funnel) that improves the coupling efficiency of light into the waveguiding structure. © 1995 Optical Society of America

It has been established for several years that spatial Kerr-type solitons induce guidance of a typically much weaker beam[1,2] through cross-phase modulation. In fact, the optical control of one beam by another has interesting potential applications in all-optical switching and beam-steering waveguide devices.[3,4] All these effects are based on Kerr-type solitons, and, as such, they carry over their characteristic properties: (i) waveguides induced by bright Kerr solitons exist only in one transverse dimension[1] (implying that all potential device applications must be planar), (ii) the dimensions of the induced waveguide depend on the soliton intensity, and (iii) the guided beam is much weaker than the soliton (guiding) beam.[1]

Photorefractive solitons[5] have been shown to exist in several forms. Quasi-steady-state solitons[5-13] appear during the slow screening process of a field applied externally to a photorefractive crystal. Solitons of this type are transient by nature, and we refer to their time window of existence as a quasi-steady state. Their most distinct properties are independence of the absolute light intensity[5-8,12,13] (for intensities much larger than the dark irradiance) and the capability of trapping in both transverse dimensions.[7-9,12,13] Experimental observations have proved the existence of one- and two-dimensional bright solitons,[7-9] planar dark solitons, and vortex solitons.[12,13] The second type of photorefractive soliton is the screening soliton,[14] which appears in the steady state, after the external field is screened nonuniformly as a result of the transversely nonuniform intensity distribution. This effect is local and results in an index perturbation that is inversely proportional to the sum of the optical and dark irradiances. Recent experimental observations have confirmed the existence of one- and two-dimensional screening solitons.[15,16] The third type of photorefractive soliton exists in materials that are both photorefractive and photovoltaic. These photovoltaic solitons[17] stem from photovoltaic currents that generate an index perturbation analogous to the nonlinearity in a saturable absorber. A recent observation[18] confirmed the existence of dark photovoltaic solitons in $LiNbO_3$. Some of these experimental observations[18,19] have shown that illumination of the crystal by a second (uniform) beam in the presence of the soliton leads to guidance of light in the soliton region. Finally, a recent paper predicted the existence of photorefractive vector solitons.[20]

In this Letter we show that quasi-steady-state photorefractive spatial solitons may serve as optical waveguides for other optical beams. Photorefractive solitons are especially attractive for light-induced waveguiding because they form in two transverse dimensions and require very little power (they exist even at microwatts or less). Furthermore, since the nonlinearity is based on space-charge fields that result from charges occupying deep traps, all photorefractive solitons leave behind them a waveguide structure that persists in the dark. One can utilize this memory property further by using the induced waveguides to guide light of nonphotosensitive wavelengths (typically much longer than that of the soliton) that cannot photoexcite the trapped charges. In this scheme a very weak photorefractive soliton beam can guide and control a very intense beam. Another interesting manifestation of the soliton guidance is the evolution from a relatively broad input beam into a narrow channel, where the photorefractive soliton induces a tapered waveguide, or an optical funnel. We study the guidance properties and measure the lifetime of these soliton-induced waveguides. We then use these waveguides to guide a near-infrared beam of intensity 2×10^4 W/cm^2, approximately 5 orders of magnitude larger than that of the soliton beam (roughly 0.1 W/cm^2). Finally, we point out that the two-dimensional soliton trapping properties[7-9,12,13,15] hold the promise of forming light needles (two-dimensional waveguides) in a bulk material. These and related two-dimensional guidance experiments by bright and

0146-9592/95/202066-03$6.00/0

Proceedings of the Applied Diamond Conference 1995, p 283-6 vol.1, 1995

Applications of Diamond Films and Related Materials: Third International Conference, 1995
Editors: A. Feldman, Y. Tzeng, W. A. Yarbrough, M. Yoshikawa, and M. Murakawa

LASER PROCESSING OF DIAMOND SUBSTRATES FOR MULTICHIP MODULES: PART II

Syed Jamil, M.H. Gordon, G.J. Salamo, H.A. Naseem, W.D. Brown and A.P. Malshe

High Density Electronics Center (HiDEC), University of Arkansas, Fayetteville, AR 72701

Key words: diamond, laser, MCM, metallization, polishing

Abstract

The development of new techniques for post-synthesis processing such as polishing and metallization is of intense current interest due to the potential use of diamond as an MCM thermal management substrate. In our laboratory, we have been able to demonstrate chemically clean laser induced coarse polishing and selective laser-assisted metal deposition on diamond substrates. Our technique is based on the use of a liquid ambient as a reactive medium for the laser processing of diamond substrates.

1. Introduction

Rapid changes in the electronic industry are driven by the attractiveness of faster, smaller, and lighter weight electronics. Much of the real estate on a typical semiconductor wafer is occupied by interconnecting electrical lines. The electronic "chips" themselves are so small that a further reduction in chip dimension would not appreciably reduce the size or weight of the electronic package, nor would it result in faster speed of operation. One solution to this obstacle is the concept of the MCM. The term MCM refers to the concept of developing high density electronics by reducing the space taken by interconnects by using multi-layered structures.

For the MCM concept or any high density electronic packaging concept to be successful, thermal management is an essential requirement. High density means high power dissipation. As chips are packed closely together the power density levels are very high. Since CVD diamond has a very high thermal conductivity (1000-1500 W/m°C), and is now available at a reasonable cost, it is now plausible to consider free

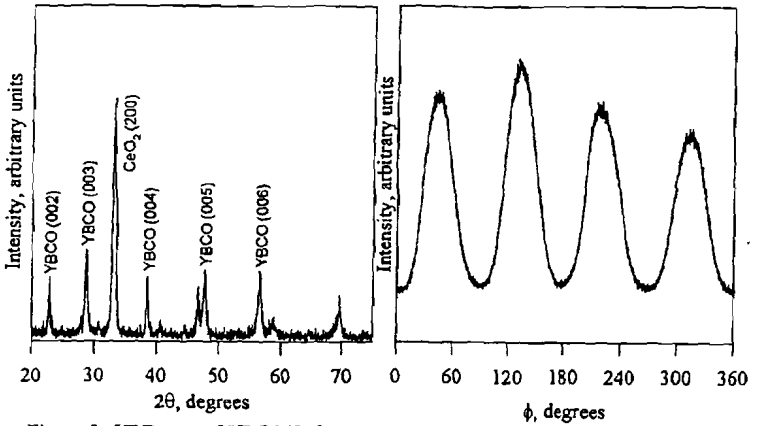

Figure 5. XRD scan of $YBCO/CeO_2$ deposited on Pyrex with IBAD.

Figure 6. Phi scan of YBCO (103) family of peaks on CeO_2/Pyrex.

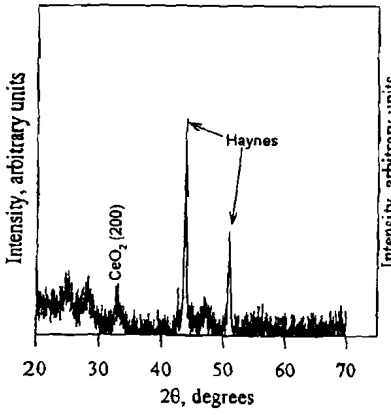

Figure 7. XRD scan of CeO_2 deposited on Haynes without IBAD.

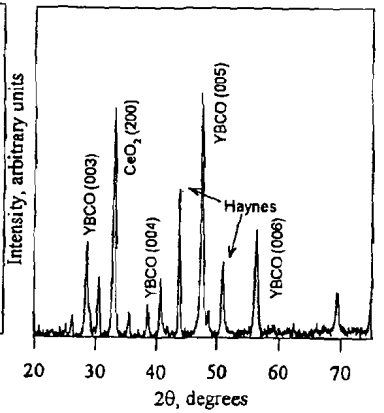

Figure 8. XRD scan of $YBCO/CeO_2$ deposited on Haynes with IBAD.

EPITAXIAL GROWTH OF SUPERCONDUCTING $YBa_2Cu_3O_{7-x}$ FILMS ON $Sr(Al_{0.5}Ta_{0.5})O_3$ BUFFERED MgO SUBSTRATES

K. Y. Chen, S. Afonso, R. C. Wang*, Y. Q. Tang, G. Salamo, and F. T. Chan

Department of Physics/High Density Electronics Center, University of Arkansas, Fayetteville, AR 72701

R. Guo, and A. Bhalla

Material Research Laboratory, Pennsylvania State University, University Park, PA 16802

ABSTRACT

High quality $YBa_2Cu_3O_{7-x}$ films have been epitaxially grown on MgO substrates with a $Sr(Al_{0.5}Ta_{0.5})O_3$ (SAT) buffer layer using pulsed laser deposition(PLD). SAT thin films were first deposited on MgO (001) substrates by PLD. X-ray diffraction shows that SAT grows with the c-axis highly oriented normal to the substrate plane. The subsequently deposited $YBa_2Cu_3O_{7-x}$ films on SAT/MgO exhibit highly epitaxial growth with a rocking curve width of 0.68° and a ϕ scan peak width of 1.67°. The T_c value is 91 K with a transition width less than 1 K. The critical current densities are higher than 2.7×10^6 A/cm² at 77 K.

INTRODUCTION

There have been great efforts in developing high T_c superconducting thin films for device applications since the discovery of the high T_c superconductors. Although high T_c YBCO films have been successfully grown on a number of substrates, such as $SrTiO_3$, $LaAlO_3$, MgO, YSZ, and $LaGaO_3$, these substrates have some drawbacks for certain electronic applications . In high-frequency electronic applications, such as superconducting multi-chip modules (MCM's), one requires substrates and dielectric layer materials with a low dielectric constant and a low loss tangent. On the other hand, the substrates should have good lattice match with YBCO films to provide epitaxial growth of YBCO layer. In recent years, significant efforts have been made in searching for substrates and dielectric intermediate layer materials which can meet these requirements for specific electronic applications as well as the

Proceedings of the Applied Diamond Conference 1995, p 761-4 vol.1, 1995

Applications of Diamond Films and Related Materials: Third International Conference, 1995
Editors: A. Feldman, Y. Tzeng, W. A. Yarbrough, M. Yoshikawa, and M. Murakawa

plantation
of muscle
erchrome

DIAMOND-LIKE CARBON FOR HIGH TEMPERATURE SUPERCONDUCTOR ENCAPSULATION

R. A. Beera, W. D. Brown, S. Afonso, F. T. Chan, G. J. Salamo, H. A. Naseem, and A. P. Malshe

High Density Electronics Center (HiDEC),
University of Arkansas, Fayetteville, AR 72701

Key words: DLC, degradation, encapsulation, lonsdaleite, r-f PECVD, YBCO

Abstract

Diamond-like carbon (DLC), a thermodynamically, metastable, amorphous form of carbon, has been a material of recent interest due to its wide range of applications. Depending on the activation agent and deposition conditions, the quality of DLC film varies and can be used for applications ranging from optics to tools. DLC is hard and chemically inert. In the present study, these properties of DLC have been used for the protection of high temperature superconductor (HTSC) thin films. DLC films were deposited on HTSC thin films using an r-f chemical vapor deposition system with methane gas at 30°C. Films were tested for superconducting transition temperature (Tc) and critical current density (Jc) before and after DLC encapsulation. Such encapsulated HTSC films were later exposed to moisture to test the corrosion resistance of DLC:HTSC structures.

1. Introduction

The unique properties of diamond-like carbon films make them suitable materials for electrical, mechanical and optical applications. Among their more attractive properties are extreme hardness, infrared transparency under certain deposition conditions, chemical inertness, good thermal conductivity, and low electrical conductivity [1]. $YBa_2Cu_3O_{7-x}$ is a very interesting material with a high potential for application in electronics and other industrial applications. It has been improved considerably since its discovery to transition temperatures of about 90 K and critical current densities of greater than 10^6 A/cm^2. The fact that the properties of YBCO superconductors degrade with exposure to air or water will limit the use of this material in many potential applications. Applications of these materials, such as electrical interconnects for multichip modules (MCM), magnetic sensors,

The good agreement between Equation (6) and the data confirms again that inter-system crossing is not an important process in our compounds with acetonitrile solvent. It is interesting to note that inter-system crossing is mainly responsible for populating the triplet state in both C_{60} molecules and phthalocyanine derivatives [2]-[5]. This is because our cluster compounds are notably different from C_{60} and phthalocyanine derivatives in containing many ionizable low valence IB elements and chalcogenide. Perhaps more importantly, the ESA behavior of our compounds was observed in acetonitrile whereas the nonlinear transmission measurements of were conducted in toluene. Acetonitrile is much more polar solvent as compared to toluene and capable of facilitating ionization process.

CONCLUSION

The excited-state absorption of cubane-like transition metal clusters in acetonitrile is observed with nanosecond laser pulses of wavelengths ranging from 532 to 700 nm. Pulse narrowing in the time-resolved transmission measurement suggests that the excited-state absorption should be dominated by triplet-triplet transitions. The measured fluence-dependent transmission is compared with a excited-state absorption model. In this model, two singlet states, two triplet states and one ionized state are involved. The population of the triplet states is predominantly generated by the ionization and subsequent recombination. The triplet-triplet transitions are responsible for the optical limiting effect.

Reference:

[1] L. W. Tutt and A. Kost, Nature **356**, 255 (1992).
[2] F. Henari, J. Callaghan, H. Stiel, W. Blau, and D. J. Cardin, Chem. Phys. Lett. **199**, 144 (1992).
[3] D. G. McLean, R. L. Sutherland, M. C. Brant, D. M. Brandelik, P. A. Fleitz, and T. Pottenger, Opt. Lett. **18**, 858 (1993).
[4] T. H. Wei, D. J. Hagan, M. J. Sence, E. W. Van Stryland, J. W. Perry, and D. R. Coulter, Appl. Phys. B **54**, 46 (1992).
[5] J. W. Perry, K. Mansour, S. R.Marder, K. J. Perry, D. Alvarez, Jr., and I. Choong, Opt. Lett. **19**, 525 (1994).
[6] S. Shi, W. Ji, P. Lang, and X. Q. Xin, J. Phys. Chem. **98**, 3570 (1994).
[7] S. Shi, W. Ji, S. H. Tang, H. C. Zeng and X. Q. Xin, J. Am. Chem. Soc. **116**, 3615 (1994).
[8] G. A. Abakumov, V. B. Koloxsky, B. I. Polyakov, and A. P. Simonov, Chem. Phys. Lett. **182**, 321 (1992).
[9] G. A. Abakumov, B. I. Polyakov, A. P. Simonov, T. M. Skavinskaya, and V. T. Yaroslavtsev, Opt. Spectrosc. **74**, 641 (1993).
[10] J.B. Birks, Photophyiscs in aromatic molecules, (Wiley-Interscience 1970), p.398.

Materials Research Society Symposium - Proceedings, v 374, p 137-150, 1995.

PHOTOREFRACTIVE OPTICAL LIMITERS

Gregory J. Salamo*, Galen C. Duree Jr.*, Matthew Morin*, Edward J. Sharp**, Gary L. Wood**, and Ramakar R. Neurgaonkar***.

* University of Arkansas, Physics Department, Fayetteville, AR 72701
** Army Research Laboratory, Fort Belvoir, VA 22060-5838
*** Rockwell International Science Center, Thousand Oaks, CA 91360

ABSTRACT

We consider the application of photorefractive beam fanning as an optical limiter. Results indicate that by focusing the incident laser light into the photorefractive crystal and by applying electric fields that limiting is possible at the 10μJ range with an optical density or O. D. of 3. These results are independent of the incident optical pulse width.

OVERVIEW OF THE PROBLEM

The existence of high powered lasers is a severe threat to all optical sensors. Widespread use of lasers as range finders and target designators makes this threat a present and immediate danger. The human eye, as well as man-made detectors such as the many FLIR devices presently employed in the battlefield, are extremely vulnerable to stray and directed laser radiation. The eye is easily attacked by light from a laser source at a considerable distance. Damage caused to optical sensors is extensive and crippling. With the success of many military operations dependent on effective use of optical sensors, the development of sensor protection is imperative.

The laser threat itself is highly agile. The high powered output radiation can occur in a short pulse or continuously, while the wavelength of the output radiation can be either fixed, shifted, or mixed. One example of a threat laser is the short-pulsed neodymium-doped yttrium aluminum garnet or YAG laser. The output wavelength of the laser is in the near infrared at about one micron. However, it can easily be altered via frequency doubling, a process which produces an additional output in the green at about 0.5 microns. The output can be further modified, producing laser radiation at a series of wavelengths scattered over the visible spectrum via the process called Raman scattering. This type of laser threat can, therefore, deliver several laser frequencies simultaneously onto a sensor. It is commonly referred to as a "rainbow" or "white-light" laser. The actual spectrum of the output laser light can be varied and difficult to predict.

While the output of the YAG laser is usually a short pulse, there are also serious laser threats which can provide a continuous output of laser light. The argon-ion and krypton-ion lasers are prime examples. These lasers emit radiation at seven to eight wavelengths simultaneously and can be regarded as continuous wave "rainbow" or "white-light" lasers. While the spectral output of these lasers is fixed, the development of continuously tunable dye lasers and solid state lasers presents a threat with a complex and variable spectral structure.

The ideal protector must provide complete blocking of laser radiation above a predetermined threshold value. It must:

(i) be sensitive over a broad spectral range;
(ii) not significantly degrade or attenuate the desired scene to be interrogated;
(iii) operate with a large field-of-view;
(iv) provide protection against continuous and pulsed laser sources;
(v) protect against laser radiation coming from any direction;
(vi) be capable of simultaneously blocking multi-wavelength laser radiation emitted from a single source.

No such protection device presently exists.

Epitaxial $Sr_2(AlTa)O_6$ films as buffer layers on MgO for $YBa_2Cu_3O_{7-x}$ thin film growth

K. Y. Chen, S. Afonso, R. C. Wang,[a] Y. Q. Tang, G. Salamo, and F. T. Chan
Department of Physics/High Density Electronics Center, University of Arkansas, Fayetteville, Arkansas 72701

R. Guo and A. S. Bhalla
Material Research Laboratory, Pennsylvania State University, University Park, Pennsylvania 16802

(Received 27 March 1995; accepted for publication 19 April 1995)

$Sr_2(AlTa)O_6$ thin films (2000–3000 Å) have been deposited on MgO (001) substrates using pulsed laser deposition (PLD). X-ray-diffraction analysis shows that the $Sr_2(AlTa)O_6$ grows with the c axis highly oriented normal to the substrate plane and very good in-plane epitaxy. The subsequently deposited $YBa_2Cu_3O_{7-x}$ films using PLD on $Sr_2(AlTa)O_6$ buffered MgO substrates exhibit excellent epitaxial growth with a narrow rocking curve width and a small ϕ scan peak width. The critical temperature T_{c0} of 90–92 K has been achieved reproducibly and the critical current density is over 2.7×10^6 A/cm^2 at 77 K. © *1995 American Institute of Physics.*

High-T_c superconducting $YBa_2Cu_3O_{7-x}$ (YBCO) films have been successfully grown on a number of substrates, such as $SrTiO_3$, $LaAlO_3$, MgO, YSZ, and $LaGaO_3$. In many high-frequency electronic applications, such as superconducting multichip modules, one requires substrates and dielectric layer materials with a low dielectric constant and a low loss tangent. In recent years, great efforts have been made in searching for substrates and dielectric intermediate layer materials which can meet these requirements for specific electronic applications as well as the requirements for growth of superconducting films.[1–5] Several materials such as $SrTiO_3$,[2,4] MgO,[2,3] YSZ,[1] and CeO_2,[3,5] have been used as buffer layers for fabricating $YBa_2Cu_3O_{7-x}$ films on some substrates of application interest. The dielectric constant of $SrTiO_3$, however, is too high to be useful in some high-frequency devices, whereas MgO and YSZ have a relatively large lattice mismatch with superconducting materials. Another cubic perovskite material $Sr_2(AlTa)O_6$ (SAT) has recently become of interest as a buffer layer and dielectric interlayer for thin films of oxide superconductors[6,7] because it has a good lattice match with the high-T_c superconductors. Ordered SAT arises from the alternate ordered distribution of Al and Ta atoms on the octahedral site of the primitive perovskite unit cell, resulting in a doubling of the lattice constant. In disordered SAT, Al and Ta atoms randomly occupy the octahedral site. Both ordered and disordered structures are closely lattice matched to the a-b plane of YBCO. Another advantage of SAT is that it has a lower dielectric constant than that of $SrTiO_3$, YSZ, and CeO_2. Table I shows the dielectric properties of SAT ceramic samples measured at both room and liquid nitrogen temperatures. Moreover, the thermal expansion coefficient of SAT is 9.7×10^{-6} °C in the temperature range from room temperature to 600 °C, which is highly compatible with that of YBCO, and there are no structural phase transitions and twinning behavior observed. These properties indicate that SAT is suitable as a buffer layer material for high-T_c thin films in device applications.

In this communication, we report our experimental results on fabricating SAT buffer layers on MgO substrates and YBCO/SAT/MgO multilayers. We chose MgO as a substrate material in this work because it has a relatively low dielectric constant (ϵ=10) and is inexpensive compared to other substrates such as $SrTiO_3$ and $LaAlO_3$. The main disadvantage of using MgO for making superconducting films is the large lattice mismatch between it and YBCO. As a result, the critical temperature of YBCO grown directly onto MgO is usually limited to 88 K.[4] The motivation of this study is to use SAT as a buffer layer to overcome the drawback of MgO. Furthermore, MgO has been successfully used as a first buffer layer on a few substrates such as MgF_2 and Si.[2,8] This suggests, therefore, that if SAT can be successfully deposited onto MgO, it can be used as a second buffer layer for growing YBCO films.

SAT and YBCO films were deposited using the pulsed laser deposition technique. A 193 nm laser beam generated by an excimer laser was focused to provide an energy density of ~1.3 J/cm^2. The laser repetition rate was 6 Hz. An oxygen pressure was maintained in the vacuum chamber at 200–250 mTorr during deposition of both the SAT and YBCO films. The quality of the SAT and YBCO films was examined by x-ray diffraction, and four-probe T_c and J_c measurements.

The SAT target used was a ceramic pellet of the ordered phase with a lattice constant a_0=7.777 Å prepared using

TABLE I. Dielectric properties of ceramic SAT with 97% theoretical density.

	Room temperature		Low temperature (77 K)	
	10 kHz	Microwave	10 kHz	Microwave
ϵ	11.8	10.7 (11.0 GHz)	11.8	···
tan δ ($\times10^{-4}$)	16.8	3.64 (7.64 GHz)	0.42	2.09 (7.64 GHz)

[a]Permanent address: Department of Materials Science, Fudan University, Shanghai, People's Republic of China.

 0021-8979/95/78(3)/2138/3/$6.00

Epitaxial $Tl_2Ba_2CaCu_2O_8$ superconducting thin film on $Sr_2(AlTa)O_6$ buffer layer

Y. Q. Tang, K. Y. Chen, S. Afonso, X. L. Xu,[a] Q. Xiong, G. Salamo, and F. T. Chan
Department of Physics/High Density Electronic Center, University of Arkansas, Fayetteville, Arkansas 72701

R. Guo and A. Bhalla
Materials Research Laboratory, Pennsylvania State University, University Park, Pennsylvania 16802

(Received 19 June 1995; accepted for publication 17 August 1995)

Epitaxial $Tl_2Ba_2CaCu_2O_8$ superconducting films have been successfully grown on the dielectric $Sr_2(AlTa)O_6$ (SAT) buffer layers. X-ray diffraction data showed that the films were highly c-axis oriented with a rocking curve full width half maximum as narrow as 0.3°. The films also had an excellent in-plane epitaxy with $Tl_2Ba_2CaCu_2O_8$[100] aligned with SAT[100] and MgO[100] of the substrate. The zero resistance temperature T_c of the superconducting films ranged from 95 to 103 K and the transport critical current density J_c in zero field was 3×10^5 A/cm^2 at 77 K. © *1995 American Institute of Physics.*

In the study of high-temperature superconducting films, buffer layers have been extensively used[1–6] because being interposed between the substrate and the film of interest, these layers can alleviate a variety of problems such as chemical incompatibility, thermal or lattice mismatch.[7] As a new dielectric compound, $Sr_2(AlTa)O_6$ (SAT) was synthesized to be one of the potential substrate materials for the growth of high T_c superconducting films.[8] Because of its relatively low dielectric constant[9,10] and good thermal expansion coefficient and lattice match with YBCO,[8–11] SAT was successfully used as a buffer layer material for the growth of YBCO thin films.[10,11] Recent studies have shown that by depositing an epitaxial SAT buffer layer on MgO, the lattice mismatch problem between a MgO substrate and a YBCO superconducting film was reduced, leading to an improvement of superconducting properties.[10]

$Tl_2Ba_2CaCu_2O_8$ superconducting films, while exhibiting higher T_c and lower surface resistance than YBCO,[12] are much more difficult to prepare with good qualities due to the high volatility and chemical reactivity of thallium and the high reaction temperature. Although best films with transport J_c of $1.06–5.3\times10^6$ A/cm^2 were obtained by carefully optimizing the thallination procedure and using suitable substrates such as $LaAlO_3$,[13–15] or $SrTiO_3$,[16] the high cost and high dielectric constants of such substrates can limit further applications of $Tl_2Ba_2CaCu_2O_8$ films in microelectronics. Some other substrates of low cost and low dielectric constants such as sapphire, silica, and MgO suffer from the chemical incompatibility or large lattice mismatch with $Tl_2Ba_2CaCu_2O_8$ and consequently yield poor film quality and low J_c. To resolve these problems, a suitable buffer layer compatible both with the $Tl_2Ba_2CaCu_2O_8$ film and with the substrate should be used. By choosing CeO_2 as buffer layers, Holstein *et al.* were able to avoid the chemical reaction of the $Tl_2Ba_2CaCu_2O_8$ films with the sapphire substrates and produced epitaxial $Tl_2Ba_2CaCu_2O_8$ films with T_c of 97–98 K and transport J_c of 2.8×10^5 A/cm^2 at 75 K.[3]

The crystallographic phase of ordered SAT has a double cell cubic perovskite structure with a lattice constant a_0=7.777 Å[10] or $a_0/2$=3.888 Å, while a_0=3.895 Å in the disordered cubic perovskite.[9] These lattice constants are close to those of Tl-based superconductors (a_0=3.85–3.86 Å). In fact, SAT has better lattice match to the TlBaCaCuO superconductors than many other substrates such as MgO (a_0=4.213 Å), YSZ ($a_0/\sqrt{2}$=3.639 Å), $LaAlO_3$ (a_0=3.792 Å), and even $SrTiO_3$ (a_0=3.905 Å). Moreover, SAT is similar to $SrTiO_3$ in structure and was tested to be chemically stable at high temperature.[8,9] Therefore, it should also be a good candidate to act as a buffer layer in the fabrication of Tl-based superconducting films. In this communication, we report for the first time the preparation of epitaxial

FIG. 1. SEM photograph of a $Tl_2Ba_2CaCu_2O_8$ superconducting film on SAT/MgO.

[a]Permanent address: Ion Beam Laboratory, Shanghai Institute of Metallurgy, Chinese Academy of Sciences, Shanghai 200050, China.

 0021-8979/95/78(11)/6846/3/$6.00

CLEO '95. (IEEE Cat. No. 95CH35800), p 259, 1995

CThA2 **8:15 am**

Photorefractive dark and vortex solitons

Greg Salamo, Galen Duree, Matthew Morin, Mordechai Segev, Bruno Crosignani, Paolo Di Porto, Amnon Yariv, *Department of Physics, University of Arkansas, Fayetteville, Arkansas 72701*

Spatial solitons in photorefractive (PR) materials[1] have been the object of growing interest during the last two years. Until now, three different types of PR solitons have been investigated. The first type stems from the nonlocal nature of the PR effect, as manifested in the dependence of the perturbation in the refractive index on the transverse derivatives of the light-intensity distribution.[1,2] Solitons of this type evolve when diffraction is exactly balanced by self-scattering (two-wave mixing) of the spatial (plane wave) components of the soliton beam. Observation of PR bright solitons of the first type[3,4] reveals that, unlike the Kerr-like solitons, these solitons may be trapped in two transverse dimensions[5] (although the self-trapping effects are inherently asymmetric with respect to the two transverse dimensions) and maintain their stability.[5] The most distinct properties of these solitons are independence of the absolute light intensity[1-3] (for intensities much larger than the dark irradiance) and (ii) the capability of trapping in two transverse dimensions.[3-5] The second and the third types of PR solitons, called the screening soliton[6] and the photovoltaic soliton,[7] respectively, result from steady-state nonuniform screening (the former) or from photovoltaic fields (the latter). Unlike the first type of PR soliton, these two are both local effects (the index perturbation at any location is a function of the light intensity at the same location). As such, the shape and width (cross section) of these solitons are dependent on their intensity.

Here we report on the experimental observation of PR dark solitons and vortex solitons, both belonging to the first (nonlocal) type. To observe the planar dark solitons, we launch a dark notch with the necessary π phase jump in its center by inserting a thin glass slide in one half of the beam. Photographs taken above the crystal are shown in Fig. 1, where a 21-μm-wide dark soliton (nondiffracting dark notch) and a normally diffracting (from 21 to 35 μm) notch are shown (top and bottom photographs, respectively). The external field required to trap the dark soliton is –400 V/cm, applied parallel to the trapping direction. An interferometric measurement verified the π phase jump at the center of the dark soliton. The asymmetry between the direction of trapping arises when the input beam is rotated so that the external field is perpendicular to the narrow dimension of the beam. In this case, the dark notch could not be trapped, even at fields as high as –1000 V/cm. An important signature of the nonlocal PR solitons is their independence of the absolute light intensity. To verify this we varied the input power over 2 orders of magnitude, from 3 to 300 μW (intensities of 0.3–30 W/cm^2), we observed no change in the shape or the size of the dark soliton.

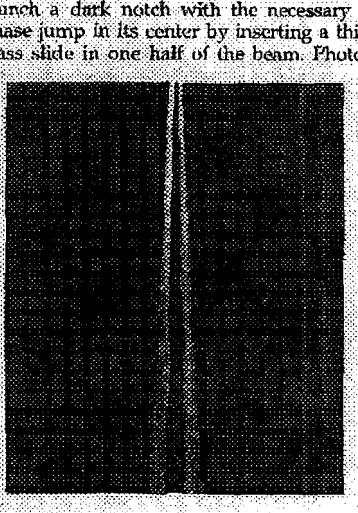

CThA2 Fig. 1. Top view photographs of a 11 μm wide (FWHM) photorefractive dark spatial soliton (top) and a normally-diffracting dark notch, propagating (from left to right) in a 5 mm long crystal.

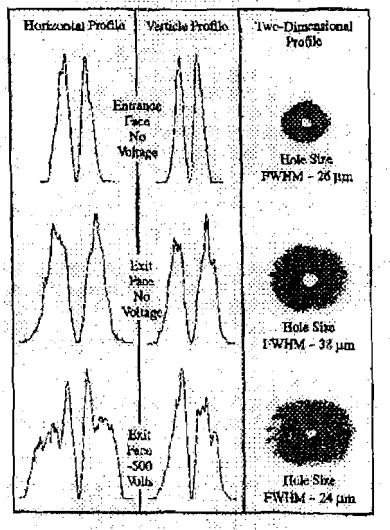

CThA2 Fig. 2. Two-dimensional transverse profiles and photographs of the input (upper) and diffracting optical vortices (middle) and of the photorefractive vortex soliton (lower).

To observe the PR vortex solitons, it was necessary to launch a beam with a transverse phase of exp($im\theta$). We used two techniques to generate the desired phase dependence at the input face of the crystal. First, we used the coherent doughnut mode of the laser and, second, we constructed the doughnut mode by using a sum of two beams, one with a vertical notch and the other with a horizontal notch, with an appropriate $\pi/2$ relative phase between them. Both methods produced a Gauss–Laguerre beam that possessed the desired phase dependence. Our results are shown in Fig. 2, where the horizontal (left column) and vertical (middle) cross sections of the cylindrical beam are shown together with the actual photographs (right column; darker regions represent regions of higher optical intensity) under various conditions. The upper and the middle rows show the beam profiles at the entrance and the exit faces of the crystal with no applied voltage. It is apparent that the bright regions and the dark regions diffract in the same manner. When a negative voltage is applied (lower row) the central two-dimensional region (the optical vortex) becomes self-trapped, whereas the bright regions increase their diffraction significantly (indicative of self-defocusing behavior). Comparison to observations of optical-vortex solitons in Kerr media reveal that all the differences in the properties of both types, as discussed for dark solitons, persist for the vortex solitons.

Department of Electrical Engineering, Princeton University, Princeton, New Jersey 09544; Department of Physics, University of Aquila, 67010 L'Aquila, Italy; California Institute of Technology, 128-95, Pasadena California 91125.

1. M. Segev, B. Crosignani, A. Yariv, B. Fischer, Phys. Rev. Lett. 68, 923 (1992).
2. B. Crosignani, M. Segev, D. Engin, P. DiPorto, A. Yariv, G. Salamo, J. Opt. Soc. Am. B 10, 446 (1993).
3. G. Duree, J. L. Shultz, G. Salamo, M. Segev, A. Yariv, B. Crosignani, P. DiPorto, E. Sharp, R. Neurgaonkar, Phys. Rev. Lett. 71, 533 (1993).
4. M. Segev, A. Yariv, G. Salamo, G. Duree, J. Shultz, B. Crosignani, P. DiPorto, E. Sharp, Opt. Photon. News 4, 8 (1993).
5. M. Segev, A. Yariv, B. Crosignani, P. DiPorto, G. Duree, G. Salamo, E. Sharp, Opt. Lett. 19, 1296 (1994); ibid., 1195 (1994).
6. M. Segev, G. C. Valley, B. Crosignani, P. DiPorto, A. Yariv, "Steady-state spatial screening-solitons in photorefractive media with applied field," in Phys. Rev. Lett., in press.
7. G. C. Valley, M. Segev, B. Crosignani, A. Yariv, M. M. Fejer, M. Bashaw, "Bright and dark photovoltaic spatial solitons," Phys. Rev. A, in press.

CThA3 (Invited) **8:30 am**

Regimes of double phase conjugate mirror operation

A. V. Mamaev, V. V. Shkunov, *Institute for Problems in Mechanics RAS, Vernadskogo 101 Moscow 117526, Russia*

Classical geometry of double phase conjugate mirror (DPCM) operation is usually associated with self-excitation of the so-called common grating which is recorded simultaneously by two separate interference patterns—of a first pump with a signal backward to a second pump, and of the second pump with a signal backward to the first one.[1,2] There was proposed also a more sophisticated DPCM model which allows generation of some intermediate fanning waves inside crystal if a particular sample demonstrates a rather high total two-wave gain.[3,4]

These two models utilize a plain-wave formalism, i.e. it is a priory assumed there that i) all the beams which participate in the mixing are the plane waves, and that ii) if any two of them are counterpropagating they are automatically phase conjugated to each other. It is rather clear that both these simplifying assumptions are very far from the experimental reality because the waves, which are self generated inside the crystal and which are inevitable participants for all DPCM scenar-

Epitaxial $Tl_2Ba_2CaCu_2O_8$ superconducting thin film on $Sr_2(AlTa)O_6$ buffer layer

Y. Q. Tang, K. Y. Chen, S. Afonso, X. L. Xu,[a] Q. Xiong, G. Salamo, and F. T. Chan
Department of Physics/High Density Electronic Center, University of Arkansas, Fayetteville, Arkansas 72701

R. Guo and A. Bhalla
Materials Research Laboratory, Pennsylvania State University, University Park, Pennsylvania 16802

(Received 19 June 1995; accepted for publication 17 August 1995)

Epitaxial $Tl_2Ba_2CaCu_2O_8$ superconducting films have been successfully grown on the dielectric $Sr_2(AlTa)O_6$ (SAT) buffer layers. X-ray diffraction data showed that the films were highly c-axis oriented with a rocking curve full width half maximum as narrow as 0.3°. The films also had an excellent in-plane epitaxy with $Tl_2Ba_2CaCu_2O_8$[100] aligned with SAT[100] and MgO[100] of the substrate. The zero resistance temperature T_c of the superconducting films ranged from 95 to 103 K and the transport critical current density J_c in zero field was 3×10^5 A/cm^2 at 77 K. © *1995 American Institute of Physics.*

In the study of high-temperature superconducting films, buffer layers have been extensively used[1–6] because being interposed between the substrate and the film of interest, these layers can alleviate a variety of problems such as chemical incompatibility, thermal or lattice mismatch.[7] As a new dielectric compound, $Sr_2(AlTa)O_6$ (SAT) was synthesized to be one of the potential substrate materials for the growth of high T_c superconducting films.[8] Because of its relatively low dielectric constant[9,10] and good thermal expansion coefficient and lattice match with YBCO,[8–11] SAT was successfully used as a buffer layer material for the growth of YBCO thin films.[10,11] Recent studies have shown that by depositing an epitaxial SAT buffer layer on MgO, the lattice mismatch problem between a MgO substrate and a YBCO superconducting film was reduced, leading to an improvement of superconducting properties.[10]

$Tl_2Ba_2CaCu_2O_8$ superconducting films, while exhibiting higher T_c and lower surface resistance than YBCO,[12] are much more difficult to prepare with good qualities due to the high volatility and chemical reactivity of thallium and the high reaction temperature. Although best films with transport J_c of $1.06–5.3\times10^6$ A/cm^2 were obtained by carefully optimizing the thallination procedure and using suitable substrates such as $LaAlO_3$[13–15] or $SrTiO_3$,[16] the high cost and high dielectric constants of such substrates can limit further applications of $Tl_2Ba_2CaCu_2O_8$ films in microelectronics. Some other substrates of low cost and low dielectric constants such as sapphire, silica, and MgO suffer from the chemical incompatibility or large lattice mismatch with $Tl_2Ba_2CaCu_2O_8$ and consequently yield poor film quality and low J_c. To resolve these problems, a suitable buffer layer compatible both with the $Tl_2Ba_2CaCu_2O_8$ film and with the substrate should be used. By choosing CeO_2 as buffer layers, Holstein *et al.* were able to avoid the chemical reaction of the $Tl_2Ba_2CaCu_2O_8$ films with the sapphire substrates and produced epitaxial $Tl_2Ba_2CaCu_2O_8$ films with T_c of 97–98 K and transport J_c of 2.8×10^5 A/cm^2 at 75 K.[3]

The crystallographic phase of ordered SAT has a double cell cubic perovskite structure with a lattice constant a_0=7.777 Å[10] or $a_0/2$=3.888 Å, while a_0=3.895 Å in the disordered cubic perovskite.[9] These lattice constants are close to those of Tl-based superconductors (a_0=3.85–3.86 Å). In fact, SAT has better lattice match to the TlBaCaCuO superconductors than many other substrates such as MgO (a_0=4.213 Å), YSZ ($a_0/\sqrt{2}$=3.639 Å), $LaAlO_3$ (a_0=3.792 Å), and even $SrTiO_3$ (a_0=3.905 Å). Moreover, SAT is similar to $SrTiO_3$ in structure and was tested to be chemically stable at high temperature.[8,9] Therefore, it should also be a good candidate to act as a buffer layer in the fabrication of Tl-based superconducting films. In this communication, we report for the first time the preparation of epitaxial

FIG. 1. SEM photograph of a $Tl_2Ba_2CaCu_2O_8$ superconducting film on SAT/MgO.

[a]Permanent address: Ion Beam Laboratory, Shanghai Institute of Metallurgy, Chinese Academy of Sciences, Shanghai 200050, China.

 0021-8979/95/78(11)/6846/3/$6.00

High-resolution phase-conjugate imaging in double-pumped phase conjugators

Jan M. Yarrison-Rice, Edward J. Sharp, Gary L. Wood, Gregory J. Salamo, Robert Klank, and Ratnakar R. Neurgaonkar

Phase-conjugate images with a resolution greater than 250 lines/mm are obtained through the use of a bridge, double-pumped phase conjugator. We demonstrate that this conjugator can carry out image-processing tasks, such as the addition and subtraction of complex spatial distributions, with a spatial resolution of >100 lines/mm. These results represent a significant improvement over previously reported resolutions obtained from photorefractive mutually pumped phase conjugators and approach the theoretical limit imposed by the grating spacing and cross talk.

Key words: Phase-conjugate imaging, double-phase conjugation, photorefraction, high spatial resolution.

1. Introduction

Photorefractive ferroelectric crystals have been the subject of numerous recent investigations owing to the particular ability of these materials to display high optical nonlinearities with only milliwatt-level input powers. In particular, a significant volume of research in recent years has centered on the development of techniques for optical communications, neural networks, real-time holography, optical correlation, and image processing.[1] For many of these applications the essential feature is the ability to generate a phase-conjugate replica of an input beam. A number of effective methods have been developed to produce phase-conjugate waves through the use of photorefractive crystals. These methods include four-wave mixing, self-pumped phase conjugation, and mutually pumped phase conjugation. Mutually pumped phase conjugators (MPPC's) are based on the simultaneous introduction of two mutually incoherent laser beams into a photorefractive crystal, resulting in the formation of two phase-conjugate wave fronts (double-phase conjugation).[2,3] These devices are unique to photorefraction and have been demonstrated in a variety of geometries.[4]

MPPC's are formed when two mutually incoherent laser beams are coupled in one or more shared-volume holograms within the crystal. When the beams are initially introduced into the crystal they simply undergo refraction as they pass through the crystal. As a result of the photorefractive effect, however, each refracted beam interferes with its own weakly scattered light and writes a set of beam-fanning gratings. The two beam fans bend toward one another, resembling a bridge, and share a common set of fan gratings.[3] This process is self-aligning and provides automatic Bragg matching between the two mutually incoherent beams. In the steady state this device exhibits stable phase-conjugate output signals after some characteristic buildup time. The buildup time and the phase-conjugate reflectivities depend on the particular crystal being used and also on several other factors associated with the geometry and pumping conditions, such as beam intensities, angles of incidence, the relative coherence of the pumping beams, and the spot size of the pumping beams. To date, the spatial resolution of images conjugated in MPPC's has been disappointing. In most cases the reported spatial resolution is only ~6 to 10 lines/mm.[2,4-8]

Only recently has attention been given to the fidelity and the resolution of phase-conjugate images obtained with MPPC's.[9-11] Segev *et al.*[9] indicate that high phase-conjugation fidelity can be obtained

J. M. Yarrison-Rice is with the Department of Physics, Miami University, Oxford, Ohio 45056; E. J. Sharp and G. L. Wood are with the U.S. Army Research Laboratory, Ft. Belvoir, Virginia 22060; G. J. Salamo is with the Department of Physics, University of Arkansas, Fayettville, Arkansas 72701; R. Klank is with the Department of Physics, University of Connecticut, Storrs, Connecticut 06286; and R. R. Neurgaonkar is with the Rockwell International Service Center, Thousand Oaks, California 91360.

Received 29 November 1994; revised manuscript received 20 July 1995.

0003-6935/95/327597-07$06.00/0.

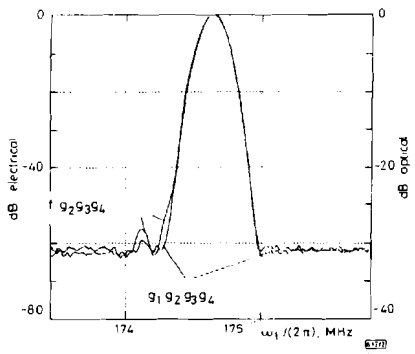

Fig. 2 *Measured functions fg_3g_4 and $g_1g_2g_3g_4$ in four-stage polarimeter*

The functions fg_3g_4 and $g_1g_2g_3g_4$ were measured in a spectrum analyser at detection frequencies $3\omega_1 + 4\omega_2$ and $4\omega_1 + 4\omega_2$, respectively, while ω_1 and ω_2 were tuned proportionally (Fig. 2). The centre frequencies were $\omega_1 = 2\pi \times 174.635$MHz, and $\omega_2 = 2\pi \times 174.985$MHz. The 3dB bandwidth was 0.22MHz, equivalent to a 2nm optical bandwidth. Sidelobes were suppressed by >28dB, which seems to confirm the theoretical value of 28dB. However, electrical powers were chosen relatively low ($P_{1,2}$ = 13.2dBm, $P_{3,4}$ = 16dBm), and due to the reduced mode conversion, a higher sidelobe suppression of roughly 35dB would have been expected. We believe the main source of limited experimental sidelobe attenuation was waveguide birefringence nonuniformity which can be minimised if a longitudinally variable chip temperature profile is applied. The noise floor level at -31dB optical was determined by a low detected optical power of -7dBm, incomplete mode conversion, a noisy electrical amplifier (not shown in Fig. 1) and resolution bandwidths of 100Hz (fg_3g_4) and 10Hz ($g_1g_2g_3g_4$).

Also, in a two-stage polarimeter setup with unused stages 3 and 4, sidelobe suppressions of >12 and >16dB for fg_3 and g_1g_2 were measured at the detection frequencies $3\omega_1$ and $4\omega_1$, respectively. In our single-stage polarimeter [6] experimental sidelobe attenuations of 5.6, 5.4, and 12.3dB were obtained for f, q, and g_1, respectively. These results demonstrate the validity of the multistage concept.

Conclusion: A multistage, instead of a single-stage, spectral polarimeter based on acousto-optical TE-TM converters has increased stopband attenuation. A stopband attenuation of >28dB has been achieved in a four-stage spectral polarimeter experiment. The pigtailed chip has a 2.4dB fibre-to-fibre loss and a 57dB return loss.

Acknowledgments: We are grateful to C. Harizi, R. Ricken, S. Westenhöfer, and W. Sohler for device fabrication and pigtailing know-how, and to G. Mrozynski for the loan of the DFB laser.

17 March 1995
Electronics Letters Online No: 19950545

R. Noé, M. Rehage and F. Tian (*University of Paderborn, Warburger Str. 100, D-33098 Paderborn, Germany*)

References

1 HAUGE, P.S.: 'Survey of methods for the complete determination of a state of polarisation', *Proc. SPIE*, 1976, **88**, pp. 3–10
2 POOLE, C.D.: 'Polarisation fluctuations in a 147km undersea lightwave cable during installation', *Electron. Lett.*, 1987, **23**, pp. 1113–1115
3 NAMIHIRA, Y.: 'Polarisation fluctuations of optical fibre submarine cable in 6000m deep sea trial', *Electron. Lett.*, 1988, **24**, pp. 582–583
4 FRANGEN, J.: 'Integrated optical, aeoustically tunable wavelength filter', *Electron. Lett.*, 1989, **25**, pp. 1583–1584
5 HERRMANN, H., SMITH, D.A., and SOHLER, W.: 'Integrated optical, acoustically tunable wavelength filters and switches and their network applications'. Proc. ECIO 1993, Neuchâtel, Switzerland, 1993, pp. 10.1–10.3
6 REHAGE, M., and NOÉ, R.: 'Wavelength-selective optical polarisation analyser with Ti:$LiNbO_3$ acoustically tunable integrated TE-TM converter', *Electron. Lett.*, 1994, **30**, (14), pp. 1130–1131
7 NOE, R.: 'Depolariser based on acousto-optical TE-TM converters for suppression of polarisation hole burning in long haul EDFA links', *Electron. Lett.*, 1994, **30**, (18), pp. 1500–1501

Observation of two-dimensional steady-state photorefractive screening solitons

M.-F. Shih, M. Segev, G.C. Valley, G. Salamo, B. Crosignani and P. Di Porto

Indexing terms: Photorefractive materials, Solitons

The first observation of two-dimensional steady-state photorefractive solitons is reported. Application of an electric field of 5.8kV/cm to strontium barium niobate yields solitons with diameters as small as 9.6μm at microwatt power levels.

Recent work on spatial solitons in photorefractive media has shown theoretically, and demonstrated experimentally that the application of a suitable external field to these materials enables long-lived, but transient, solitons [1 – 9]. A related study has shown that photovoltaic materials (such as $LiNbO_3$) support bright and dark steady-state planar solitons [10, 11]. In a recent paper [12], we have shown theoretically that the application of an external electric field also enables steady-state solitons in photorefractive materials. These solitons result from optical excitation of carriers, their migration in the presence of the external field and finally their trapping that results in nonuniform screening of the electric field. Thus, the magnitude of the electric field is lowered in regions of higher optical intensity, and this modifies the refractive index via the Pockel effect and traps the beam (or the dark notch in the beam, depending on the sign of the index perturbation). The resulting refractive index perturbation is proportional to the inverse of the sum of the light intensity and the dark irradiance. We named these steady-state solitons 'screening solitons' and pointed out that they differ from those studied previously in their physical origin, properties and dependence on the light intensity [12]. We also note that a recent observation of steady-state one-dimensional self-focusing effects in BTO [13] may eventually lead to observing screening solitons in that crystal.

We report the first observation of steady-state screening solitons. We observe solitons in strontium barium niobate (SBN:60) that are as narrow as 9.6μm (full width half maximum (FWHM)) in both the horizontal and the vertical directions.

In one transverse dimension, our calculations [12] show that the narrowest screening solitons should be obtained for peak intensities roughly three times larger than the dark irradiance. However, since the dark irradiance is very small in all dielectric photorefractive media (of the order of μW/cm²), this limits the applicable observation range to three alternatives. The first is operation at ultralow powers. This is not physically feasible since the soliton formation time is of the order of the dielectric relaxation time, which in turn is inversely proportional to the soliton intensity. The soliton formation time would be of the order of hours or more, and small vibrations would eliminate any observation. The second alternative corresponds to operating at very large voltages and keeping the soliton intensity within a reasonable range. In this case, however, an ~1μW soliton is at least 10^6 times more intense than the dark irradiance, which implies a required trapping voltage of more than 10^6V, to be applied across 5mm electrodes; also physically infeasible. The third choice is to generate 'artificial' dark irradiance, using uniform background illumination, and controlling its magnitude relative to the soliton peak intensity. We have used this alternative and generated the background irradiance with a laser beam polarised orthogonal to the soliton beam, so that they could be easily separated.

The experimental setup is similar to that in [3 – 6]. We generate the screening solitons in 5.5mm long strontium barium niobate (SBN:60) by launching an extraordinarily polarised TEM_{00} beam

Optically induced quasi-phase matching in strontium barium niobate

Anthony S. Kewitsch[a)]
Department of Applied Physics, Caltech, Pasadena, California 91125

Terrence W. Towe and Gregory J. Salamo
Department of Physics, University of Arkansas, Fayetteville, Arkansas 72701

Amnon Yariv and Min Zhang
Department of Applied Physics, Caltech, Pasadena, California 91125

Mordechai Segev
Department of Electrical Engineering, Princeton University, Princeton, New Jersey 08544

Edward J. Sharp
Army Research Laboratory, Fort Belvoir, Virginia 22060

Ratnakar R. Neurgaonkar
Rockwell International Science Center, Thousand Oaks, California 91360

(Received 8 November 1994; accepted for publication 13 February 1995)

We observe dynamic ferroelectric domain gratings in strontium barium niobate (SBN) induced by photorefractive space charge fields. The optically induced modulation of the spontaneous polarization attains a maximum of 1%. Quasi-phase matched second harmonic enhancements are observed above the ferroelectric-paraelectric phase transition due to the glassy ferroelectric nature of SBN. We find that the second harmonic power is significantly enhanced by recording gratings in optically fatigued rather than electrically poled crystals. © *1995 American Institute of Physics.*

We have recently demonstrated that ferroelectric domains align with the local photorefractive space charge fields in $Sr_xBa_{1-x}Nb_2O_6$(SBN:x).[1,2] The resulting dynamic domain gratings respond nearly instantaneously to changes in the photogenerated space charge field and modulate the ferroelectric polarization. We used these gratings to perform tunable quasi-phase matched second harmonic generation (QPM-SHG) with spectral widths of the QPM enhancement as narrow as 0.175 nm, across the fundamental tuning range of 880–990 nm. In this letter we apply this technique to SBN:61 and explore the temperature dependence of the phenomenon. We demonstrate that space charge field induced QPM-SHG can be achieved even in the paraelectric phase. In addition, we observe that an optically fatigued crystal displays significantly stronger QPM-SHG than an electrically poled crystal. We also find that a strong broad-band second harmonic enhancement occurs automatically in optically depoled crystals.[3,4] In fact, this broad-band enhancement can attain values several orders of magnitude larger than the QPM enhancement. We propose an explanation of this latter result based on charge compensation and fringe stability requirements.

The experimental setup for writing dynamic domain gratings and simultaneously generating the second harmonic is identical to that reported in Ref. 2. A tunable, mode-locked Ti-sapphire laser is frequency doubled within the 45° cut, Ce-doped SBN:61 crystal (4.5×4.5×5.5 mm). This crystal exhibits a ferroelectric-paraelectric phase transition at 75 °C. The fundamental infrared beam is focused to a 60 μm beam diameter, producing a peak fundamental intensity of 17 MW cm^{-2} at the beam waist. A 2–6.6 W argon-ion laser at 514.5 nm records a domain grating throughout the entire crystal volume. To maintain the poled state at elevated temperatures, a poling field of 8000 V cm^{-1} is applied between optical exposures (Fig. 1).

The angular spectrum of the second harmonic wave reveals the spatial modulation of the spontaneous polarization and nonlinear optical susceptibility.[5–7] Upon recording a domain grating in an initially poled crystal, we observe a collimated QPM second harmonic beam [Fig. 1(a)], in addition to a non-phase matched streak. This streak exits the crystal at an angular displacement of approximately 10° below the QPM spot. The origin of this angular walk-off between the two distinct second harmonic beams is the 45° inclination of the c axis relative to horizontal [Fig. 1(b)]. The broad extent of the streak along the x direction and the narrow extent in the y direction indicates that domains are extremely narrow in diameter, while being elongated along the c axis. Typical dimensions of microdomains are tens of nanometers in diameter and hundreds of nanometers in length. Figure 1(b) depicts the resulting range of grating vectors generated by the randomly distributed microdomains, representing a multiplicity of grating vectors with different magnitudes directed nearly normal to the c axis and all sharing a common origin. The momentum conservation relation for the interaction is $2\mathbf{k}^{\omega}+\mathbf{k}_g=\mathbf{k}^{2\omega}$, where $\mathbf{k}^{\omega}$ is the fundamental wave vector and $\mathbf{k}^{2\omega}$ is the second harmonic wave vector. The second harmonic far field profile will be directed to a spot (upon interacting with grating periodicity $\mathbf{k}_g$) and a streak (upon interacting with the ensemble of grating periodicities $\mathbf{k}_{random}$). For a random distribution of microdomains of diameter 10 nm, the distribution of $\mathbf{k}_{random}$ is also random up to grating vectors as large as 6×10^8 m^{-1}.

The total second harmonic power in the streak can attain

a)Electronic mail: kewitsch@cco.caltech.edu

SINGLE-BEAM ADAPTIVE HOLOGRAPHIC INTERFEROMETRY-AHI AND SMALL SIZE DEVICES FOR INDUSTRIAL INSPECTION

G.Dovgalenko, Y.Onistchenko, I.Loutchkina, G.Salamo

Optic Laboratory,105 Physic Bld,University of Arkansas, Fayetteville, AR,72701,USA

ABSTRACT

We propose a new technique of AHI which combines the high speed operation advantages of dynamic holographic interferometry and a real-time, high resolution, high stability, Denisyuk's holograms [1]. Based on a new high sensitive phototerfractive reversible crystals group 23 doped (P and Cu) a small power CW laser was used for continuously hologram read and read-out processing. Portable wariant of a small size AHI sensor and practical demonstration of this technique are described.

1.INTRODUCTION

For many years Holographic Interferometry -HI was used in many different fields (flow visualization, plasmas diagnostics, non-destructive testing of materials and structures, vibration analysis, medical applications, to visualize physical phenomena and to give qualitative and quantitative explanations [2].

In most cases, experimentally were achieved in laboratory environment Unfortunately no commercially available holographic systems compact and reliable with fast image processing were created [2].

An objective of this work is creating more commercial holographic system compact and reliable with a fast image processing.

The new branch of AHI based on using of the reversible holographic materials was created in a last decade [3]. Unfortunately a large time consuming, a high power laser radiation, and weak reversibility of these materials have been restricting a usage for commercial applications. In [1] was demonstrated AHI for testing a fast moving biological object under water (living fish) using a small power (4 mW) He-Ne laser. The BTO crystal in this experiment generated 10 holograms per second in continuous hologram registration regime.

We propose a new type of BTO crystals doped P and Cu as a media for continuous hologram registration which used a high resolution reflected Denisyuk's holograms. These crystals combine a high speed hologram formation (0.01sec.) and a good hologram conservation (some days) with a high reversibility (more than 10^6 cycles) and high resolution (3000 lines/mm).

0-8194-1684-3/95/$6.00

Portable holographic interferometric device for aircraft inspecting

George Dovgalenko
The University of Arkansas, Department of Physics, Fayetteville, AR 72701
Yuri Onischenko, Irina Loutchkina
"Geluon" laboratory, P.O. Box 15, Kiev, 252141, Ukraine
Gregory Salamo
The University of Arkansas, Department of Physics, Fayetteville, AR 72701

ABSTRACT

A new single-beam technique for a continuous reconstruction of volume holograms in photorefractive crystals of symmetry 23 is presented. The doped crystal $Bi_{12}TiO_{20}$ (Fe, P) possessing diffraction efficiency above 70 % is used for real-time holographic interferometry. The major advantage of this technique is an automatic self-adjustment of diffraction in volume holograms, continuous reconstruction of volume holograms, high diffraction efficiency without application of external electric field, high resolution (more than 3000 lines/mm), high vibroprotection stability, low cost using of He-Ne or diode lasers, portability (single-beam device). A 1 mm crack was detected at a depth 1.5 mm in airplane wings near a rivet zone using portable adaptive holographic interferometer - AHI.

Keywords: adaptive holographic interferometer, photorefractive crystals, portability, detecting cracks, aircraft wings.

1. INTRODUCTION

Inspecting and maintaining a fleet of aircraft that may include planes 20 year or older is a crucial responsibility for every airline. Electrical eddy current inspection is standard inspection technique for detecting cracks around aircraft fuselage rivets, which secure the lap joints in an airplane's exterior aluminum surface, or skin. These lap joints are vulnerable to corrosion and fatigue, and cracks near the rivets may indicate the beginning of structural failure. Unfortunately only 53 percent of inspectors achieved detection rates exceeding 95 percent for cracks at one-tenth of an inch because collected data depend on contact measurements, time on task, surface conditions (painted or unpainted), inspector tedium, and boredom [1].

For many years Holographic Interferometry was used in many different fields (flow visualization, plasma diagnostics, non-destructive testing of materials and structures, vibration analysis, medical applications, to visualize physical phenomena and to give qualitative and quantitative explanations. In most cases, results were achieved in a laboratory environment. Unfortunately no commercially available holographic systems

0-8194-1904-4/95/$6.00

IEEE International Symposium on Applications of Ferroelectrics, p 633-635, 1994

The Use of Applied Electric Fields on the Photorefractive Tungsten Bronze Ferroelectrics

Nianyu Bei[1], Galen C. Duree[1], and Gregory J. Salamo[1], Rakesh Kapoor[2], Edward J. Sharp[3], and Ratnaker R. Neurgaonkar[4]

[1]Physics Department of the University of Arkansas, Fayetteville, Arkansas 72701
[2]Physics Department of Alabama A&M, Normal, Alabama 35762
[3]Army Research Laboratory, Fort Belvoir, Virginia 20060
[4]Rockwell International Science Center, Thousand Oaks, California 91360

Abstract--The traditional method of determining the photorefractive effective charge density is to plot the photorefractive space charge field versus the crossing angle in a two-beam coupling experiment. The difficulty with this traditional measurement technique is that the apparatus must be moved several times in order to obtain data over the sufficient number of crossing angles needed for an accurate fit with theory. Moreover, with small crossing angles the overlap between the two crossing beams can easily extend over the entire crystal, while with larger crossing angles the overlap between the two beams becomes less certain.

In this paper we demonstrate an alternative method of determining the photorefractive charge density. In this approach we measure the phase shiift between the optical intensity pattern in the crystal and the resulting index pattern, as a function of the magnitude of an applied d.c. field. By comparing the measured value of the d.c. field which produces a minimum phase shift with that predicted by theory the photorefractive effective charge density is found. In this case, only the magnitude of the applied field is varied and the apparatus remains fixed. The result is obtained quickly and with little error.

INTRODUCTION

In this paper we discuss a technique to measure the trap density in photorefractive crystals. The technique is based on the use of interfering two laser beams in a crystal in the presence of an applied electric field. In the crystal the two light waves can be expressed as

$$E_T(x,z) = E_{T0}\exp[i(k_x x + k_z z)] \quad (1)$$

$$E_D(x,z) = E_{D0}\exp[i(-k_x x + k_z z)] \quad (2)$$

where k_x and k_z are components of the wavevector. The two light beams cross at an angle 2θ in the crystal with each beam making an angle θ with the normal to the incident surface. If ϕ is the phase shift between the grating and the interference pattern, the intensities of the output beams from the crystal can be written [Ref. 1] as

$$I_T(d) = I_T\cos^2(\kappa d) + I_D\sin^2(\kappa d) - (I_T I_D)^{1/2}\sin(2\kappa d)\sin\varphi \quad (3)$$

$$I_D(d) = I_D\cos^2(\kappa d) + I_T\sin^2(\kappa d) + (I_T I_D)^{1/2}\sin(2\kappa d)\sin\varphi \quad (4)$$

where I_T and I_D are the incident intensities and $I_T(d)$ and $I_D(d)$ are their intensities after passing through a crystal of thickness d with a coupling coefficient κ. In expressions (3) and (4), the first term corresponds to the transmitted component, the second term is the diffracted component, and the third term is the energy-exchange component between the two beams. From expressions (3) and (4) we can write the diffraction efficiency η as

$$\eta = \sin^2(\kappa d) \quad (5)$$

If the intensity of both beams is adjusted to be equal at the entrance of the crystal we can write the energy exchange efficiency in terms of the diffraction efficiency as

$$\varepsilon = 2[\eta(1-\eta)]^{1/2}\sin\varphi \quad (6)$$

Therefore, expression (6) yields an expression for the phase shift between the intensity pattern and the index grating and is given by

$$\sin\varphi = \varepsilon/[2[\eta(1-\eta)]^{1/2}] \quad (7)$$

$$\sin\varphi = I_\varepsilon/[2[I_d(I_0 - I_d)]^{1/2}] \quad (8)$$

where I_ε, I_d and I_0 are the magnitude of the energy exchange, the diffraction signal and the intensity of the transmitted beam. From these expressions we can see that by measuring I_d, I_ε, and I_0, ϕ can be determined [Ref 2,3,4].

EXPERIMENTAL TECHNIQUE

The apparatus which we used to measure ϕ as a function of applied d.c. electric field consisted of a HeNe laser oscillating at 6328A with an output power of 5mw. We used ordinary polarized beams in order to minimize beam fanning and the corresponding intensity fluctuations which appear in energy exchange signals. After the polarizer, the laser beam was split into two beams I_D and I_T which intersected inside a thin sample of SBN 60 with 0.015% Cesium as a dopant (static dielectric constant $\epsilon' = 950$) such that the grating vector is parallel to the c-axis. The beam splitter is 50% /50% to make the beam I_D have the same intensity as I_T. The angle 2θ

CH3416-5 0-7803-1847-1/95/$4.00©1995IEEE

Cooperative photorefractive beam fanning in $BaSrKNaNb_5O_{15}$

Steven R. Montgomery and Michael P. Gallagher

Department of Physics, U.S. Naval Academy, Annapolis, Maryland 21402

Gregory J. Salamo

Department of Physics, University of Arkansas, Fayetteville, Arkansas 72701

Edward J. Sharp and Gary L. Wood

U.S. Army Research Laboratory, Fort Belvoir, Virginia 22060-5028

Ratnakar R. Neurgaonkar

Rockwell International Science Center, Thousand Oaks, California 91360

Received October 22, 1993

A multiline laser beam incident upon a $BaSrKNaNb_5O_{15}$ crystal causes rings to form in the beam fan by means of cooperative photorefractive fanning between the different wavelengths. We examine the novel case in which the input beam consists of two lines from an argon-ion laser with independently controlled linear polarizations as well as the single-line case with equal amounts of ordinary and extraordinary light. We compute the expected rings in each case, taking full account of the crystal birefringence, and compare them with the experimental data. Applications of the rings to crystallography and cryptology are presented.

INTRODUCTION

Several studies have shown that beam fanning[1] can cause cones of light to emerge from a photorefractive crystal, displaying rings when the cones are projected onto a viewing screen.[2–7] A single extraordinary polarized input beam has been shown to result in an ordinary ring[2] in barium titanate, whereas other studies have used crossed-beam arrangements[3,4] in which the crossing beams have had different polarizations[5] or wavelengths.[6] Earlier reports[7,8] showed that linearly polarized input consisting of several lines from an argon-ion laser produces a multicolored ring or a rainbow pattern with the same polarization as the input light. For the study reported here the photorefractive rings in the beam fan of a cerium-doped $BaSrKNaNb_5O_{15}$ (BSKNN) crystal[9] are examined when the input beam is composed of two lines that have orthogonal or parallel polarizations. We also examine the case in which the input beam consists of a single linearly polarized laser line with the polarization rotated so that there are equal amounts of ordinary and extraordinary polarization incident upon the crystal. In each of these cases the input beam can be imagined to be composed of light in two different states, with each state of the light being determined by its wavelengths and polarization. The resulting rings are shown to depend on cooperative scattering by phase-matched gratings from each state. A geometrical argument for predicting the rings is developed and is the basis for a computer program that plots the appearance of the rings. Finally, the predictions are compared with the experiment.

THEORY

The beam fan for a single beam entering a photorefractive crystal is formed by the energy exchange between the incident beam and the light scattered by imperfections and impurities in the crystal.[1] Corresponding to each fan wave vector there is written in the crystal a photorefractive grating that satisfies the vector relation

$$\mathbf{k}^g = \mathbf{k}^f - \mathbf{k}^i, \tag{1}$$

where $\mathbf{k}^g$, $\mathbf{k}^f$, and $\mathbf{k}^i$ represent wave vectors for the grating, the fanned light, and the incident light, respectively. As shown in Fig. 1, the fan wave vectors and the incident wave vector must terminate on the k-space index surface. Although the set of extraordinary grating vectors is not the same as the set of ordinary grating vectors because the ordinary and the extraordinary surfaces have different shapes (see Fig. 1), there can be a subset of gratings that is common to each, which we determine with a process first presented in Ref. 2 to explain the appearance of an anisotropically scattered ordinary ring that appears when extraordinary light is incident upon a barium titanate crystal.

Initially, for simplicity, consider the case of a linearly polarized input beam from a single laser line that is incident upon the a face of the crystal. If the beam is polarized so that components of ordinary and extraordinary light are present, then a beam fan will be formed for each component. If there are members of the ensemble of extraordinary gratings that scatter ordinary light, then

0740-3224/94/091694-06$06.00

Stability of photorefractive spatial solitons

Mordechai Segev,* Bruno Crosignani,† Paolo Di Porto,† and Amnon Yariv

California Institute of Technology, 128-95, Pasadena, California 91125

Galen Duree, Gregory Salamo, and Edward Sharp‡

Department of Physics, University of Arkansas, Fayetteville, Arkansas 72701

Received February 10, 1994

We present a theoretical analysis of the stability of photorefractive spatial solitons along with experimental results that show that the solitons are stable for small-scale perturbations but break down when the perturbations exhibit a transverse scale comparable with the soliton size (cross section).

Self-trapping of optical beams in photorefractive (PR) media occurs when diffraction is exactly balanced by self-scattering of the spatial components of the soliton beam.[1,2] Our recent observation of the first PR spatial solitons[3,4] revealed, among a variety of other properties (such as independence of the absolute light intensity and self-trapping in both transverse dimensions), that the PR soliton is stable and may be observed despite index inhomogeneities that are always present in PR materials. Furthermore, we observed that the PR soliton is capable of evolving from an arbitrary input waveform (Fig. 4 of Ref. 3).

In this Letter we provide a theoretical stability analysis and show experimental results that illustrate that the soliton is indeed stable under small-scale perturbations but breaks down when the index perturbations are of a transverse scale comparable with the soliton size. The evolution property of the PR solitons may be viewed as another manifestation of their stability, but, since the evolution stage encompasses other properties (such as modulation instability), we here study stability alone.

We recall the basics of our model[1,2] and point out that our analysis is restricted to two (transverse x and longitudinal z) dimensions and cannot explain trapping in two transverse dimensions. Elsewhere[5] we showed experimentally that the self-trapping effects in the direction parallel to the external electric field (x direction) exist regardless of the size of the beam in the other transverse dimension (y). Self-trapping in the y direction (perpendicular to the field), however, is generated by tilted gratings and fully depends on the finite extent of the beam in x. In this spirit, we demonstrated in Ref. 5 that sheet solitons (of a single transverse dimension) exist for trapping along x but not along y and concluded that trapping in x is independent of trapping in y but not vice versa. A full theoretical model for trapping in both transverse dimensions is under investigation. We therefore restrict our stability analysis to perturbations in this single transverse direction. Fortunately, in most ferroelectric PR crystals inhomogeneities consist primarily of index variations parallel to the crystalline c axis, which is also the growth direction and our transverse axis x. This permits experimental study of the soliton stability to perturbations in one transverse dimension.

We start by recalling the paraxial nonlinear wave equation

$$\left(\frac{\partial}{\partial z} - \frac{i}{2k}\frac{\partial^2}{\partial x^2}\right)A(x, z) = \frac{ik}{n_1}\delta n(x, z)A(x, z), \quad (1)$$

where A is the slowly varying complex amplitude of the beam, $k = \omega n_1/c$ is the wave number, and n_1 is the unperturbed index of refraction of the medium. The nonlinear term $\delta n(x, z)$ is obtained by consideration of the mixing process between each pair of plane-wave components:

$$\delta n(x, z) = \frac{1}{|A(x, z)|^2} \times \iint A(x - \rho, z)A^*(x + \rho', z)g(\rho, \rho')\mathrm{d}\rho\mathrm{d}\rho', \quad (2)$$

where

$$g(\rho, \rho') = \iint \widehat{\delta n}(q_1, q_2)\exp[i(q_1\rho + q_2\rho')]\mathrm{d}q_1\mathrm{d}q_2 \quad (3)$$

is the two-dimensional Fourier transform of the coupling coefficient $\widehat{\delta n}(q_1, q_2)$ (which, if multiplied by $-2\pi i/\lambda$, is identical to γ, the commonly used expression for the PR coupling coefficient) and q_1 and q_2 are the projections of the wave vectors of the plane-wave components in the transverse (x) direction ($0 \le |q| \le k$). The requirement for a spatial soliton,

$$A(x, z) = U(x)\exp(i\gamma z), \quad (4)$$

leads to

$$\gamma - a\frac{U''}{U} + b\left(\frac{U'}{U}\right)^2 = 0, \quad (5)$$

where $a = (1/2k) + (k/n_1)I_{20}$ and $b = (k/n_1)I_{11}$, with I_{11} and I_{20} being the real parts of the coefficients of the Taylor expansion of $\widehat{\delta n}(q_1, q_2)$, as explained in Ref. 2.

0146-9592/94/171296-03$6.00/0

Ferroelectric Domain Gratings in Strontium Barium Niobate Induced by Photorefractive Space Charge Fields

Anthony S. Kewitsch,[1] Mordechai Segev,[1,*] Amnon Yariv,[1] Gregory J. Salamo,[2] Terrence W. Towe,[2] Edward J. Sharp,[3] and Ratnakar R. Neurgaonkar[4]

[1]*Department of Applied Physics, Caltech, Pasadena, California 91125*
[2]*Department of Physics, University of Arkansas, Fayetteville, Arkansas 72701*
[3]*Army Research Laboratory, Fort Belvoir, Virginia 22060*
[4]*Rockwell International Science Center, Thousand Oaks, California 91360*

(Received February 1994)

We demonstrate that illuminating a photoconducting strontium barium niobate crystal with a low intensity optical standing wave generates space charge fields which induce ferroelectric domain gratings. We study the formation and decay kinetics of these domain gratings using a short exposure technique and present a thermodynamic model of the fixing mechanism.

PACS numbers: 77.84.Dy

Ferroelectric domain gratings in strontium barium niobate (SBN) are typically generated by applying external depoling electric fields [1,2] under illumination, in geometries where photoinduced space charge fields do not invert domains. However, light interference patterns photoexcite mobile charge and generate spatially modulated space charge fields with periods of typically 0.1 to 100 μm in photorefractive crystals. A fundamental question is whether these periodic space charge fields alone can spatially modulate the ferroelectric polarization in materials which possess a coercive field of the order of the space charge field, an effect not previously reported in the literature. In this Letter we present experimental evidence demonstrating that this is indeed the case in $Sr_{0.75}Ba_{0.25}Nb_2O_6$ (SBN:75). Light induced space charge fields dynamically modify the positions of ions within the unit cell. We report on observations of dynamic domain gratings which adiabatically follow the space charge field in time, in addition to permanent domain gratings, which persist long after the space charge fields are depleted. We propose a thermodynamic model of the fixing mechanism based on the glassy ferroelectric properties of SBN. This technique holds great promise in a broad range of applications in optics and acoustics, and we demonstrate its application to second harmonic generation and holographic storage.

We use two techniques to study the optically induced modulation of the ferroelectric polarization: the second harmonic enhancement produced by a quasi-phase matched domain grating [3] and optical diffraction from the domain hologram. Using the first technique, we measure the temporal evolution in second harmonic power generated within the crystal while recording and erasing the domain grating. The experimental setup is illustrated in Fig. 1. We record a domain grating with a period equal to twice the coherence length, defined as $l_c = \lambda/4(n^{2\omega} - n^{\omega})$, appropriate for quasi-phase matching between a colinear fundamental and second harmonic beam. λ is the wavelength (in vacuum) of the fundamental beam, n^{ω} the index of refraction at the fundamental wavelength and $n^{2\omega}$ the index at the second harmonic. The technique to compensate for the phase mismatch between the fundamental and second harmonic beams by using periodically poled crystals is an example of quasi-phase matching (QPM). By monitoring the peak second harmonic power at the center wavelength of the QPM peak, we determine the evolution of the polarization grating in time. The fundamental beam is generated by a tunable, mode-locked Ti-sapphire laser and propagates at 45° to the c axis. An argon-ion laser (488 or 515 nm) writes a domain grating oriented at 45° to the c axis.

Figure 2 illustrates the buildup and decay of the second harmonic power, which is proportional to the square of the Fourier component of the polarization modulation at the period $2\,l_c$. The time to enhance the second harmonic by writing a phase matched polarization grating is typical of the buildup time of the electro-optic or photorefractive grating under the influence of a spatially periodic space charge field (~1 sec at 1 W cm^{-2}). Since the nonlinear optical polarizability responsible for second harmonic generation and the linear electro-optic effect arises primarily from the distortion of the covalent

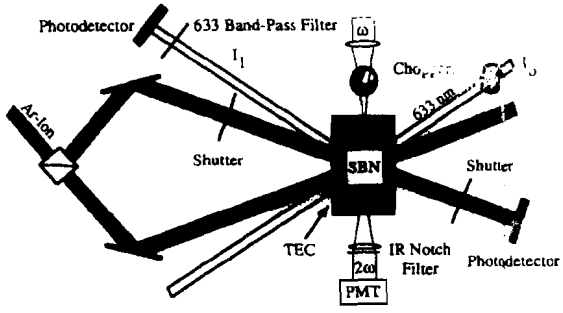

FIG. 1. The experimental setup for recording a polarization grating and monitoring its strength by Bragg diffraction and quasi-phase matched second harmonic generation.

0031-9007/94/73(8)/1174(4)$06.00

Tunable quasi-phase matching using *dynamic* ferroelectric domain gratings induced by photorefractive space-charge fields

Anthony S. Kewitsch, Mordechai Segev, and Amnon Yariv
Department of Applied Physics, California Institute of Technology, Pasadena, California 91125

Gregory J. Salamo and Terrence W. Towe
Department of Physics, University of Arkansas, Fayetteville, Arkansas 72701

Edward J. Sharp
Army Research Laboratory, Fort Belvoir, Virginia 22060

Ratnakar R. Neurgaonkar
Rockwell International Science Center, Thousand Oaks, California 91360

(Received 13 January 1994; accepted for publication 5 April 1994)

We demonstrate a method of dynamic, tunable quasi-phase matched second-harmonic generation using optically induced polarization gratings with periods equal to twice the coherence length. These gratings increase the peak second-harmonic conversion efficiency by a factor of 17 above a poled strontium barium niobate crystal, to 0.01% for fundamental beam intensities of 0.8 MW cm^{-2}. We generate quasi-phase matching spectral response peaks as narrow as 0.175 nm and tailor the response by writing an ensemble of gratings in the same volume, each of which enhances the second-harmonic generation at a predetermined wavelength.

Quasi-phase matching (QPM)[1,2] is a technique to periodically compensate for the phase mismatch between the fundamental and second-harmonic beams. This technique relaxes the stringent phase matching requirements based on birefringence[3] or modal dispersion in waveguides.[4] QPM can be achieved by periodically poling a ferroelectric crystal so that the relevant nonlinear coefficients for second-harmonic generation (SHG) are spatially modulated with a period equal to twice the coherence length. For colinear beams, the coherence length is $l_c=\lambda/4\ (n^{2\omega}-n^{\omega})$, where λ is the wavelength in vacuum of the fundamental beam, n^{ω} is the index of refraction at the fundamental wavelength, and $n^{2\omega}$ is the index at the second harmonic. In the absence of periodic domain inversion, the coherence length is the maximum effective crystal length that is useful in generating the second-harmonic power. Coherence lengths exceeding a few mm are needed in practice for efficient conversion. In ferroelectric crystals such as $LiNbO_3$ and $Sr_{0.75}Ba_{0.25}Nb_2O_6$ (SBN:75), the coherence length is on the order of a few microns for SHG in the visible; consequently, the non-phase matched conversion is negligibly small despite the relatively large nonlinear coefficients. For these and many other highly nonlinear materials, QPM is a means of increasing the effective interaction length.

QPM by periodic poling has been demonstrated during growth,[5] by indiffusion,[6,7] by applying external electric fields,[8,9] electron beams,[10] or SiO_2 masks.[11] Typically, only a very narrow frequency band is converted efficiently and it is difficult or impossible to tune the center frequency dynamically, except over a small range using temperature or angle tuning. Fabrication constraints often restrict the region of polarization modulation to a thin layer on the surface or to thin waveguides rather than throughout the entire crystal volume. These periodic domain gratings are typically static and permanent.

In this letter we demonstrate tunable QPM using *dynamic* domain gratings that respond nearly instantaneously to changes in the photogenerated space-charge field. This technique uses photoinduced space-charge fields alone to modulate the ferroelectric polarization of the crystalline unit cell[12,14] rather than photoinduced screening of external electric fields.[9] We exploit the dynamic nature of these domain gratings to perform tunable QPM with spectral widths as narrow as 0.175 nm across the fundamental tuning range of 880–990 nm. This technique is of great fundamental interest because light interference patterns dynamically modify the position of ions with the crystalline unit cell and tailor the optical, electronic, and acoustic properties of the crystal.

Figure 1 illustrates the experimental setup for writing dynamic domain gratings and simultaneously generating the second harmonic. A tunable, mode-locked Ti-sapphire laser with 2 ps transform-limited pulses and 250 W peak power is frequency doubled within the SBN:75 crystal. The fundamental beam is loosely focused with a 20 cm lens to a 100 μm beam diameter at the center of the SBN crystal, produc-

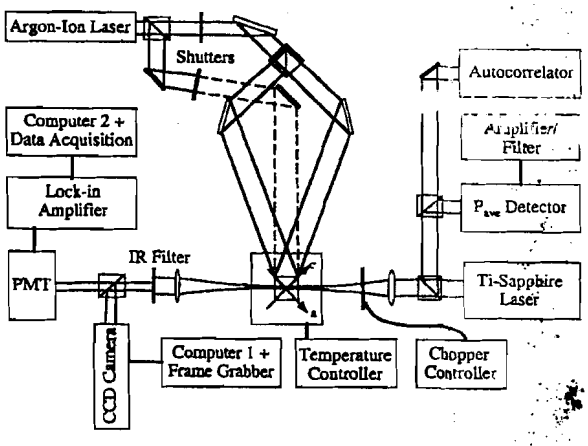

FIG. 1. Experimental setup for writing polarization gratings and generating the second harmonic.

 0003-6951/94/64(23)/3068/3/$6.00

Dimensionality and size of photorefractive spatial solitons

Galen Duree and Gregory Salamo

Department of Physics, University of Arkansas, Fayetteville, Arkansas 72701

Mordechai Segev* and Amnon Yariv

California Institute of Technology, 128-95, Pasadena, California 91125

Bruno Crosignani and Paolo Di Porto

Dipartimento di Fisica, Università dell'Aquila, L'Aquila, Italy, and Fondazione Ugo Bordoni, Roma, Italy

Edward Sharp

Army Research Laboratory, Fort Belvoir, Virginia 22060

Received March 10, 1994

We study experimentally self-trapping of optical beams in photorefractive media and show that the trapping is inherently asymmetric with respect to the two (transverse) trapping dimensions. We also present experimental results that show how the sizes of the resultant photorefractive spatial solitons are independent (within their range of existence) of the amplitude of the externally applied electric field used to generate them.

Self-trapping of optical beams in photorefractive (PR) media occurs when diffraction is exactly balanced by self-scattering (two-wave mixing) of the spatial (plane-wave) components the soliton beam.[1,2] Intuitively, since diffraction involves accumulation, by each plane-wave component of a beam, of a phase that is linear in the propagation distance, it is desirable to balance the diffraction by nonlinear phase coupling that leaves the complex amplitudes of the plane-wave components unchanged. PR materials, however, typically exhibit amplitude coupling (energy-exchange interaction) that is due to a dominant diffusion transport mechanism for the redistribution of the photogenerated charge carriers, which, inherently, cannot compensate for diffraction since it alters the amplitudes of the plane-wave components rather than balancing their phases. The presence of an external bias field, however, can cause strong phase coupling and is therefore required for the formation of PR solitons. We have predicted that PR solitons exist for a well-defined range of external fields, and, within this range, the soliton size (cross section) is independent of this external field. This property is a consequence of the optical nonlinear property of the medium: the perturbation in the refractive index is proportional to the light-induced space-charge fields, which depend primarily on the beam profile.

Our recent observation of what is to our knowledge the first PR spatial solitons[3,4] revealed, among a variety of features (such as independence of the absolute light intensity), that, unlike the Kerr-like solitons, the PR solitons may be trapped in two transverse dimensions and maintain their stability. We have also shown theoretically and experimentally[5] that the PR solitons are stable for perturbations in their waveforms that are much smaller (in size) than their transverse cross sections but break down for perturbations that are comparable with their cross sections. Our theoretical model, however, is at this point limited to a single transverse dimension and cannot fully explain the trapping in two transverse dimensions.

In this Letter we present experimental results that address the two-transverse-dimensional problem and point out where a one-dimensional analysis is valid. Furthermore, we find experimentally, in agreement with our predictions,[1,2] that the size of the PR soliton is independent (within the range of its existence) of the externally applied voltage used to generate it.

First, we address the trapping in two transverse dimensions. Assuming the anisotropy of the PR medium to be negligible, the only remaining asymmetry between the transverse dimensions can be associated with the direction of the external field. With this in mind, we recall that the influence of the external field is maximal for gratings whose **K** vectors are parallel (or antiparallel) to its direction and vanishes for gratings that are perpendicular to it. Consequently, we study the behavior of a beam that is narrow in one transverse dimension but very wide (virtually uniform) along the other direction, and we expect to observe a fundamental difference between self-trapping of beams that are uniform in the direction of the applied field and those that are uniform in the direction perpendicular to it. We perform this qualitative experiment using the setup shown in Fig. 1 of Ref. 3. As described there, the solitons are observed in a quasi-steady state, that is, after the gratings have been formed but before the external voltage has been screened. Our experimental observations indicate that the typical time for screening is roughly 2 orders of magnitude larger than the soliton formation time. By use of low in-

0146-9592/94/161195-03$6.00/0

Vector tensor algorithm for optimization of hologram images in photorefractive gyroanisotropic media

G.E. Dovgalenko, G.J. Salamo, I.I. Loutchkiha

Optics Laboratory, 105 Physics Bld., University of Arkansas, Fayetteville, Arkansas 72701, U.S.

ABSTRACT

Given is a tensor-vector generalization for anisotropic crystal of nonlinear optic interaction in arbritrary incidence of two plane waves transmitting regular nonhomogeneous nonlinear gyroanisotropic media. The solution is represented for arbitrary polarization of interacting waves, taking into account the real parameter of media: bipolar conductivity, natural and induced anisotropy by electric, optics, etc. external fields. A compact matrix-vector algorithm is demonstrated for a fast estimation 3D space evolution of the optic fields in arbitrary crystal symmetries and is usable to optimization the experimental condition and crystal parameters measurement. As example the theoretical predicted of selfdiffraction gyrotropy and energy exchange effects in crystal of 23 class at orthogonal polarization counterpropagating waves is given. The giant value of the self-diffraction effect was found experimentally and applied in continously hologram registration interferometer. The concentration of impurity centers was found 3. $8 \cdot 10^{14}$ cm $^{-3}$.

0-8194-1302-X/94/$6.00

NEW TECHNIQUES FOR MEASURING STRAIN AT FRACTURE OF THIN FILM MATERIALS

R.C. GOFORTH, B. CHANDRAN, S. NASRAZADANI, AND G.J. SALAMO
University of Arkansas, Fayetteville, AR 72701

ABSTRACT

The High Density Electronics Center (HiDEC) at the University of Arkansas is developing advanced electronic packaging methods including multi-chip modules which utilize high temperature superconductor interconnects. A wide variety of materials have been proposed and investigated for these applications. Good knowledge of the mechanical properties of the candidate thin film materials is important for reliable device design.

Two new techniques have been developed to measure strain at fracture of thin film materials. The first is an acoustic technique in which an accelerometer is attached to the film. The film is then gradually strained. When the film fractures, an acoustic wave propagates through the film thereby creating a transient signal from the accelerometer. This signal is used to trigger an oscilloscope. The second technique is similar except that it utilizes a laser probe to detect the acoustic wave. In this photo-acoustic technique, the laser is reflected from the film onto a bi-sectional photodetector while the film is gradually strained. Upon film fracture, the acoustic wave modulates the laser beam and a transient voltage pulse is produced by the photodetector. Both techniques are capable of detecting extremely small cracks.

INTRODUCTION

Thin film materials used in multi-chip modules (MCM's) are often subjected to large mechanical stresses resulting from specific deposition conditions, temperature changes during processing and in service, and from the presence of passivation coatings. A good knowledge of the mechanical properties of the thin film materials is essential for improving the reliability of multi-chip module designs.

The High Density Electronics Center (HiDEC) at the University of Arkansas is developing MCM's which utilize high temperature superconductor (HTSC) thin films for the interconnects. Ceramics such as the HTSC films are brittle materials with inherently low toughness. Since the mechanical properties of thin film superconductors — which differ from their bulk properties — are not well known, it is important that they be characterized. Furthermore, the mechanical properties are dependent on temperature. Thus, the techniques used to measure the mechanical properties of HTSC thin films should ideally be able to make accurate measurements at low temperatures (approx. 100 K). This paper describes the progress we have made in developing and verifying new techniques for the determination of the strain at fracture of thin film materials.

Two new techniques have been developed to determine the strain at fracture of thin film materials. Both techniques should be suitable for measurements from cryogenic temperatures to several hundred degrees celsius although they have not yet been demonstrated at cryogenic

Mat. Res. Soc. Symp. Proc. Vol. 323. ©1994 Materials Research Society

Photorefractive self-focusing and defocusing as an optical limiter

Galen C. Duree Jr. and Gregory J. Salamo

University of Arkansas
Physics Department
Fayetteville, Arkansas 72701

Mordechai Segev and Amnon Yariv

California Institute of Technology
Department of Applied Phyiscs
Pasadena, California 91125

Edward J. Sharp

Army Research Laboratory
Fort Belvoir, Virginia 22060

and

Ratnakar R. Neurgankar

Rockwell International Science Center
Thousand Oaks, California 91360

ABSTRACT

Focusing and defocusing of laser light has been observed for many years. Optical Kerr type materials exhibit this effect only for high intensities. We show experimental evidence that photorefractive materials can also produce dramatic focusing and defocusing. Whereas Kerr materials produce this effect for high intensities, photorefractive materials produce these effects independent of intensity indicating that this effect would be ideal for an optical limiter. We compare the characteristics of Kerr and photorefractive materials, discuss the physical models for both materials and present experimental evidence for photorefractive defocusing. Self-focusing and defocusing was observed for any incident polarization although the effect was more pronounced using extraordinary polarized light. In addition, self-focusing or defocusing could be observed depending on the direction of the applied electric field. When the applied field was in the same direction as the crystal spontaneous polarization, focusing was observed. When the applied field was opposite the material spontaneous polarization, the incident laser light was dramatically defocused.

0-8194-1533-2/94/$6.00

Appl. Phys. A 56, 303–305 (1993)

Applied Physics A Solids and Surfaces

Manifestation of Circular Photogalvanic Current by Dynamic Holography in $BaTiO_3$

N. Kukhtarev[1,*], G. Dovgalenko[1,], J. Shultz[1], G. Salamo[1], E. J. Sharp[2], B. A. Wechsler[3], M. B. Klein[3]**

[1] University of Arkansas, Physics Department, Fayetteville, AR 72701, USA (FAX: +1-501/575-4580)
[2] Army Research Laboratory, Fort Belvoir, VA 22060-5028, USA
[3] Hughes Research Laboratories, 3011 Malibu Canyon Road, Malibu, CA 90265, USA

Received 10 July 1992/Accepted 11 December 1992

Abstract. We report the first measurement of the photogalvanic circular current antisymmetric tensor component in $BaTiO_3$: Co. The measurement gives a value of this coefficient, for extraordinary beam amplification, of 4×10^{-9} A/W using a nonstationary measurement technique at a wavelength of 0.632 μm.

PACS: 42.40, 42.65, 42.70

A photogalvanic current is a nonlinear optical effect [1, 2] which can be utilized for hologram writing in a noncentrosymmetrical crystal. This current can be represented as a function of a light-wave electric field with components E_k, E_l as:

$$j_n^{ph} = \beta_{nkl} E_k E_l + i\beta_{nl}[\mathbf{E} \times \mathbf{E}^*]_l . \tag{1}$$

In this expression, the first term is the symmetric part of the photogalvanic current. This part of the tensor has components which satisfy the relationship

$$\beta_{nlk} = (\beta_{nkl})^* . \tag{2}$$

The second term in (1) represents the antisymmetric part of the photogalvanic current and has tensor components β_{nl} which have transformation properties that are similar to the properties of the gyration tensor [1–2].

The antisymmetric components of the photogalvanic current, sometimes called the circular photogalvanic current because it can be generated using elliptically polarized light, can produce interesting results. For example, the fact that the antisymmetric component can couple orthogonally polarized waves makes possible polarization recording and restoration [3, 4]. In fact, the circular photogalvanic current has been shown in $LiNbO_3$: Fe to be the main mechanism for phase conjugation with polarization restoration for images transmitted in multi-node fibers [5].

In this paper we report the first quantitative measurements of the circular photogalvanic current in $BaTiO_3$: Co using the dynamic holographic grating technique. Writing the electric field of the incident light waves as a superposition

$$\mathbf{E} = \sum_s [\mathbf{C}_s e^{i\eta_s} + \text{c.c.}] , \tag{3}$$

where $\eta_s \equiv \omega t - \mathbf{k}_s \cdot \mathbf{r}$, the amplitude of each coefficient $\mathbf{C}_s$ can be found using the Maxwell wave equation to give:

$$(\mathbf{k}_s \cdot \nabla)\mathbf{C}_s = -\frac{ik_0^2}{2} \langle (\delta\hat{\varepsilon}\mathbf{E}) e^{-i\eta_s} \rangle . \tag{4}$$

In this expression the birefringence is included in the wave vector $\mathbf{k}_s$, and $\mathbf{k}_0$ is the wave vector in a vacuum and the angular brackets denote usual time and space averages. The change in the permittivity tensor $\delta\hat{\varepsilon}$ is governed by the linear electro-optic effect given by

$$\delta\varepsilon_{ij} = -(\hat{\varepsilon}(\hat{r}\mathbf{E})\hat{\varepsilon})_{ij} , \tag{5}$$

where $\hat{r}$ is the electro-optic tensor, $\mathbf{E}$ the photo-induced electro-static field, and $\hat{\varepsilon}$ the permittivity tensor of the nonlinear crystal. In the case of $BaTiO_3$ with crystal symmetry 4 mm, the components of $\delta\varepsilon_{ij}$ are given by

$$\begin{aligned} \delta\varepsilon_{xx} &= \delta\varepsilon_{yy} = -n_o^4 r_{13} E_z , \\ \delta\varepsilon_{zz} &= -n_e^4 r_{33} E_z , \\ \delta\varepsilon_{xz} &= -(n_o n_e)^2 r_{51} E_x , \\ \delta\varepsilon_{yz} &= -(n_o n_e)^2 r_{51} E_y , \end{aligned} \tag{6}$$

where z is along the $\mathbf{c}$ or optic axis as shown in Fig. 1.

The photo-induced electro-static field or space charge field can be calculated using the continuity and Poisson equations for the electric current and net charge distribution. These two equations may be written as

$$\begin{aligned} \frac{\partial\rho}{\partial t} &= -\nabla \cdot \mathbf{j} , \\ \nabla \cdot \varepsilon\mathbf{E} &= 4\pi\rho . \end{aligned} \tag{7}$$

* Professor N. Kukhtarev is on leave from the Institute of Physics in the Ukraine and is supported by the NSF

** Dr. G. Dovgalenko is on leave from the IRPA "Rotor-Control" research laboratory of the Ukraine and is supported by the University of Arkansas

Superconducting $TlSr_2(Ca,Cr)Cu_2O_7$ thin films with critical current density up to 10^6 A/cm^2

Y. Q. Tang, K. Y. Chen, I. N. Chan, Z. Y. Chen, Y. J. Shi, G. J. Salamo, F. T. Chan, and Z. Z. Sheng
Department of Physics, University of Arkansas, Fayetteville, Arkansas 72701

(Received 8 March 1993; accepted for publication 13 June 1993)

Superconducting $TlSr_2(Ca,Cr)Cu_2O_7$ thin films with zero resistance temperature T_c up to 102 K and critical current density J_c as high as 10^6 A/cm^2 at 77.7 K have been successfully prepared via laser ablation and thallium diffusion. Prolonged low temperature annealing in air was used for film processing. X-ray diffraction patterns indicated that the films were highly oriented 1212 phase with c axes normal to the $LaAlO_3(100)$ or MgO(100) substrates.

Among the Tl-based high T_c superconductors,[1–4] the single Tl-O layered Tl-1212 and Tl-1223 compounds have drawn more and more attention in applied superconductivity.[5–7] Since the distance between Cu-O conducting planes in these compounds is shorter than in the compounds with two Tl-O layers (2212 and 2223), leading to stronger interlayer coupling, it is suggested that the thermally activated flux motion in Tl-1212 and Tl-1223 phases may not be as severe as that in double Tl-O layered compounds.[8] It is also believed that the single Tl-O layered compounds have higher critical current density J_c and their superconducting performances are less influenced by magnetic field.[5,8,9] These advantages make Tl-1223 and Tl-1212 phases good candidates for the fabrication of superconducting wires and thin films.

Based on the work of the 105 K $TlSr_2(Ca,Cr)Cu_2O_7$ bulk material in which Cr primarily takes the position of Ca,[10] we have recently prepared this kind of 1212 phase film by chemical deposition[11] and by laser ablation.[12] It was found that the new 1212 films were easy to prepare and could sustain a wide range of processing conditions. However, the superconducting properties of the films should be further improved in order to meet the requirements of practical application.

In this communication, we report the preparation of highly oriented Cr-substituted 1212 phase $TlSr_2(Ca,Cr)Cu_2O_7$ films of good quality. The films were produced by a two-step process via laser ablation and post-annealing in Tl vapor. By carefully controlling annealing conditions, we have successfully obtained superconducting $TlSr_2(Ca,Cr)Cu_2O_7$ films with T_c of 98–102 K and J_c of 1×10^6 A/cm^2 at 77.7 K. To our knowledge, the J_c value is among the highest values achieved in 1212 phase Tl-based thin films.

The precursor films with a fixed starting composition of $Sr_2CaCr_{0.2}Cu_2O_z$ were first deposited onto MgO(100) or $LaAlO_3(100)$ substrates using an Ar-F excimer laser. This starting composition was chosen according to the optimum range of Cr amount in the nominal compositions $TlSr_2CaCr_yCu_2O_z$ (y=0.15–0.25) of bulk material.[10] The laser operated with a wavelength of 193 nm at 10 Hz. The pulse energy was 125 mJ. The oxygen pressure in the deposition chamber was 200 mTorr and the deposition time was 20–30 min. The substrate temperature was controlled in the range of 250–350 °C during ablation. It was found that the substrate temperature was not critical during deposition as long as it was lower than 600 °C. With a thickness of 0.3–0.8 μm, the precursor films had a dark brown color and looked mirror-like.

The as-deposited precursor films were then annealed in Tl vapor. One unfired pellet with the nominal composition $Tl_xSr_2CaCr_{0.2}Cu_2O_z$ (x=1 or 1.3) was used as the main Tl vapor source, and some fired pellets were used as supports and as an auxiliary Tl source. We determined that x=1 in the nominal composition corresponded to the ideal Tl amount for synthesizing the 105 K 1212-phase bulk material. This ratio did not seem adequate for prolonged film annealing. Therefore, x=1.3 was chosen to enhance the concentration of Tl vapor during the annealing process. Two kinds of slightly different configurations were used in the film annealing. One was the so-called "untouched method," in which the unfired pellet was placed about 1 mm above the precursor film in a covered alumina boat. The other was called the "touched method," where the film was sandwiched between two pellets vertically placed in a closed alumina cylinder with the film surface confined to the unfired pellet. Annealing was carried out in a programmable tube furnace at 860–870 °C, about 50 °C lower than the calcining temperature for bulk material.[10] A lower annealing temperature proved to be helpful in improving the properties of superconducting films.[13,14] A cooling rate as low as 2 °C/min was used to ensure the final film quality.[12] The T_c and J_c of the fabricated superconducting films were then measured either by the four-probe or by the self-inductance[15] method.

In previous work, annealing was carried out in a flowing oxygen atmosphere for less than 3 h and the nominal $TlSr_2CaCr_{0.2}Cu_2O_y$ pellets were used as a Tl vapor source.[11,12] In the present work, however, we annealed the films in air and prolonged the annealing time to 5–20 h. These modifications played an important role in improving the quality of the resulting films. Studies on the effect of oxygen pressure on the formation of Tl-based superconductors show that the decrease of oxygen pressure can reduce the temperature of phase formation and enable the reaction at lower temperature.[14,16] The oxygen pressure in air (0.2 atm) is much lower than the 1 atm flowing oxygen; thus, the formation of superconducting film at low anneal-

 0021-8979/93/74(6)/4259/3/$6.00

10. D. Ceperley, *Phys. Rev.* **B18**, 3126 (1978).
11. G. Vignale and K. S. Singwi, *Phys. Rev.* **32**, 2156 (1985).
12. T. K. Ng and K. S. Singwi, *Phys. Rev.* **B34**, 7738 (1986).
13. G. Vignale, *Phys. Rev.* **B38**, 6445 (1988).
14. C. A. Kukkonen and A. W. Overhauser, *Phys. Rev.* **B20**, 550 (1979).
15. D. R. Penn, *Phys. Rev.* **B22**, 2677 (1980).
16. H. Yasuhara, Y. Ousaka, and H. Suehiro, *J. Phys.* **C20**, 2511 (1988).
17. S. Yarlagadda and G. F. Giuliani, *Phys. Rev.* **B38**, 10966 (1988).
18. Y. Takada, *Phys. Rev.* **B43**, 5979 (1991).
19. H. Yasuhara and Y. Takada, *Phys. Rev.* **B43**, 7200 (1991).
20. Y. Takada and H. Yasuhara, *Phys. Rev.* **B44**, 7879 (1991).

Modern Physics Letters B, Vol. 7, No. 1 (1993) 19–23

HIGH-QUALITY $Tl_2Ba_2Ca_2Cu_3O_{10}$ THIN FILMS FABRICATED VIA LASER ABLATION

W. A. LUO,* Y. Q. TANG,† Y. Z. CHEN,‡ I. N. CHAN, K. Y. CHEN,
Y. J. SHI, X. C. WANG, M. YOUNG, S. NASRAZADANI,§
Z. Z. SHENG, G. J. SALAMO, and F. T. CHAN
Physics Department and HiDEC, University of Arkansas,
Fayetteville, AR 72701, USA

Received 25 November 1992

In this letter, we describe results obtained via laser ablation to fabricate $Tl_2Ba_2Ca_2Cu_3$-O_{10} superconducting thin films using a two-step process. We found that the zero-resistance temperatures are up to 121 K, while the onset temperatures are up to 125 K. The T_c and J_c are mainly determined by a non-contact new technique for high-T_c films. The typical critical current density, J_c, is about 10^6 A/cm^2 at 77 K. X-ray diffraction showed that the superconducting thin films are nearly single 2223 phase and are highly oriented.

The potential application of high-T_c superconductors in the field of advanced microelectronic depends on the development of low cost and high quality superconducting thin films. With the advantage of high-T_c and J_c, low noise, and low microwave surface resistivity, the Tl-based superconducting thin films are considered to be a viable candidate for practical applications at liquid-nitrogen temperature. Consequently, a wide variety of deposition methods have been adopted to fabricate Tl-based superconductor thin films.[1–5] Due to the high volatility of Tl oxides, it is difficult to control both Tl and oxygen stoichiometry during deposition. Hence, recent works have been focused on refining the subsequent thermal annealing processes. In this letter, we describe high-quality $Tl_2Ba_2Ca_2Cu_3O_{10}$ thin films fabricated via laser ablation using a "two-step" process.[6,7]

In the first step, a target of $Ba_2Ca_{2.3}Cu_3O_x$ sintered at 870°C for 15 hours is placed in a vacuum chamber at 200–300 mTorr oxygen. An excimer laser beam is then focused into the chamber and onto the target. The high power laser then results in ablation and deposition of the target material onto the substrate. The

*Permanent address: Department of Materials Science, Fudan University, Shanghai 200433, China.
†Permanent address: Analysis & Research Center, East China Institute of Chemical Technology, Shanghai 200237, China
‡Permanent address: Department of Applied Chemistry, University of Science & Technology, Hefei, Anhui 230026, China
§Department of Mechanical Engineering, University of Arkansas, USA.

Optics Communications 101 (1993) 397–402
North-Holland

OPTICS
COMMUNICATIONS

Enhancing the photorefractive effect

Galen C. Duree Jr., John L. Shultz, Nianyu Bei, Gregory J. Salamo
University of Arkansas, Physics Department, Fayetteville, AR 72701, USA

Edward J. Sharp, Gary L. Wood
Army Research Laboratory, Fort Belvoir, VA 22060-5028, USA

Steven Montgomery
Naval Academy, Annapolis, MD, USA

and

Ratnakar R. Neurgaonkar
Rockwell International Science Center, Thousand Oaks, CA 91360, USA

Received 2 March 1993

The transient response for beam fanning in photorefractive tungsten bronze crystals with an applied electric field and a focused laser beam is studied. Response times on the order of 1 ms for an incident power of 1 mW observed for incident beams focused to a 30 μm diameter in the crystal. This improved response time is accomplished without the significant reduction in the magnitude of the photorefractive effect normally observed for focused beams.

1. Introduction

Photorefractive crystals have potential for applications in the fields of dynamic holography and optical phase conjugation. This is basically due to the fact that these crystals exhibit large changes in their index of refraction with milliwatts of incident laser power. At the same time, however, these crystals suffer from a reputation of having a response time that is considered very slow. In this paper, we demonstrate that milliwatt lasers can in fact produce large index changes with fast response times in many photorefractive crystals available today. Our experimental results are compared with theory and show some salient features not previously observed.

Given a laser power of 1 mW in a 1 mm diameter beam incident on a tungsten bronze photorefractive crystal, the typical photorefractive response time is on the order of 1 to 10 s. This response time is considered relatively slow for such applications as optical limiting or image processing. In order to improve the response time, two techniques can be used. The first takes advantage of the fact that the photorefractive response time goes inversely with the incident intensity. By focusing the laser beam to a small area in the crystal, the incident intensity can be increased and consequently a dramatic improvement in the response time may be expected. However, when the incident laser light is focused to a small spot, the magnitude of the photorefractive effect decreases and nearly vanishes [1]. The physical reason for the decrease in the strength of the effect is due to the fact that the gain–length product for a 30 μm diameter beam is extremely small when compared to that of a millimeter beam. As a result, while focusing the incident laser light is attractive, it proves to be impractical. One method of overcoming the gain–length reduction is the use of a cylindrical lens for focusing the incident light into the crystal [2]. In this case, the intensity is increased by focusing only in one

Optics Communications 104 (1993) 23–28
North-Holland

OPTICS
COMMUNICATIONS

Reflection holographic gratings in [111] cut $Bi_{12}TiO_{20}$ crystal for real time interferometry

N. Kukhtarev, Bo Su Chen, P. Venkateswarlu
Physics Department, Alabama A & M University, Normal, AL 35762, USA

G. Salamo
Physics Department, University of Arkansas, Fayetteville, AR 72701, USA

and

M. Klein
Hughes Aircraft Corporation, MS RL64, Malibu, CA 90265, USA

Received 30 March 1993; revised manuscript received 6 August 1993

It is shown that reflection grating in [111] $Bi_{12}TiO_{20}$ crystal can be used for dynamic interferometry with a low power HeNe laser, giving a diffraction efficiency of 0.14%. Predicted and confirmed is the possibility of hologram recording by orthogonal polarized waves, using as advantage natural optical activity.

1. Introduction

Recording of holographic gratings for real-time dynamic holographic interferometry (DHI) with photorefractive crystals was demonstrated in previous work [1,2] in transmission grating. Another promising geometry, reflection grating, was demonstrated as useful for DHI [3].

In this paper we present both theoretical and experimental investigation of reflection gratings in $Bi_{12}TiO_{20}$ (BTO) crystal. We use [111] cut crystal which provides for holographic grating vector $K \| [111]$ isotropic recording and reading, without introducing birefringence.

We also show that the natural optical activity of the crystal which usually hampers holographic recording in transmission grating [1,2,4] can be used as an advantage to allow to write grating by orthogonal polarized waves.

The basic features of DHI with reflection gratings is shown in fig. 1. Two counter-propagating beams intersect in the crystal, beam a acts like an object and beam b as reference. The interference pattern is recorded in crystal via modulation of crystal refractive index by electro-optic effect [1–3].

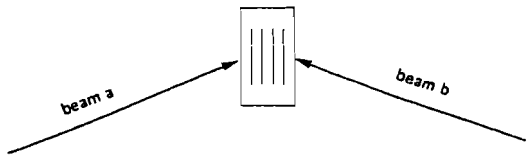

Fig. 1. Standard reflection grating set-up.

Beam b at the same time can participate in reading out in real time, producing beam a_d which may be different by polarization from the transmitted object beam a_t. This polarization difference allows to select a diffracted signal by analyzer.

If some changes occur in the object beam, which results in small deviation of interference pattern, then a new grating begins to form in the crystal and the old grating is erasing. This leads to simultaneous appearance of two diffracted beams from old and new holographic gratings. That generates interference

Observation of Self-Trapping of an Optical Beam Due to the Photorefractive Effect

Galen C. Duree, Jr., John L. Shultz, and Gregory J. Salamo
Department of Physics, University of Arkansas, Fayetteville, Arkansas 72701

Mordechai Segev and Amnon Yariv
California Institute of Technology, Department of Applied Physics, Pasadena, California 91125

Bruno Crosignani and Paolo Di Porto
Dipartimento di Fisica, Università dell'Aquila, L'Aquila, Italy and Fondazione Ugo Bordoni, Roma, Italy

Edward J. Sharp
Army Research Laboratory, Fort Belvoir, Virginia 22060

Ratnakar R. Neurgaonkar
Rockwell International Science Center, Thousand Oaks, California 91360
(Received 19 April 1993)

We report on the first observation of self-trapping of an optical beam due to the photorefractive effect. The self-trapping occurs at microwatt light power levels, is intensity independent, and results in significant spatial pulse reshaping.

PACS numbers: 42.65.Jx, 42.50.Rh, 42.65.Hw

Self-trapping of laser beams in nonlinear Kerr media is a well studied phenomenon [1–6] in which the diffraction effects are exactly compensated by focusing effects caused by a light induced index change. In these cases, the propagation of a light beam is spatially confined and a shape-preserving transverse profile or spatial soliton is observed. Recently, a new type of spatial soliton has been suggested [7]. It has been predicted to occur in a photorefractive medium and differs from Kerr solitons by the fact that the focusing effect is produced by an internal nonlocal space-charge dc field, as opposed to the local intensity dependent Kerr effect. A dramatic consequence of the difference in the focusing origin is that the photorefractive soliton is observable at low light powers on the order of 10 μW (intensities of about 200 mW/cm^2) or less while the observation of "bright" [5] or "dark" [6] Kerr solitons requires much higher powers. Moreover, photorefractive solitons are independent of the laser light power. As a result, they propagate while maintaining their spatial profile even in the presence of loss or gain.

In this Letter, we report the observation of photorefractive solitons. These solitons preserve their profile, which are independent of input power, and can be observed at low light powers of less than 10 μW. The degree of self-focusing due to the photorefractive index change is shown to be controllable by an applied dc voltage across the photorefractive crystal. For small applied voltages, diffraction is seen to exceed the photorefractive focusing effect and the transmitted beam is observed to diverge through the crystal. For large applied voltages, the photorefractive focusing effect exceeds diffraction and the transmitted beam is observed to converge throughout the crystal. Only for a small range of applied voltages is a shape-preserving spatial profile observed to propagate throughout the crystal. This voltage range has been predicted in Ref. [7] and is dictated by the crystal parameters, such as its electro-optic coefficients, the dielectric constant, the density of traps, and the light wavelength and polarization. For very large applied voltages, photorefractive focusing greatly exceeds diffraction and the incident beam converges in the crystal to a spot size smaller than its original waist. Following the formation of the new waist, the beam diverges and is then trapped as diffraction is once again compensated for by the focusing produced via photorefraction. In all cases, the laser beam is observed to reshape and take on a "smooth" spatial profile.

For photorefractive solitons the photorefractively induced change in the index of refraction of the medium can be thought of as arising from the photorefractive two-wave mixing between all possible pairs of the plane-wave spatial-frequency spectrum of the incident laser beam [7,8]. That is, for each pair of plane-wave components of the incident beam which interferes and produces an interference grating throughout the crystal, a perturbation in the refractive index is generated $\delta n(r,z)$, where z is along the propagation direction and r is in the plane perpendicular to z. Each corresponding index grating may be viewed as a composition of two grating components: One is in phase, spatially, with the original interference pattern and the other is 90° out of phase. The in-phase component is responsible for phase coupling between the plane waves, and therefore can compensate for diffraction while the 90° phase shift component is responsible for energy exchange between each pair of spatial-frequency plane-wave components of the incident beam and for stimulated scattering or "beam fanning" [9,10]. In order to generate a nondiffracting light beam, we require $\delta n(r,z) = \delta n(-r,z)$, for all z, since diffraction is symmetric about the z axis. Following the discussion in Ref. [7] on the symmetry properties of the coupling coefficient, δn in the simple scalar 2D case, we have used

0031-9007/93/71(4)/533(4)$06.00

Mutually pumped phase conjugator as a moving-object correlator

Richard J. Anderson

National Science Foundation, Washington, D.C. 20550

Edward J. Sharp, Gary L. Wood, William W. Clark III, and Quochien Vuong

U.S. Army Research Laboratory, Fort Belvoir, Virginia 22060-5028

Gregory J. Salamo

Department of Physics, University of Arkansas, Fayetteville, Arkansas 72701

Ratnakar R. Neurgaonkar

Rockwell International Science Center, Thousand Oaks, California 91360

Received November 23, 1992

Cross talk is observed in a photorefractive bridge mutually pumped phase conjugator during the transient time of photorefractive grating formation and is utilized to construct a moving-object correlator. The correlation of various input images has been demonstrated and compared with calculated results. The device is currently capable of a resolution of approximately 4 to 6 lines/mm.

Photorefractive crystals have been used for a number of optical processing applications arising from multiwave mixing.[1] For example, with images spatially impressed on one or more of the beams in four-wave-mixing geometries, correlation/convolution operations have been demonstrated.[2–4] Recently a new class of phase conjugator, called the mutually pumped phase conjugator (MPPC), has been demonstrated in a variety of materials and geometries. These conjugators can be classified by the number of internal reflections the beams experience before conjugation; zero,[5–7] one,[8] two,[9] or three.[10] In these devices, two phase-conjugate outputs (double phase conjugation) are produced simultaneously by the interaction of two mutually incoherent beams of the same wavelength within the photorefractive crystal.

In this Letter we describe how the occurrence of cross talk in MPPC's can be used to demonstrate a correlator. Whereas there are similarities between the device discussed here and the concept of a photorefractive novelty filter,[11] the distinction is that the MPPC device not only detects moving objects but identifies them as well. In addition, unlike other four-wave-mixing correlators, this device selectively identifies only moving objects and ignores stationary objects.

The no-cross-talk criterion[12] established for MPPC's refers to steady-state conjugate signals (a time that is long compared with the photorefractive response time of the particular crystal being used). For example, suppose that the double phase-conjugate mirror is formed by a plane wave and an image-bearing beam. After steady state is reached there is no observed cross talk between the two beams, i.e., there is no evidence of an image present in the phase-conjugate signal of the plane wave. If, however, while the MPPC is operating in the steady state, the amplitudes of the input beams are spatially modulated in a time that is short compared with the photorefractive response time, then cross talk between the input beams is observed.[13] After a time corresponding to the photorefractive response time of the crystal, the cross talk is observed to disappear. If the object is suddenly moved, however, the image is again instantaneously present on the phase-conjugate signal of the plane-wave beam.

To understand the correlation process in the bridge MPPC consider the diagram shown in Fig. 1, which schematically shows the bridge MPPC operating in the steady state. The two input beams are of

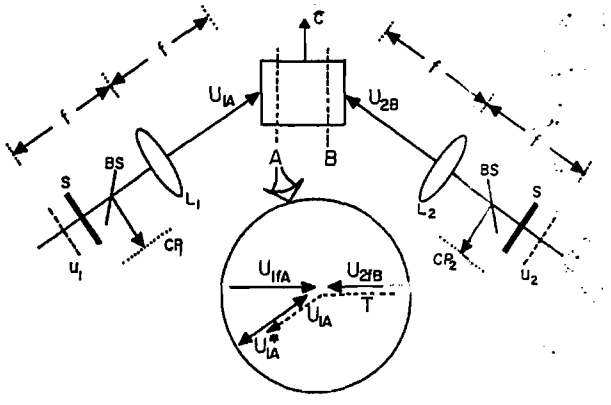

Fig. 1. Optical correlator that uses the bridge MPPC: L_1, L_2, Fourier-transform lenses; S's, shutters; CP_1, CP_2, correlation planes; u_1, u_2, objects; BS's, beam splitters; A, B, regions of dynamic holography. Region A is expanded in the inset.

0146-9592/93/120986-03$6.00/0

Self-trapping of optical beams in photorefractive media

Bruno Crosignani

Dipartimento di Fisica, Università dell'Aquila, L'Aquila, Italy, and Fondazione Ugo Bordoni, Rome, Italy

Mordechai Segev and Doruk Engin

California Institute of Technology, Pasadena, California 91125

Paolo Di Porto

Dipartimento di Fisica, Università dell'Aquila, L'Aquila, Italy, and Fondazione Ugo Bordoni, Rome, Italy

Amnon Yariv

California Institute of Technology, Pasadena, California 91125

Greg Salamo

Department of Physics, University of Arkansas, Fayetteville, Arkansas 72701

Received July 16, 1992; revised manuscript received October 9, 1992

We study the possibility of self-trapping of an optical beam in a photorefractive medium under the combined influence of diffraction and self-scattering (two-wave mixing) of its spatial frequency components. We investigate the spectrum of solutions for the resulting photorefractive spatial solitons and discuss their unique properties. Design considerations and material requirements for experimental realization of these solitons, together with specific examples, are given.

1. INTRODUCTION

Self-trapping of light beams in nonlinear self-focusing Kerr media has been explored intensively during the past three decades. The self-trapped beams, often in the form of spatial solitons, evolve from nonlinear changes in the refractive index of the material that are induced by the intensity distribution of the light when the confining effect of the refractive index exactly compensates for the defocusing effect of diffraction. After self-focusing of light beams[1] in the presence of the optical Kerr effect was observed experimentally, a theoretical solution for the resulting spatial solitons was found.[2,3] This solution was followed by demonstrations of self-trapping in vapors[4] and liquids,[5] and finally, within the past few years, spatial solitons in solid (glass) media were also observed.[6] However, the index changes needed for Kerr-like spatial solitons require high intensities, intensities often exceeding 1 MW/cm^2.

In a recent paper[7] we suggested a new type of spatial soliton that is associated with the photorefractive (PR) effect in a crystal. The intensity profile of the beam modulates the refractive index by means of the PR effect, which results in an exact compensation for the effects of diffraction and causes the light beam to propagate with an unvarying profile. These new solitons arise from the nonlocal PR effect rather than from the local Kerr effect. They can be generated even at moderate light intensities, since the efficiency of the PR effect is independent of the absolute light intensity.

In this paper we provide a detailed derivation of the equation governing propagation in a PR material and explore the spectrum of its solutions that pertain to distortionless propagation. We discuss the properties of the PR solitons and specify the material requirements and the design considerations for an experimental realization. Finally, we evaluate the minimal nonlinearity that is required for trapping a light beam and consider a specific example of self-trapping in strontium barium niobate (SBN).

2. BEAM PROPAGATION IN PHOTOREFRACTIVE MEDIA

The PR solitons are found among the steady-state solutions of the nonlinear wave equation that describe beam propagation in PR media and account for both diffraction and the mutual interaction between each pair of spatial components of the beam. Since the key to this nonlinear scattering process is grating formation by a continuum of Fourier (plane-wave) components of the beam, we cannot resort to the two-plane-wave analysis that is commonly applied to PR materials. Our general formalism accounts for the transverse spatial structure of the beam.

We start by deriving the nonlinear wave equation that describes the propagation of a monochromatic optical beam of a given frequency (ω) and polarization that is traveling in the positive direction of an arbitrary axis z. We assume the absence of nonlinear interactions between orthogonal polarizations (anisotropic scattering[8]), so that

0740-3224/93/030446-08$05.00

Single Beam Polarization Holographic Grating Recording

Nickolai Kukhtarev,* George Dovgalenko, Galen C. Duree, Jr., and Gregory J. Salamo
Physics Department, University of Arkansas, Fayetteville, Arkansas 72701

Edward J. Sharp
U.S. Army Research Laboratory, Fort Belvoir, Virginia 22060

Barry A. Wechsler and Marvin B. Klein
Hughes Research Laboratories, 3011 Malibu Canyon Road, Malibu, California 90265
(Received 17 August 1992; revised manuscript received 27 July 1993)

Single beam holographic grating recording, based on the photogalvanic coupling between orthogonal birefringent modes, is demonstrated in a photorefractive $BaTiO_3$ crystal.

PACS numbers: 42.70.Nq, 42.25.Ja, 78.20.−e

In holography, two waves, signal and reference, are needed to record information about the phase and amplitude of the signal wave. This is normally accomplished using one optical beam for the signal wave and a separate beam for the reference wave.

In this paper, we demonstrate both theoretically and experimentally the possibility of hologram recording using only one input beam, which is automatically split into two eigenmodes in a birefringent photogalvanic crystal. The interaction between the two orthogonally polarized eigenmodes, ordinary (o) and extraordinary (e), in the crystal, via a photogalvanic current [1–5], then writes a holographic grating. This grating is subsequently read using the same single recording beam either in real time or at a later time. Consequently, the great advantage of this technique is that there are reduced restrictions on the coherence length and alignment of the incident laser light since the reference and signal beams are formed inside the crystal.

The coupling between orthogonal waves inside the crystal is depicted in Fig. 1. An optical beam is incident onto a crystal at angle θ. The incident field then splits into two crystal eigenfunctions characterized by the ordinary and extraordinary wave vectors $\mathbf{k}_o$ and $\mathbf{k}_e$. In the region of overlap between the two eigenwaves in the crystal, a holographic grating is written. More formally, the electric field of the incident light in the crystal can be written as a superposition of quasiplane waves,

$$\mathbf{E}=\sum_s [\mathbf{C}_s e^{i\eta_s}+\text{c.c.}]\,, \tag{1}$$

where $\eta_s=\omega t-\mathbf{k}_s\cdot\mathbf{r}$ and "s" is a sum over the ordinary and extraordinary crystal eigenmodes. In this expression, the birefringence of the photorefractive crystal is contained in the wave vector $\mathbf{k}_s$ and ω is the optical frequency of the incident field.

The propagation of the electric field in the crystal is described by Maxwell's wave equation:

$$\nabla\times(\nabla\times\mathbf{E})+\frac{1}{c^2}\frac{\partial^2\mathbf{D}}{\partial^2 t}=0\,. \tag{2}$$

To take into account the fact that our coefficients of the expansion in Eq. (1) are time dependent we write the displacement vector as

$$\mathbf{D}=\hat{\varepsilon}\mathbf{E}+\delta\mathbf{D}\,. \tag{3}$$

Substituting Eqs. (1) and (3) into the wave equation, while making the slowly varying envelope approximation, we get an expression [6] for the wave amplitudes C_s:

$$(\mathbf{k}_s\cdot\nabla)\mathbf{C}_s=-\frac{i\omega^2}{2c^2}\langle\delta\mathbf{D}e^{-i\eta_s}\rangle_{t,r}$$
$$=-\frac{i\omega^2}{2c^2}\langle\delta\hat{\varepsilon}\mathbf{E}e^{-i\eta_s}\rangle_{t,\tau}\,, \tag{4}$$

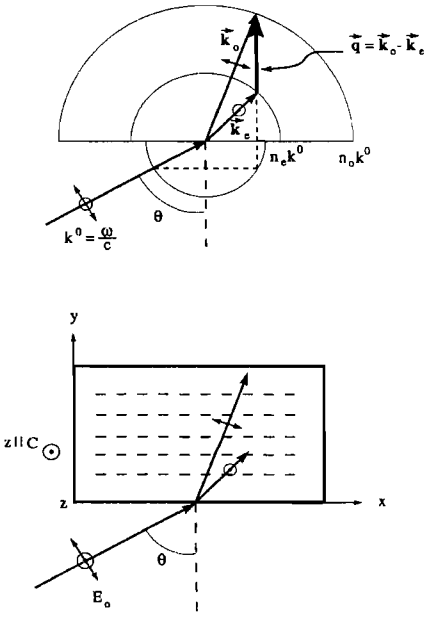

FIG. 1. $BaTiO_3$ in crystallographic system of axes with k-vector diagram.

0031-9007/93/71(26)/4330(4)$06.00

Supercond. Sci. Technol. 6 (1993) 173–175. Printed in the UK

Preparation of $Tl_2Ba_2Ca_2Cu_3O_{10}$ thin films via low-temperature Tl-diffusion

Y Q Tang†, Z Z Sheng†, W A Lou†, Z Y Chen†, Y N Chan†, Y F Li†, F T Chan†, G J Salamo†, D O Pederson†, T H Dhayagude‡, S S Ang‡ and W D Brown‡

† Department of Physics, University of Arkansas, Fayetteville, Arkansas 72701 USA
‡ Department of Electrical Engineering, University of Arkansas, Fayetteville, Arkansas 72701 USA

Received 24 November 1992

Abstract. Superconducting $Tl_2Ba_2Ca_2Cu_3O_{10}$ thin films with T_c ($\rho = 0$) up to 121 K were successfully prepared via the deposition of a BaCaCuO precursor (by laser ablation or sputtering) and thallium diffusion under 1 atmosphere of air. Instead of a short annealing time at high temperature, we use a prolonged annealing time (up to 60 hours) at lower temperature (800–815 °C). The films obtained with this procedure are generally good in morphology, highly oriented and exhibit a critical current density, J_c, of about $1–2 \times 10^6$ A cm^{-2} on MgO(100) and up to 1.5×10^6 A cm^{-2} on $LaAl_3$(100) at 77 K. Both T_c and J_c values reported here are comparable to the best Tl-2223 films prepared by the pseudo-one-step process.

1. Introduction

Since the discovery of Tl-based superconductors [1–2], the compound $Tl_2Ba_2Ca_2Cu_3O_{10}$ (Tl-2223 or 2223) has been found to have the highest T_c ($\rho = 0$) up to 127 K [3–4]. With high sintering temperature (>850 °C), it is usually not difficult to prepare and reproduce bulk 2223 materials with T_c about 120 K. However, to further improve the T_c, a sophisticated post-annealing procedure, involving low-temperature treatment and oxygen adjusting, must be introduced. By encapsulating the 2223 samples in evacuated quartz tubes and post annealing at low temperatures (750–760 °C) for about 10 days or more, the T_c can be increased to 127 K [3–4]. Moreover, reduced partial oxygen pressure has proved useful in decreasing the synthesis temperature of the 2223 phase [5] and in increasing its T_c [3].

In the fabrication of Tl-2223 thin films, where post annealing is still necessary for both pseudo-one-step or two-step processes [6], reduction of annealing temperature is of particular importance because it not only leads to the formation of high-quality films but is also a necessary step towards a real one-step process such as that for Tl-1212 film [7]. Previous annealing procedures for 2223 films generally use high temperatures (>850 °C) and short times (5–60 min), which usually generate relatively rough film surface and poor J_c. Lee *et al* recently reported the low temperature formation of 2223 films in reduced O_2 pressure [8]. With their pseudo-one-step procedure, the quality of the 2223 film was improved significantly. Their best films were shiny to the eye and showed a T_c as high as 121 K and a J_c of 1.6×10^6 A cm^{-2} at 77 K. However, their technique was somewhat complicated. Our recent work on spray pyrolysis also showed that, even under 1 atmosphere of oxygen, 2223 films with T_c up to 121 K can still form at relatively low annealing temperature if the annealing time is long enough [6].

In this paper, we report the two-step formation of 2223 films at low annealing temperature in 1 atmosphere of air. Under optimum conditions, the T_c ranged from 117 K to 121 K, and J_c is $1–2 \times 10^5$ A cm^{-2} for the films on MgO(100) substrates and up to 1.5×10^6 A cm^{-2} on $LaAlO_3$ at 77 K.

2. Experimental details

The substrates used for film production were MgO(100) and $LaAlO_3$(100). The BaCaCuO precursor films were deposited by laser ablation or sputtering. The details of the equipment for these methods are described elsewhere [9, 10]. The substrates were heated at 400–500 °C for the laser ablation but were kept at room temperature during sputtering. The precursor films deposited by laser were 0.4–0.5 μm thick while those by sputtering were about 0.8 μm. Thallium was then introduced by annealing the as-deposited BaCaCuO films with crude $Tl_{1.7}Ba_2Ca_{2.3}Cu_3O_x$ pellets in a closed alumina boat. The films were placed in a free-surface configuration with the pellet positioned about 1 mm above the film. The pellets were prepared using high purity Tl_2O_3, BaO_2, CaO and CuO powder [11]. The annealing temperature was 750–820 °C, 80–150 °C lower than the conventional temperature for bulk formation and at least 50 °C lower than the generally used

0953-2048/93/030173 + 03 $07.50

SUPERCONDUCTING Tl-Ba-Ca-Cu-O THIN FILMS

by

M. Young, X-L. Yang, Y.F. Li, Y.G. Tang, Z.Z. Sheng
G.J. Salamo, R.J. Anderson*, and F.T. Chan

Physics Department/HIDEC
University of Arkansas
Fayetteville, Arkansas 72701

AIP Conference Proceedings, n 251, p 76-83, 1992

ABSTRACT

Tl-Ba-Ca-Cu-O superconducting thin films have been prepared using both laser ablation and "fog" spray techniques. The zero resistance temperature varied between 92 K and 119 K.

INTRODUCTION

The potential application of high T_c superconductors in the field of advanced microelectronics depends on the development of low cost high quality superconducting thin films. In this paper we will describe results obtained using two techniques to produce Tl-Ba-Ca-Cu-O superconducting thin films. The first technique is laser ablation while the second involves the use of a chemical "fog" spray.

LASER ABLATION

Results using the laser ablation technique on an alumina substrate are shown in Figure 1. A very low resistance is maintained until a T_c of up to 92 K. The technique used to fabricate these films employs a simple two-step process[1, 2]. In the first step a target of $Ba_2Ca_2Cu_3O_x$ is placed in a vacuum chamber. The output of an excimer laser is then focused into the chamber and onto the target. The high laser intensity at the target then results in ablation of the target material. The resulting spray of material then deposits onto an alumina substrate. The experimental apparatus for the deposition of the thin film is shown in Figure 2. In the second step the sample is removed from the chamber and placed in an oven along with a boat of $Tl_2Ba_2Ca_2Cu_3O_x$ powder. The sample is then heated at 830° C for approximately five minutes and then cooled and removed for testing.

*National Science Foundation, Washington, D.C.

The excimer laser shown in Figure 2 was operated using ar producing about 100 millijoules in a 10 nanosecond pulse at a wa nanometers. The output of the laser was focused, using a quartz lens (mm, into the vacuum chamber housing the Ca-Ba-Cu target and alumi focused laser spot size at the target was about 100 μ × 200 μ. At th rate of 20 Hz the time for forming a 2 micron thick film was about 40 r average deposition rate of about 0.8 nanometers per second. The vacu maintained at a background pressure of 10-5 torr while the alumi maintained at a temperature of 200° C. The angle θ between the inc and the normal to the substrate was fixed at 30° and the distance betwe substrate was 3 cm. These values were chosen to optimize the unifo film formed on the substrate. Several alumina substrates were trie varying from 10 μ to .25 μ. Results were similar to that shown in case. However, a higher T_c was generally found for smoother sample Figure 3(a) and (b) shows plots of the surface smoothness for two dif before laser deposition. Substrate (a) yielded the higher T_c of 92 K sh substrate (b) gave the results in 3(d). Figure 4, shows both the subst and the corresponding film smoothness for our best alumina samples (that the film smoothness is similar to that of the substrate. The improv with increased substrate smoothness is also supported by our measur when polished sapphire was used as a substrate. Similar high quality also been obtained using MgO as a substrate. Results from a sc microscope, shown in Figures 5(a), (b), and (c) show in more deta smoothness for the alumina superconducting samples.

As mentioned earlier, once the $Ca_2Ba_2Cu_3O_x$ thin film is prepar an oven and heated along with a boat containing about 10 grams of Tl powder. The oven temperature is maintained at 830° C for approximat and then allowed to cool to room temperature. In this way, the interact thalium and substrate is only possible, at elevated temperatures, fo minutes. This relatively brief interaction time is believed to be resp successful growth of the films without the need for buffer layers. In heating for periods longer than five minutes results in the loss of the Figure 1.

The microstructure of the thalium thin films on alumina was als using x-ray diffraction. Figure 6 shows a typical x-ray diffraction pa film after baking in thalium vapor. The data reveals that the supercondu composed of the (2212) low phase and the (2223) high phase. Each p present. This observation agrees with the fact that the measured T_c which is between the bulk T_c temperatures of 80 K and 120 K for th phases. Corresponding data for sapphire and MgO substrates have not y

CHEMICAL FOG SPRAY

The second technique used to produce thin films involves the us "fog" spray. This technique is one of the simplest but useful methods thin film superconductors. A solution of Tl-Ba-Ca-Cu-O (Tl: Ba: Ca: 3) and .05 M concentration was prepared using high-purity Tl NO_3, B $(NO_3)_2$, and Cu $(NO_3)_2$. The solution was sprayed on using a fog spra

Enhancing the response time for photorefractive beam fanning

John L. Shultz and Gregory J. Salamo

University of Arkansas
Physics Department
Fayetteville, Arkansas 72701

Edward J. Sharp and Gary L. Wood

CECOM Center for Night Vision and Electro-Optics
Fort Belvoir, Virginia 22060-5677

Richard J. Anderson

National Science Foundation
Washington, D.C.

and

Ratnakar R. Neurgaonkar

Rockwell International Science Center
Thousand Oaks, California 91360

ABSTRACT

Two types of optical limiting devices which have been demonstrated using photorefractive crystals are the "beam fanning" limiter and the "two-beam coupling" limiter. Experimental demonstrations of these two devices have revealed an interesting difference in behavior between those two limiter types. The two-beam coupling limiter is consistently faster than the beam fanning limiter for the same incident intensity. This is somewhat surprising since the beam fanning limiter is based on two-beam coupling phenomena. Our recent experiments show, however, that the relative speed of the two devices can be made more alike using a phase grating at the entrance face of the beam fanning limiter. While the phase grating scatters only about 1% to 5% of the incident light it apparently provides sufficient seeding to significantly enhance the beam fanning response time. Since the diffracted light is only about 1% the distortion to vision through the limiter due to dispersion is minimal. In the presentation we will present results from an experimental investigation of the effect of seeding on the "beam fanning" limiter response time. In particular, we have examined the response time dependence on the intensity and direction of the seed beam. Comparison with theory will also be presented.

0-8194-0857-3/92/$4.00

Incoherent-to-coherent conversion using a photorefractive self-pumped phase conjugator

Edward J. Sharp, Gary L. Wood, and William W. Clark III

Night Vision and Electro-Optics Directorate, Fort Belvoir, Virginia 22060

Gregory J. Salamo

Department of Physics, University of Arkansas, Fayetteville, Arkansas 72701

Ratnakar R. Neurgaonkar

Rockwell International Science Center, Thousand Oaks, California 91360

Received August 28, 1991

The principle of incoherent-to-coherent conversion is demonstrated in several photorefractive oxide crystals using a self-pumped phase-conjugator geometry. Resolution in excess of 30 line pairs/mm has been obtained for writing beams of a few milliwatts of power. The combined read/write function for a single frame showed a time response of approximately 140 ms at an intensity of 1 W/cm^2 for the crystals used in these demonstrations.

Spatial light modulators (SLM's) play a key role in the architecture of optical processing systems, and numerous SLM concepts have been demonstrated based on a wide variety of physical phenomena and materials. One of these techniques makes use of the real-time grating formation in photorefractive crystals to produce successfully coherent replicas of incoherent images.[1–4] A number of devices that can convert incoherent images into coherent images have been demonstrated by using either two[3,4] or three[2,5] input plane waves. All these devices use an incoherent image-bearing beam to erase selectively a uniformly recorded volume hologram so that the spatial information contained in the image-bearing beam is transferred to a coherent readout beam when the hologram is reconstructed.

In another method the incoherent scene is imaged into the crystal after it passes through a Ronchi ruling.[6] As a result, the imaged Ronchi ruling and incoherent scene form an encoded grating in the crystal. The coherent reading beam then diffracts off the incoherently written grating, and the coherent signal beam bears its encoded incoherent image. This technique has been recently used in a single crystal of Ce-doped strontium barium niobate (SBN:75) to demonstrate multichannel photorefractive incoherent-to-coherent optical conversion.[7]

In this Letter we demonstrate incoherent-to-coherent conversion using a self-pumped phase conjugator.[8] In this geometry the incident input wave is reflected from self-generated gratings in the crystal to form the conjugate beam (signal beam). The experimental arrangement used for this demonstration is shown in Fig. 1. An extraordinary-polarized beam at 514 nm from an argon-ion laser was used as the self-pumping beam (recording beam). It was expanded to 4 mm in diameter and had an intensity of 37 mW/cm^2. The conjugate signal was produced with a reflectivity of approximately 5% and was imaged with lens L_2 onto an observation screen positioned in front of detector D_1. A counterpropagating beam (writing beam) approximately 1 mm in diameter consisted of either a laser beam or a white-light source (xenon lamp). The lasers producing the write beam were either an argon-ion laser using a single line or all lines or a He–Cd laser at 442 nm. The amplitude of the writing beam could be spatially modulated by passing it through a binary transparency (U.S. Air Force resolution chart). Lens L_1, with a focal length of 75 mm, was used to image the writing beam into the crystal without magnification. The amplitude-modulated writing beam alters the volume phase gratings responsible for the phase-conjugate signal by means of selective era-

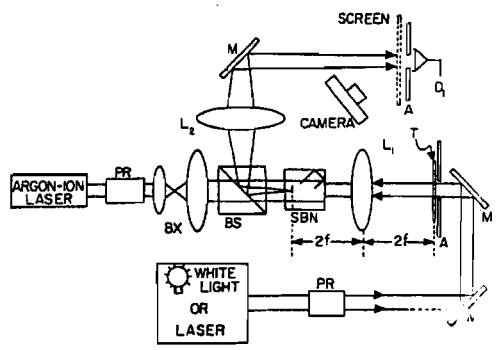

Fig. 1. Experimental arrangement used to demonstrate the principle of incoherent-to-coherent conversion in a self-pumped phase conjugator. PR's, polarization rotators; BX, beam expander; T, binary transparency; BS, beam splitter; A, 1-mm-diameter aperture; M's, mirrors. The incoherent white-light source is a xenon lamp.

0146-9592/92/030207-03$5.00/0

Jpn. J. Appl. Phys. Vol. 31 (1992) pp. 3851-3852
Part 1, No. 12A, December 1992

Short Note

Fabrication of Superconducting $TlSr_2(Ca, Cr)Cu_2O_7$ Thin Films by Laser Ablation and Thallium Diffusion

Yongqiu TANG, Weiang LUO, Zuyao CHEN, Seifollah NASRAZADANI*, Fui T. CHAN, Gregory SALAMO, Donald O. PEDERSON and Zhengzhi SHENG
Department of Physics, The University of Arkansas, Fayetteville, Arkansas 72701, USA

(Received June 29, 1992; accepted for publication September 19, 1992)

Superconducting $TlSr_2(Ca, Cr)Cu_2O_7$ thin films have been prepared on MgO(100) substrates via laser ablation and thallium diffusion. Precursor SrCaCrCuO films were first deposited by an excimer laser; thallium was then incorporated by annealing the precursor films between un-fired TlSrCaCrCuO bulk pellets. The product superconducting films are 1212 phase and exhibit $T_c(\rho=0)$ up to 90 K and J_c(transport) up to 10^4 A/cm^2.

KEYWORDS: superconducting thin film, high T_c superconductor, Tl-Sr-Ca-Cu-O system, "1212" phase, Cr addition, laser ablation

Among M-substituted (M=Pb, Bi, Cr or rare earth) 1212-type phase (Tl, M)Sr_2(Ca, M)Cu_2O_7 compounds,[1-7] the Cr-substituted $TlSr_2(Ca, Cr)Cu_2O_7$ exhibits a T_c as high as 110 K and is easy to synthesize.[7] Motivated by this easy formation and high T_c, we have successfully prepared 100 K $TlSr_2(Ca, Cr)Cu_2O_7$ superconducting films via spray pyrolysis and thallium diffusion.[8] However, the films obtained by the spray technique are generally thick and rough on surface which may not be suitable for certain electronic applications. In this paper, we report the preparation of $TlSr_2(Ca, Cr)Cu_2O_7$ superconducting films on MgO(100) substrates using laser ablation and thallium diffusion. Zero-resistance temperature $T_c(\rho=0)$ of the best films was 90 K, and the critical transport current J_c was about 10^4 A/cm^2 at 77 K.

The laser ablation target with nominal composition of $Cr_{0.2}Sr_2CaCu_2O_x$ was prepared by sintering a pellet of properly mixed powder of Cr_2O_3, SrO, CaO and CuO at 880°C for 24 h. Precursor films were deposited onto MgO(100) substrates at 260-280°C using a Kr-F excimer laser with a wavelength of 248 nm. The laser operated at 20 Hz with a power of 200 mJ. The oxygen pressure in the deposition chamber was 200 mTorr and the deposition time was 7-20 min. The as-deposited precursor films were then put between unfired $TlCr_{0.2}Sr_2CaCu_2O_x$ bulk pellets in a covered alumina cylinder, and were heated in a programmable tube-furnace at 860-880°C for 30-180 min in an oxygen atmosphere. A high temperature worked with a short annealing time while the lower temperature treatment took longer. In the cooling step, some films were cooled in argon while others were cooled in oxygen. Different cooling rates were used. The methods and instruments used for investigating the thickness, morphology, X-ray diffraction patterns as well as the T_c and J_c of films were all described in ref. 8.

The precursor films deposited by laser ablation were mirror-like with a shiny dark brown color and were not conducting. The thickness of the films varied from 0.3-0.8 μm depending on the deposition time. After the Tl-diffusion procedure, the films turned black, and were superconducting. Although the preparation conditions for TlSrCaCrCuO films were much less sensitive than that for TlBaCaCuO superconducting films,[8] the annealing procedure was still very crucial for the superconducting properties.

Table I lists the processing conditions and T_c and J_c for some films. It shows clearly that both annealing temperature and cooling rate play very important roles in the film properties. Film S1 was annealed at 880°C for 30 min in an oxygen flow. The X-ray diffraction pattern of this film (Fig. 1) shows that the film is single 1212 phase $TlSr_2(Ca, Cr)Cu_2O_7$ and exhibits a strong orientation with c-axis perpendicular to the surface of the MgO(100) substrate. However, $T_c(\rho=0)$ of the film is only 82 K and the J_c is also low ($<10^3$ A/cm^2). The SEM photograph (Fig. 2(a)) illustrates that the film consists of uniform crystalline grains with an average size of 2 μm, but the morphology is porous. Obviously, it is the porosity that causes the poor J_c of film. In contrast, films processed at lower temperature have random orientation but are more dense (Fig. 2(b)). These films exhibit higher $T_c(\rho=0)$ and J_c. By decreasing the temperature from 880°C to 865°C, T_c is increased from 82 K to 90 K (also see Fig. 3). A rapid cool-

Table I. Annealing condition and $T_c(\rho=0)$ and J_c for some films.

Sample	Annealing condition	T_c(K)	J_c(A/cm^2)
S1	880°C, 30 min (O_2), cooling rate: 50°C/min (Ar)	82	6×10^2
S2	875°C, 60 min (O_2), cooling rate: 50°C/min (Ar)	85	1×10^3
S3	870°C, 90 min (O_2), cooling rate: 50°C/min (Ar)	86	2×10^3
S4	870°C, 90 min (O_2), cooling rate: 50°C/min (O_2)	87	2×10^3
S5	865°C, 150 min (O_2), cooling rate: 2°C/min (O_2)	90	1×10^4
S6	860°C, 180 min (O_2), cooling rate: 2°C/min (O_2)	90	1×10^4

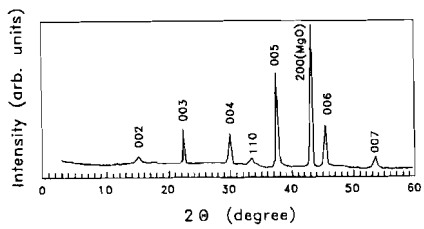

Fig. 1. X-ray diffraction pattern for the superconducting $TlSr_2(Ca, Cr)Cu_2O_7$ film S1 in Table I. It shows that this film is single 1212 phase and is highly oriented.

*Department of Mechanical Engineering, The University of Arkansas.

Improved photorefractive time response using a cylindrical lens

Gregory J. Salamo, Brian D. Monson, William W. Clark III, Gary L. Wood, Edward J. Sharp, and Ratnakar R. Neurgaonkar

Experimental observations are reported which demonstrate that the response time for beam fanning, self-pumped phase conjugation, and double phase conjugation can be shortened by more than an order of magnitude without a significant reduction in coupling strength by using a cyclindrical lens to focus incident laser light into a photorefractive crystal. These results are compared with those obtained using a spherical lens where a reduction in the photorefractive response time is accompanied by a corresponding reduction in coupling strength. It is shown that the fidelity of a phase conjugate beam is not degraded when cylindrical optics are used.

I. Introduction

Over the last few years beam fanning,[1] self-pumped phase conjugation,[2] and double phase conjugation[3] have been demonstrated in photorefractive materials. While these effects are intriguing and have potential application, one of the noted drawbacks has been the slow time response associated with high gain materials.[4] The search for new materials and the modification of existing materials are two efforts currently being pursued to improve the response time.[5–7] For presently available materials, three other methods have been used: increased intensity,[8] higher temperature,[9,10] and applied electric fields.[11,12] This paper is an investigation of the use of higher laser intensities via focusing to improve the response time. In addition, the intensity distribution of the focused spot is used to maintain a high gain-length product.

Higher laser intensities decrease the response time by increasing the rate at which charges are excited in the illuminated areas in photorefractive crystals. Higher intensities can be achieved by turning up the laser power or by focusing the available laser light to a smaller spot. Both techniques produce faster photorefractive response times but not necessarily the same coupling strength. It will be shown that the use of a spherical lens to focus the incident beam to a tight waist decreases the response time but also decreases the magnitude of the photorefractive effect for processes involving beam fanning; however, the response time can be improved without decreasing the gain by focusing with a cylindrical lens. In particular, the photorefractive response times for beam fanning, self-pumped phase conjugation, and double phase conjugation were observed to improve by use of cylindrical focusing while maintaining approximately the original coupling strength.

In addition to response time, the fidelity of phase conjugate images produced by a self-pumped phase conjugate mirror based on cerium doped strontium barium niobate (Ce-SBN:60) was compared for the cases of spherically focused, cylindrically focused, and unfocused light. A fidelity of ~70 line pairs/mm was obtained in each case.

II. Physical Description of Beam Fanning

Beam fanning is a well known photorefractive phenomenon in which coherent light is scattered asymmetrically as it passes through a high gain crystal. The beam fan originates from conventional scattered light which crosses the incident beam and writes index gratings in the crystal via the photorefractive effect. As a result of these index gratings, energy is coupled from the incident beam into the weaker scattered beams, which can result in significant depletion of the incident beam. The magnitude of the coupling depends on the number of scatterers, the gain of the

Ratnakar R. Neurgaonkar is with Rockwell International Science Center, Thousand Oaks, California 91360; G. J. Salamo and B. D. Monson are with University of Arkansas, Physics Department, Fayetteville, Arkansas 72701; and the other authors are with CECOM Center for Night Vision & Electro-Optics, Fort Belvoir, Virginia 22060-5677.

Received 14 June 1990.

Improved photorefractive time response using a cylindrical lens

Gregory J. Salamo, Brian D. Monson, William W. Clark III, Gary L. Wood, Edward J. Sharp, and Ratnakar R. Neurgaonkar

Experimental observations are reported which demonstrate that the response time for beam fanning, self-pumped phase conjugation, and double phase conjugation can be shortened by more than an order of magnitude without a significant reduction in coupling strength by using a cyclindrical lens to focus incident laser light into a photorefractive crystal. These results are compared with those obtained using a spherical lens where a reduction in the photorefractive response time is accompanied by a corresponding reduction in coupling strength. It is shown that the fidelity of a phase conjugate beam is not degraded when cylindrical optics are used.

I. Introduction

Over the last few years beam fanning,[1] self-pumped phase conjugation,[2] and double phase conjugation[3] have been demonstrated in photorefractive materials. While these effects are intriguing and have potential application, one of the noted drawbacks has been the slow time response associated with high gain materials.[4] The search for new materials and the modification of existing materials are two efforts currently being pursued to improve the response time.[5-7] For presently available materials, three other methods have been used: increased intensity,[8] higher temperature,[9,10] and applied electric fields.[11,12] This paper is an investigation of the use of higher laser intensities via focusing to improve the response time. In addition, the intensity distribution of the focused spot is used to maintain a high gain-length product.

Higher laser intensities decrease the response time by increasing the rate at which charges are excited in the illuminated areas in photorefractive crystals. Higher intensities can be achieved by turning up the laser power or by focusing the available laser light to a smaller spot. Both techniques produce faster photorefractive response times but not necessarily the same coupling strength. It will be shown that the use of a spherical lens to focus the incident beam to a tight waist decreases the response time but also decreases the magnitude of the photorefractive effect for processes involving beam fanning; however, the response time can be improved without decreasing the gain by focusing with a cylindrical lens. In particular, the photorefractive response times for beam fanning, self-pumped phase conjugation, and double phase conjugation were observed to improve by use of cylindrical focusing while maintaining approximately the original coupling strength.

In addition to response time, the fidelity of phase conjugate images produced by a self-pumped phase conjugate mirror based on cerium doped strontium barium niobate (Ce-SBN:60) was compared for the cases of spherically focused, cylindrically focused, and unfocused light. A fidelity of ~70 line pairs/mm was obtained in each case.

II. Physical Description of Beam Fanning

Beam fanning is a well known photorefractive phenomenon in which coherent light is scattered asymmetrically as it passes through a high gain crystal. The beam fan originates from conventional scattered light which crosses the incident beam and writes index gratings in the crystal via the photorefractive effect. As a result of these index gratings, energy is coupled from the incident beam into the weaker scattered beams, which can result in significant depletion of the incident beam. The magnitude of the coupling depends on the number of scatterers, the gain of the

Ratnakar R. Neurgaonkar is with Rockwell International Science Center, Thousand Oaks, California 91360; G. J. Salamo and B. D. Monson are with University of Arkansas, Physics Department, Fayetteville, Arkansas 72701; and the other authors are with CECOM Center for Night Vision & Electro-Optics, Fort Belvoir, Virginia 22060-5677.

Received 14 June 1990.

Appl. Phys. B 53, 323–329 (1991)

Applied Physics B Photophysics and Laser Chemistry

Color Imaging in Photorefractive Crystals

S. G. Rabbani[1], J. L. Shultz[1], G. J. Salamo[1], E. J. Sharp[2], W. W. Clark[2] III, M. J. Miller[2], G. L. Wood[2], and R. R. Neurgaonkar[3]

[1] University of Arkansas, Physics Department, Fayetteville, AR 72701, USA
[2] CECOM Center for Night Vision and Electro-Optics, Fort Belvoir, VA 22060-5677, USA
[3] Rockwell Science Center, Thousand Oaks, CA 91360, USA

Received 30 April 1991/Accepted 17 September 1991

Abstract. Color phase-conjugate imaging is demonstrated using a multi-colored laser beam. Speed of response, size of the image, clarity of the image, and the intensity of the image are investigated. Color images are stored and recalled without crosstalk between different colors.

PACS: 42.80. 42.30, 42.65

One of the more amazing properties of photorefractive crystals is their ability to store and manipulate optical images. This ability has been beautifully demonstrated in many experiments using monochromatic laser light. In this paper we report on several techniques, using photorefractive crystals, which demonstrate the storage and recall of color images. Each of these techniques depends on a basic photorefractive phenomenon called beam fanning.

1 Beam Fanning

Allow a monochromatic laser beam from an argon-ion laser to propagate through a photorefractive crystal [1]. Light scattered from imperfections in the crystal bulk can cross the incident beam and write an interference pattern. The interference pattern then causes charges to be selectively excited in the light areas and diffuse into the dark areas where they are re-trapped. The diffusion of charge from areas which are illuminated with laser light to areas which are dark therefore results, at equilibrium, in a charge separation. The charge separation then induces an electric field and causes a change in the index of refraction via the electro-optic effect. The resulting index change is 90° phase shifted from the original intensity interference pattern. This shift is then responsible for the selective energy transfer from the incident beam into the scattered light to one side of the crystal as seen in Fig. 1. The scattered light pattern resembles that of a fan and is therefore termed "beam fanning" [2]. This beam fanning phenomenon plays an important role in each of the color imaging techniques which will be described in this paper.

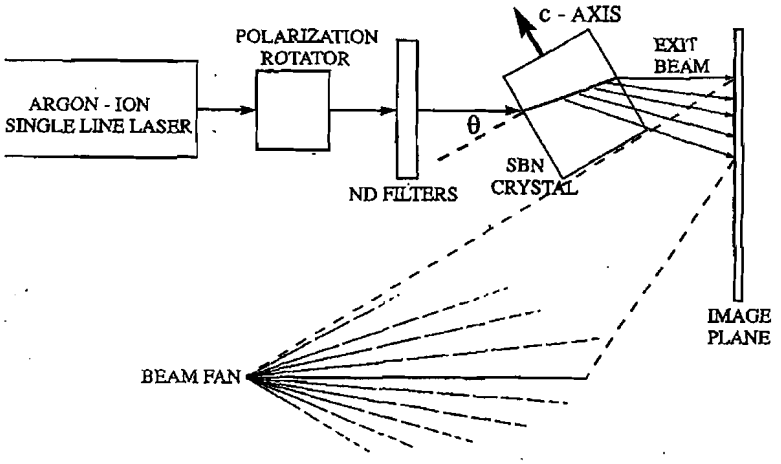

Fig. 1. Amplified scattered light pattern or "beam fan" observed in photorefractive SBN crystals

Enhanced photorefractive beam fanning due to internal and external electric fields

William W. Clark III, Gary L. Wood, Mary J. Miller, Edward J. Sharp, Gregory J. Salamo, Brian Monson, and Ratnakar R. Neurgaonkar

Significant increases (×10) in both speed and gain of the beam fanning process were obtained via three different methods in SBN and BSKNN. These methods involve the creation of a dc electric field either (1) externally, (2) by the pyroelectric effect, or (3) by thermally cycling the crystal and the presence of laser radiation. The enhanced effects were observed for both ordinary and extraordinary polarized light.
Key words: photorefraction, SBN, BSKNN, space-charge field, beam coupling.

I. Introduction

Beam fanning[1] is a well-known photorefractive phenomenon in which light from a laser is scattered asymmetrically as it passes through a high gain crystal. This is a result of the two-beam coupling[2] process where the input beam interacts with its own scattered light, forms a diffraction grating, and couples additional energy into the scattered light. This weakens the transmission in the direction of propagation and produces a broad fan of light to one side of the main beam as shown in Fig. 1.

Beam fanning has possible use in optical communications,[3] optical limiting,[4] motion detection,[5] and plays an auxiliary role in the formation of self-pumped phase conjugators[6] and double phase conjugate mirrors.[7] Most of these applications demand both fast response and high gain, but few, if any, current materials are considered able to meet both criteria. We report on experiments which show that significant increases in both speed and gain can be obtained from application of an electric field in SBN and BSKNN. In addition, these increases were obtained for ordinary as well as extraordinary polarized light. An example of the enhanced fan is shown in Fig. 2. Note that much more light appears in the enhanced fan in just two seconds than in the normal (zero-field) fan after a considerably longer time [Fig. 1(b)].

The electric field which produces the enhanced effect could be applied directly or it could be self-generated through temperature changes. In fact, three alternate techniques were used to produce enhanced effects: (1) the external field method, (2) the pyroelectric method, and (3) the thermal cycle method. In Fig. 2 the crystal was prepared using the latter method, although similar results were observed by using any of the three methods. Each of these methods along with corresponding quantitative results are presented below.

II. Experimental Apparatus

For these experiments, the amount of beam fanning was measured by observing the decrease in the straight-through transmission of a laser beam as it passed through a photorefractive crystal. As seen in Fig. 3, radiation from either a He–Cd laser (442 nm) or a He–Ne laser (633 nm) was directed normally to the (100) face of the crystal which was housed in a temperature controlled oven. The power at the crystal from each laser was ~5 mW in a TEM_{00} mode and the spot size was ~1.8 mm in diameter. After leaving the crystal, the on-axis radiation passed through an aperture (~3-mm diameter) and the decrease in transmission was measured by use of a silicon diode detector. For visual observation the aperture and detector were replaced by a screen and the transmitted light could be photographed or recorded with a video camera. Although enhanced results were observed for many of our SBN and BSKNN crystals, most of the curves and calculations which follow will be for our 0.65-cm cube of cerium doped SBN:60 (crystal 3 of Ref. 8) because of knowledge of its material properties.

Ratnakar Neurgaonkar is with Rockwell International Science Center, Thousand Oaks, California 91360; G. J. Salamo and B. Monson are with University of Arkansas, Fayetteville, Arkansas 72701; and the other authors are with CECOM Center for Night Vision & Electro-Optics, Fort Belvoir, Virginia 22060-5677.
Received 7 August 1989.
0003-6935/90/091249-10$02.00/0.

Double phase conjugation in tungsten bronze crystals

Edward J. Sharp, William W. Clark III, Mary J. Miller, Gary L. Wood, Brian Monson, Gregory J. Salamo, and Ratnakar R. Neurgaonkar

In this paper we report a new method for double phase conjugation particularly suited to the tungsten bronze crystal strontium barium niobate. It has also been observed to produce conjugate waves in $BaTiO_3$ and BSKNN. This new arrangement is called the bridge conjugator because the two beams enter opposing [100] crystal faces and fan together to form a bridge without reflection off a crystal face. Our measurements indicate that the bridge conjugator is competitive with previously reported double phase conjugate mirrors in reflectivity, response time, ease of alignment, and fidelity.

I. Introduction

New photorefractive materials have been the subject of intense research over the last few years. The motivation is provided by the unique ability of these materials to display high optical nonlinearities with milliwatt power outputs. This makes them good candidates for the fields of holography, optical processing, and nonlinear optics.

One application for photorefractive crystals is the production of the phase conjugate replica of an incident optical wave. The earliest method for producing a conjugate wave in a photorefractive crystal was by a four-wave mixing process where two of the optical waves called pumping beams were externally supplied.[1] These two beams were mixed in the crystal with a third beam, the optical wave to be conjugated, and together they produced the phase conjugated signal wave. An early simplification of this technique avoided the use of externally supplied pumping beams by using mirrors to generate the pumping beams from the input wave.[2] Later, the mirrors themselves were replaced by reflections off the crystal walls. In this "self-pumped phase conjugate mirror"[3] no external pumping beams or mirrors were required, a single laser beam was directed into the crystal and a phase conjugate replica was automatically reflected. The latest development has been the "double phase conjugate mirror" (DPCM)[4] where the photorefractive material acts as a conjugate mirror for two incoming waves simultaneously. DPCMs require no external pumping beams and the two incident beams need not be coherent with each other.

Ratnakar Neurgaonkar is with Rockwell International Science Center, Thousand Oaks, California 91360; B. Monson and G. J. Salamo are with University of Arkansas, Fayetteville, Arkansas 72701; and the other authors are with CECOM Center for Night Vision & Electro-Optics, Fort Belvoir, Virginia 22060-5677.

Received 27 March 1989.

II. Description of Experiment

In this paper, we report a new method for double phase conjugation which is particularly suited to the tungsten bronze crystal strontium barium niobate (SBN) and which has also been observed in $BaTiO_3$ and BSKNN. The geometry for this new DPCM is shown in the photographs of Fig. 1. The c-axis is directed from bottom to top in these photographs and the beams enter opposing [100] crystal faces with wave-vector components in the $+c$-direction. In Fig. 1(a) the two beams are crossing in the crystal at a time $t = 0$. After the conjugates have appeared the beams overlap each other as shown in Fig. 1(b). Because the two beams bridge together in the crystal without reflecting off a crystal face, this arrangement is called a "bridge conjugator."

To describe the operation of this new double phase conjugator, it will be useful to review a basic phenomenon that occurs when a laser beam propagates through a photorefractive material. This phenomenon is called "beam fanning."[5] When the laser beam passes through the crystal, light is scattered due to crystal imperfections. The scattered light, though weak in intensity when compared to the incident beam, can cross and interfere with the incident beam, eventually creating a weak index modulation grating by photorefractive charge transfer and the Pockel effect. This initially weak grating, however, causes asymmetric (relative to the c-axis) energy transfer[6] to the scattered light from the more intense incident beam. This process is governed by the coupled Maxwell equations described in Ref. 7 and depends on the polarization of the incident beams in conjunction with the electrooptic coefficients. As the scattered light builds in intensity it may also result in secondary scattered beams which form additional gratings. This process continues as the scattered light becomes more intense and its distributions more complex. As a result the incident beam is depleted due to the myriad of gratings formed and energy is transferred from the incident beam to the scattered light.

Self-pumped phase conjugation with nanosecond pulses in strontium barium niobate

Brian Monson and Gregory J. Salamo

Department of Physics, University of Arkansas, Fayetteville, Arkansas 72701

Andrew G. Mott, Mary J. Miller, Edward J. Sharp, William W. Clark III, and Gary L. Wood

CECOM Center for Night Vision and Electro-Optics, Fort Belvoir, Virginia 22060-5677

Ratnakar R. Neurgaonkar

Rockwell Science Center, Thousand Oaks, California 91360

Received July 25, 1989; accepted October 25, 1989

We report the observation of self-pumped phase conjugation by means of internal reflection in a photorefractive medium produced by a series of intense nanosecond pulses. Nanosecond pulses from a YAG laser ranging in intensity from 9×10^4 to 9×10^5 W/cm^2 were used. The crystal was rhodium-doped strontium barium niobate. The conjugate signal began with the first pulse, and the time to reach 63% of its equilibrium value scaled as I^{-2}. The equilibrium reflectivity was 29%. A similar cw experiment with the 514-nm line of an argon laser produced a response time that scaled as $I^{-1.1}$.

Self-pumped phase conjugation[1] occurs in many different photorefractive crystals using milliwatt-level cw lasers. In this process, extraordinarily polarized light brought into a crystal scatters asymmetrically. Some of this scattered light internally reflects from the corner and forms a loop similar to that shown in Fig. 1. The light in this loop undergoes four-wave mixing with the input beam and generates its phase conjugate. A phase conjugate can form in a few seconds with a low-power cw beam. Since previous studies have shown that the response time varies inversely with intensity, the higher intensity available from pulsed lasers should greatly reduce this response time. Phase conjugation with nanosecond pulses using three input beams in $BaTiO_3$ has been reported.[2] Self-pumped phase conjugation with short pulses has been previously demonstrated by several groups for use as phase-conjugate mirrors in dye lasers.[3-6] The previous researchers did not measure the response time as a function of input intensity or show that conjugation begins during the first pulse. We also find that the time response is different from the cw response for the same crystal.

The crystal used in our experiments is a 6.3 mm × 5.9 mm × 6.2 mm piece of rhodium-doped strontium barium niobate (SBN:60) grown at the Rockwell Science Center. The c axis is parallel to the 6.3-mm side. It was poled to a single domain, and the charge carriers were found to be negative.

The output beams of an air-cooled argon-ion laser operating at 514 nm and a Q-switched, frequency-doubled Nd:YAG laser were combined at a beam splitter and made to be collinear. The YAG laser had a pulse width of 15 nsec FWHM and a repetition rate of 10 Hz. Both lasers operated in a TEM_{00} mode and had a $1/e^2$ diameter of 2.3 mm as measured with a beam-profiling system. A fraction of the YAG beam was picked off with a wedge and sent to a calibrated detector to monitor the energy at the crystal. The conjugate return was also sampled with a wedge and sent to a second detector. The outputs of both detectors were then digitized and sent to a computer for storage and analysis. Extraordinary light was used to produce a conjugate beam. Between runs, the polarization of the argon laser was rotated to ordinary, and the beam was expanded to illuminate the crystal uniformly and erase the gratings.

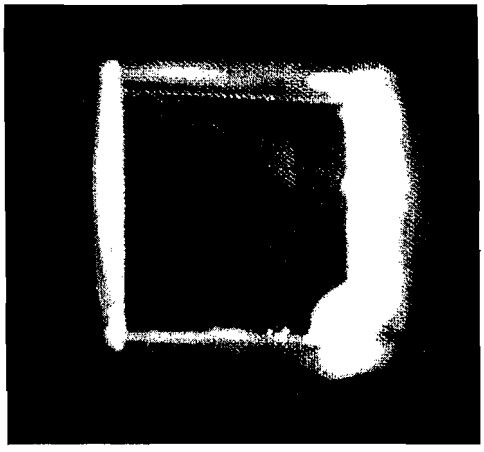

Fig. 1. Photograph of the characteristic loop of light found in the crystal while it was self-pumping after a series of 15-nsec pulses had driven the conjugate to its steady state. The photograph was made with the light of a single pulse. The laser beam enters the crystal from the right edge at an angle of ~40° below the normal. The c axis is directed from top to bottom.

0146-9592/90/010012-03$2.00/0

Electron impact excitation of the $3p(^5P)$ state of atomic oxygen

G. A. Germany, R. J. Anderson, and G. J. Salamo
University of Arkansas, Fayetteville, Arkansas 72701

(Received 21 March 1988; accepted 9 May 1988)

The 157.6 nm output from a fluorine excimer laser is focused in a vacuum chamber containing O_2 gas at a pressure of 20 mTorr. Laser photodissociation of the O_2 target gas produces $2p^4(^3P)$ and $2p^4(^1D)$ oxygen atoms with unit quantum efficiency. A low-energy electron beam is crossed with the laser beam to produce $3p(^5P)$ excited states of OI via electron impact excitation of the $2p^4(^3P)$ ground state. Intensity measurements of the 777.4 nm radiation, corresponding to the $3p(^5P)$–$3s(^5S)$ transition, are used to calculate the excitation cross section of the $3p(^5P)$ state of atomic oxygen. Absolute optical cross sections are reported for a range of incident electron energies less than 18 eV.

INTRODUCTION

Because of its prominence as an excitation mechanism for the aeronomically important states of atomic oxygen (OI), electron impact excitation has been of continuing interest to atmospheric researchers. The present experiment reflects this interest and the continuing need for additional electron excitation cross section data. It is based on the previous work of Germany *et al.*[1] in which (i) vacuum ultraviolet photodissociation of O_2 was used to produce the $O(^1D)$ state and (ii) time-resolved analysis of the resulting $2p^4(^1D)$–$2p^4(^3P)$ transition at 630.0 nm yielded its collisional deactivation cross section. Here, the VUV photodissociation technique is used to produce the $2p^4(^1D)$ metastable state as well as the $2p^4(^3P)$ ground state which is subsequently excited by low-energy electron excitation to produce a $3p(^5P)$ atomic oxygen gas sample (Fig. 1).

The $O(^5P)$ sample is monitored to determine the optical cross section for the emission of the 777.4 nm radiation corresponding to the $3p(^5P)$–$3s(^5S)$ transition of atomic oxygen. In addition, the radiative decay of the metastable $O(^1D)$ state is detected as a monitor of the atomic density of the $O(^3P)$ ground state target sample. Using this two-step photon-dissociation, electron-excitation technique, absolute values of the 777.4 nm optical cross sections for atomic oxygen are determined. Although Doering *et al.*[2] recently performed an energy-loss measurement of the $3p(^5P)$ excitation cross section for 30 eV incident electrons, the 777.4 nm optical data reported here is believed to be the first measurement of the excitation function for this important transition.

TECHNIQUE

Apparatus

The present apparatus (Fig. 2) utilizes a fluorine excimer laser (157.6 nm; 2 mJ peak; 10 Hz) to excite the parent oxygen molecule, with unit quantum efficiency,[3] to a dissociative state ($B\,^3\Sigma_u^-$) that results in the ground $2p^4(^3P)$ and metastable $2p^4(^1D)$ states of atomic oxygen. Because the photoabsorption process provides excess energy beyond that needed for the production of $O(^1D)$ and $O(^3P)$, each of the products share 0.8 eV of kinetic energy[4] (corresponding to a velocity of about 2×10^5 cm/s). Because time-resolved experimental measurements indicated that significant field-of-view signal losses occur in the present optical measurements >3 μs after the exciting laser pulse, the experiment is performed within 1.5 μs after the incident laser pulse. Therefore, field-of-view losses are not significant.

Due to high molecular oxygen absorption of the laser VUV radiation at atmospheric pressures, the laser output is coupled to the collision chamber via a flexible tube through which helium is flowed. In addition to the VUV emissions, the laser also produces visible fluorescent emissions which are discriminated against by a series of optical stops, apertures, and light traps.

The experiment is housed in a stainless steel high-vacuum collision chamber pumped by two liquid-nitrogen-trapped diffusion pumps. A calibrated leak valve is used to

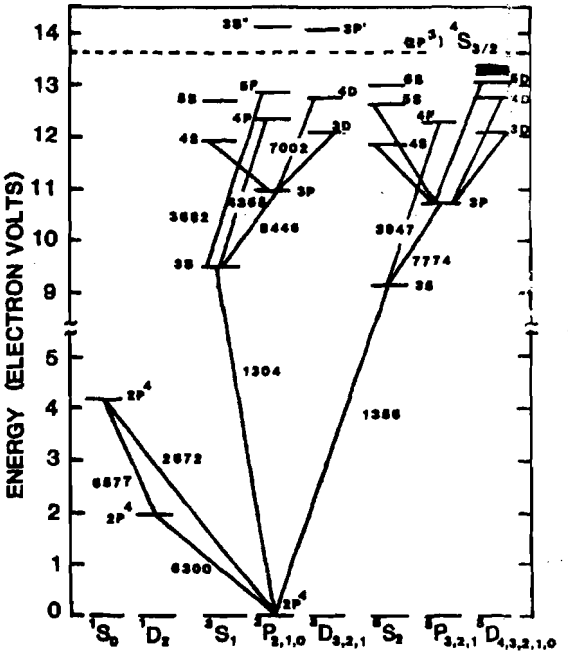

FIG. 1. Atomic oxygen energy diagram. Three manifolds of states are formed from the ground and excited state configurations. Emission cross sections for the 777.4 nm transition are reported.

 0021-9606/88/161989-04$02.10

Self-pumped phase conjugation in the red in photorefractive $Ba_{0.5}Sr_{1.5}K_{0.25}Na_{0.75}Nb_5O_{15}$ and $Sr_{0.6}Ba_{0.4}Nb_2O_6$ with cerium in 9-fold coordinated sites

Steven R. Montgomery, Jan Yarrison-Rice, Donald O. Pederson, and Gregory J. Salamo

University of Arkansas, Fayetteville, Arkansas 72701

Mary J. Miller, William W. Clark III, Gary L. Wood, and Edward J. Sharp

Center for Night Vision and Electro-Optics, Fort Belvoir, Virginia 22060-5677

Ratnakar R. Neurgaonkar

Rockwell International Science Center, Thousand Oaks, California 91360

Received January 15, 1988; accepted March 17, 1988

Self-pumped phase conjugation has been observed at selected laser wavelengths over the range 647–780 nm. Phase-conjugate reflectivities as great as 20% were measured for power levels ranging from 2 to 100 mW. In addition, phase-conjugate and beam-fanning response times were also measured. Our observations were carried out in crystals belonging to the tungsten-bronze family; these crystals were doped with cerium at the 9-fold coordinated lattice sites to give a red photorefractive response.

INTRODUCTION

We report the first observation of self-pumping[1] in barium strontium potassium sodium niobate (BSKNN) and strontium barium sodium niobate (SBN) with cerium in 9-fold coordinated sites.[2] The advantage of this dopant site is an increase in the photorefractive effect at longer wavelengths; the observations reported here were carried out at selected laser lines between 647 and 780 nm. Phase-conjugate reflectivities as great as 20% were observed, although no attempt at optimization was made. In addition, phase-conjugate formation times and beam-fanning response times were recorded.

This work extends the wavelength range over which self-pumping can be observed in BSKNN and SBN. In previous experiments using crystals with Ce in 12-fold coordinated sites, self-pumping could only be weakly observed in the red at 633 nm.[3–5] Our current observations exemplify an interesting and useful feature of tungsten-bronze crystals, i.e., the spectral response of these crystals can be significantly altered by changing the site preference of the Ce ion.

CRYSTAL PROPERTIES

Tungsten-bronze oxides[6] have a composition that is represented by either of the general formulas $(A_1)_4(A_2)_2B_{10}O_{30}$ or $(A_1)_4(A_2)_2C_4B_{10}O_{30}$, in which A_1, A_2, C, and B are 15-, 12-, 9-, and 6-fold coordinated sites, respectively. The tetragonal bronze structure is shown in Fig. 1 as a projection onto the (001) plane.[7,8] The sites A_1, A_2, C, and B are shown from a perspective perpendicular to the (001) direction in Fig. 2. For an undoped SBN crystal, the 12- and 15-fold sites are occupied by Ba^{2+} and Sr^{2+}, whereas in BSKNN these sites are occupied by Ba^{2+}, Sr^{2+}, K^+, and Na^+. For both materials the 6-fold sites are occupied by Nb^{5+}, whereas the 9-fold sites are generally empty. When doping the tungsten-bronze crystals with Ce or other rare-earth ions, the dopant ion is found to have a preference for the 12-fold sites. However, one of the inherent flexibilities of the tungsten-bronze structure is that the dopant ion can also be forced into either the 9- or 6-fold sites. As a result of the choice offered between these three sites, the material properties can be intentionally changed.

The site location of the impurity ion is distinctly identified by the color of the crystal. When the Ce ions are located in the 12-fold coordinated sites, the crystals are pink in color and have a broadband absorption spectrum ranging from 0.6 μm to the band edge, which is near 0.4 μm. On the other hand, when Ce is forced into the 9-fold coordinated sites, the color is greenish yellow and has an absorption profile that extends into the near infrared. The transmission spectra of our SBN crystals with Ce in the 12- and 9-fold coordinated sites are shown in Fig. 3. For comparison, the transmission spectrum of an undoped SBN sample is also shown in Fig. 3. The undoped sample lacked any noticeable color. For this work on SBN and BSKNN, Ce is in the 9-fold coordinated sites, making the observed photorefractive response in the red possible.

The growth of Ce-doped tungsten-bronze crystals used in these experiments is discussed in recent review papers.[9,10] These crystals exist on a $SrNb_2O_6$–$BaNb_2O_6$–$KNbO_3$–$NaNbO_3$ quaternary system and are labeled SBN:60 and

0740-3224/88/081775-08$02.00

Broadband Photorefractive Properties and Self-Pumped Phase Conjugation in Ce–SBN:60

GARY L. WOOD, WILLIAM W. CLARK III, MARY J. MILLER, MEMBER, IEEE, EDWARD J. SHARP, GREGORY J. SALAMO, AND RATNAKAR R. NEURGAONKAR

Abstract—The first use of cerium-doped $Sr_{0.6}Ba_{0.4}Nb_2O_6$ as a broadband self-pumped phase-conjugate mirror using internal reflection is reported. The phase-conjugate reflectivity at normal incidence ranged from two percent at 442 nm to seven percent at 515 nm and was zero at 633 nm. The electron-hole competition was found to be significant and had a wavelength dependence in one sample but not the other. The charge carrier density was $\sim 7 \times 10^{16}$ cm^{-3} and was wavelength independent. The absorption coefficient ranged from 2 cm^{-1} at the shorter the wavelengths to zero at longer wavelengths. The dispersion in the indexes of refraction was measured and the birefringence was -0.036. The sign of the dominant charge carriers was determined to be negative and the sign of the electrooptic coefficient, r_{13}, was positive. Using the above values, a wavelength dependent coupling coefficient has been determined. The experimental results indicate that the phase-conjugate reflectivity decreases at shorter wavelengths due to increased absorptive losses and experiences a threshold effect at longer wavelengths.

Introduction

THE ferroelectric crystal $Sr_{0.6}Ba_{0.4}Nb_2O_6$ (SBN:60) belongs to the tungsten-bronze structural family and has received considerable attention recently due to its attractiveness for electrooptic, photorefractive, pyroelectric, and millimeter wave applications [1]–[3]. It was shown to be an efficient two-beam mixing material by Megumi *et al.* [4] after the introduction of Ce-ions as impurity dopants. The first use of undoped SBN:60 as a photorefractive four-wave mixing medium employed external pumping beams and resulted in phase-conjugate reflectivities exceeding unity [5]. This was quickly followed by a demonstration of passive phase conjugation in undoped SBN:60 based on self-induced oscillation in an optical ring cavity [6]. The first use of SBN:60 as a self-pumped phase-conjugate mirror (SPPCM) requiring no external mirrors or pumping beams, yielded phase-conjugate reflectivities of 60 percent in undoped crystals and 30 percent in Ce-doped crystals at 442 nm [7]. To date only three crystals have demonstrated self-pumped phase conjugation: $BaTiO_3$ [8], SBN [7], [9], and BSKNN [10].

In this paper, we present our experimental data characterizing Ce-doped SBN:60 as a broadband photorefractive material. Specifically, we demonstrate for the first time self-pumped phase conjugation in this material over a broad spectral range in the visible. We have determined the charge carrier density, the electron-hole competition, and the gain coupling coefficient through two-beam coupling measurements at 488 nm and 633 nm. In addition, we have measured the refractive indexes, the absorption coefficient, and the poling factor. By taking the dispersion of these measured parameters into account, we provide a calculation of the wavelength dependence of the coupling coefficient and explain the relationship of absorption to self-pumped phase conjugation.

Manuscript received March 9, 1987; revised June 12, 1987.

G. L. Wood, W. W. Clark III, M. J. Miller, and E. J. Sharp are with the Center for Night Vision and Electro-Optics, Fort Belvoir, VA 22060.

G. J. Salamo is with the Department of Physics, University of Arkansas, Fayetteville, AR 72701.

R. R. Neurgaonkar is with the Rockwell International Science Center, Thousand Oaks, CA 91360.

IEEE Log Number 8717189.

Growth of Doped SBN:60 Single Crystals

A comprehensive review of the status of the growth and applications of the tungsten-bronze family crystals, with emphasis on the $Sr_{1-x}Ba_xNb_2O_6$ solid-solution system, can be found in the paper and references therein by Neurgaonkar and Cory [11]. Of particular interest in this class of materials is SBN:60 since it is the only congruent melting composition in the $SrNb_2O_6$–$BaNb_2O_6$ system [12]. Concentrated crystal growth efforts on this composition have resulted in good optical-quality doped and undoped crystals. Boules as large as 2 to 2.5 cm in diameter are now routinely grown and allow the fabrication of photorefractive crystal cubes approaching 2 cm on a side (see Fig. 1).

These large optical-quality crystals of both Ce-doped and undoped SBN:60 have been grown by suppressing the problems associated with coring and striation. The addition of cerium produces a broadband absorption in the visible which enhances the photorefractive effect considerably in this crystal [4], [13]. In the tungsten-bronze structure, Ce^{3+} and Ce^{4+} ions are expected to occupy 9- and 12-fold sites, while Fe^{2+} and Fe^{3+} ions are expected to occupy 6-fold coordinated sites. To date, attempts to suppress striations in Fe-doped SBN:60 have been unsuccessful. This suggests that the existence of striations in SBN:60 crystals depends strongly on the type of dopant and its location in the structure [11]. Table I summarizes the growth conditions and typical physical properties of Ce-doped and undoped SBN:60 crystals.

For our photorefractive and SPPCM studies, high optical-quality SBN:60 samples, both undoped and nominally-doped with cerium, were cut from different boules, optically polished, and poled to a single domain. In all,

0018-9197/87/1200-2126$01.00

Time response of a cerium-doped $Sr_{0.75}Ba_{0.25}Nb_2O_6$ self-pumped phase-conjugate mirror

Mary J. Miller, Edward J. Sharp, Gary L. Wood, and William W. Clark III

Center for Night Vision & Electro-Optics, Fort Belvoir, Virginia 22060-5677

Gregory J. Salamo

University of Arkansas, Fayetteville, Arkansas 72701

Ratnakar R. Neurgaonkar

Rockwell International Science Center, Thousand Oaks, California 91360

Received December 1, 1986; accepted February 5, 1987

Self-pumping in cerium-doped strontium barium niobate has been observed with phase-conjugate reflectivities near 6% and a formation time of 8 sec for a 200-mW/cm² beam at 442 nm. The time response for asymmetrical self-defocusing was also measured, and the observed transmissions through the crystal at normal incidence were limited to about 1.5% of the incident radiation.

A great deal of attention has been given to self-pumped photorefractive phase-conjugate mirrors for a wide variety of applications.[1-3] These mirrors exhibit a number of attractive features, including high reflectivity, a modest wavelength range of operation, and only milliwatt beam-power requirements for start-up. Self-pumped phase conjugation,[4] as reported here, operates on internal reflection and is completely self-contained, requiring no external mirrors,[5] pumping beams,[6] or applied electric fields. The only known demonstrations of self-pumping using internal reflection have been in $BaTiO_3$,[4,7] undoped and cerium-doped strontium barium niobate (SBN),[9] and cerium-doped barium strontium potassium niobate (BSKNN).[10]

In this Letter we report on self-pumped phase conjugation in a single crystal of cerium-doped $Sr_xBa_{1-x}Nb_2O_6$, $x = 0.75$ (SBN:75). The addition of cerium produces a broad absorption in the visible, which enhances the photorefractive effect considerably in this crystal.[11,12] The 0.05 wt. % cerium-doped SBN:75 crystal used in this study was an approximately 5 mm × 5 mm × 5 mm cube, poled at 8 kV/cm at a temperature well above the Curie temperature of 56°C.[13] SBN:75 is tetragonal, has a 4-mm point group symmetry, and possesses a strong transverse electro-optic coefficient, r_{33}, as do other SBN compositions. By contrast, BSKNN and $BaTiO_3$ exhibit a strong longitudinal electro-optic coefficient, r_{51}. The phase-conjugate reflectivity of SBN:75 measured at 442 nm is similar to that previously reported for $BaTiO_3$,[7] BSKNN,[10] and SBN:60.[8,9] In addition to the behavior of SBN:75 as a self-pumped phase-conjugate mirror, we also report on the time required for the onset of the phase-conjugate beam[14,15] and the time needed to deamplify the beam through asymmetrical self-defocusing (beam fanning).[8,16,17] These characteristic times were measured as a function of the pump intensity for a fixed spot size.

The phase-conjugate reflectivity and response-time measurements were recorded using the experimental arrangement depicted in Fig. 1. A He–Cd laser provided an extraordinary polarized beam at 442 nm. The incident beam was 2.5 mW, with a $1/e^2$ beam diameter of 1.8 mm at the crystal. Neutral-density filters (ND's) were used to vary the input intensity of the beam from 200 mW/cm² to a few milliwatts per square centimeter. The beam was incident upon the crystal at an angle of $\theta = -50°$ to the normal of the c axis, so that it was directed toward a crystal corner where retroreflection provided feedback for the four-wave mixing process and the subsequent phase-conjugate beam buildup. The phase-conjugate beam intensity was determined as a function of time at detector D1 (see Fig. 2). As can be seen from the data, the temporal buildup of the phase-conjugate intensity for the self-pumping configuration is nonexponential, as would be expected of a phenomenon that is a stimulat-

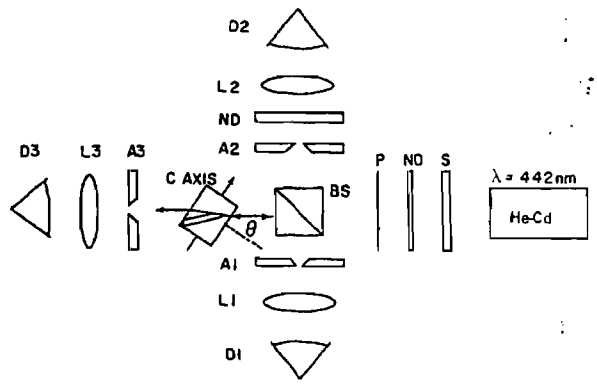

Fig. 1. Diagram of the experimental apparatus used to measure the phase-conjugate reflectivity and characteristic response times of the cerium-doped SBN:75 crystal. P, polarizer; L1, L2, lenses.

0146-9592/87/050340-03$2.00/0

BSKNN as a self-pumped phase conjugator

Juan Rodriguez, Azad Siahmakoun, Gregory Salamo, Mary J. Miller, William W. Clark III, Gary L. Wood, Edward J. Sharp, and Ratnakar R. Neurgaonkar

Self-pumping has been observed in a cerium-doped $Ba_{2-x}Sr_xK_{1-y}Na_yNb_5O_{15}$ (BSKNN) crystal at four argon-ion laser wavelengths. Phase-conjugate reflectivities as high as 30% were measured with response times inversely proportional to the 0.5 power of the input intensity. The response time for beam fanning in the crystal was determined to be inversely proportional to the 0.82 power of the input intensity.

I. Introduction

Many different nonlinear phenomena and techniques have been used to produce phase-conjugate beams.[1] Until recently, however, only barium titanate[2,3] ($BaTiO_3$) and Ce-doped strontium barium niobate[4] (SBN) have been successfully demonstrated as broadband self-pumped phase-conjugate mirrors using milliwatt beams. Self-pumped phase conjugation, as reported here, is completely self-contained and requires no external mirrors,[5,6] pumping beams,[7] or applied electric fields. In our experiments, the incident beam is directed into a crystal corner via asymmetrical self-defocusing[8] where retroreflection provides the pump beams for the four-wave mixing process and the subsequent phase conjugate build-up.

Currently, both $BaTiO_3$ and SBN crystals are leading candidates for applications in many areas, including electrooptics, photorefraction, and millimeter waves. Both of the above crystals are tetragonal at room temperature with a 4-mm point group symmetry; however, $BaTiO_3$ exhibits a strong longitudinal electrooptic coefficient (r_{51}) while tungsten-bronze SBN:60 exhibits a strong transverse electrooptic coefficient (r_{33}). At this point in time, the use of $BaTiO_3$ is somewhat limited due to the extreme difficulty in growing doped crystals of adequate size and quality for a number of applications. For this reason, Neurgaonkar *et al.* introduced the tungsten-bronze $Ba_{2-x}Sr_xK_{1-y}Na_yNb_5O_{15}$(BSKNN) solid solution system[9] and has since grown optical quality, twin-free, doped and undoped BSKNN crystals.

Specifically, $Ba_{1.5}Sr_{0.5}K_{0.75}Na_{0.25}Nb_5O_{15}$ (BSKNN-1) and $Ba_{0.5}Sr_{1.5}K_{0.5}Na_{0.5}Nb_5O_{15}$ (BSKNN-2) have been grown using an automatic, diameter-controlled Czochralski pulling technique. The growth of BSKNN-1 crystals is much more difficult than that of BSKNN-2 which indicates that BSKNN-2 is closer to the congruent melting composition in this solid solution system. These crystals resemble both SBN and $BaTiO_3$ in many respects, i.e., point group symmetry, optical properties, and ferroelectric properties. The electrooptic effect in BSKNN-2 is strongly longitudinal as in $BaTiO_3$.

In this paper we confine our photorefractive phase conjugation experiments to the BSKNN-2 composition. BSKNN-2 is characterized by a sharp anomaly in the polar-axis dielectric constant at the ferroelectric phase-transition temperature occurring between 170 and 178°C. The room temperature dielectric constants, $\epsilon_\parallel = 170$ and $\epsilon_\perp = 750$, have been measured for poled samples at 10 kHz.[9] For crystals poled to a single ferroelectric domain, the dielectric dispersion has been found to be minimal over the range of 100 Hz to 100 kHz.[9]

The sign of the electrooptic coefficient, r_{33}, has been determined to be positive by use of a calibrated compensator. This fact, coupled with the observation that extraordinary light fans toward the electrode held positive during poling, gives a negative sign for the photorefractive charge carriers, as similarly found in SBN. By comparison, the charge carriers in $BaTiO_3$ are positive and extraordinary light fans toward the negative poling electrode.[10] The transmission spectra for our BSKNN-2 samples, both doped and undoped, are shown in Fig. 1, curves *a* and *b*, respectively.

Ratnakar Neurgaonkar is with Rockwell International Science Center, Thousand Oaks, California 91360; J. Rodriguez, A. Siahmakoun, and G. Salamo are with University of Arkansas, Physics Department, Fayetteville, Arkansas 72701; the other authors are with Center for Night Vision and Electro-Optics, Fort Belvoir, Virginia 22060-5677.

Received 29 October 1986.

1252 **Spectral Characteristics of Optically Stimulable MgS:Eu,Sm Phosphor:** *V. K. Mathur* and R. J. Abbundi,* Naval Surface Weapons Center, Silver Spring, MD 20903-5000 and *M. Hill* and *J. J. Brown,* Dept. of Materials Engineering, Virginia Polytechnic Institute and State University, Blacksburg, VA 24061

Optically stimulable MgS:Eu,Sm phosphors have been synthesized from magnesium sulfate by CS_2 reduction in the presence of argon. The absorption spectrum of this phosphor consists of an absorption edge at about 260 nm and two absorption bands near 320 and 420 nm. The emission under UV excitation (250-280 nm) consists mainly of two sharp bands at 570 and 607 nm. However, the emission spectrum changes as the excitation is moved to longer wavelengths.

1253 **Dynamic Aspects of Electrochromism in Lu-diphthalocyanine Films:** *K. Aoyama,* H. Tsuda, J. Hanna,* and *H. Kokado,* Tokyo Institute of Technology, 4259, Nagatsuta-cho, Midori-ku, Yokohama, Kanagawa 227, Japan

A solid electrochromic cell consisting of Lu-diphthlocyanine and PbF_2 (solid electrolyte) exhibited essentially the same characteristics to the solution cell. The dynamics of the reaction were investigated mainly with a solution cell. The transient current at the coloring process was examined as functions of the anion concentration, the thickness and the history of electrochromic layer. The current seemed to reflect the speed of movement of the green/red interface where the electrochromic reaction is taking place.

1254 **Direct Current Electrochemiluminescence of $Ru(bpy)_3^{2+}$:** *R. Igarashi,* Y. Nosaka, H. Miyama, M. Kaneko,* and *M. Yokoyama,* Dept. of Chemistry, Technological University of Nagaoka, Kamitomioka 1603-1, Nagaoka 940-21, Japan

Direct current (dc) electrochemiluminescence (ECL) of tris(2,2'-bipyridine)ruthenium(II) [$Ru(bpy)_3^{2+}$] was observed in acetonitrile solution by using Al working electrode (W.E.) at negative potential. The dc ECL seems to originate from the excited state of $Ru(bpy)_3^{2+}$. Characteristics of the luminescence were as follows: (i) the luminescence continues for several hours, (ii) response time of the luminescence is faster than that of alternating current luminescence, and (iii) the luminescence spreads all over the W.E.

1255 **Excitonic and Edge Emissions in MOCVD Homoepitaxially Grown ZnS Crystalline Films:** *A. Sawada, Y. Kawakami, K. Kurisu, T. Taguchi,** and *A. Hiraki,* Dept. of Electrical Engineering, Faculty of Engineering, Osaka University, Suita, Osaka 565, Japan

ZnS films have successfully been grown on (100) ZnS single crystalline substrates at 400°C using low-pressure MOCVD. We describe the origins of the excitonic lines, (D^0,X) and (A^0,X), and edge emission bands in MOCVD homoepitaxially grown ZnS films using a He-Cd (325 nm) laser and luminescence excitation spectroscopy. It is pointed out that the extrinsic impurities (Na and I) and native defects involved can evaluate, as well as the sharp exciton and well-known edge emission features found in other II-VI compounds.

LUMINESCENCE AND DISPLAY MATERIALS/DIELECTRICS AND INSULATION

Materials for Fabrication Techniques for Storage Displays

1256 **Solid-State Thermoelectrochromic Display:** *S. Pantaloni, S. Passerini,* and *B. Scrosati,** Dipartimento di Chimica, Universita di Roma "La Sapienza," Roma 00185, Italy

A solid-state electrochromic display has been realized by placing into contact a lithium foil, a thin layer of a polymer electrolyte and a WO_3 film supported on a ITO-coated glass support. The response of the display is critically affected by the marked thermal dependence of the conductivity of the electrolyte. This can be conveniently exploited for the realization of devices directed to specific applications, such as electrochromic displays with optical memory, thermoelectrochromic displays, and optoelectrochromic displays.

1257 **Electrochromic Properties of Two Complexes in Erbium Phthalocyanine Compound:** *H. Yamamoto, Y. Ikuta, T. Hirota, M. Tanaka,* K. Yamada, S. Yamaguchi, K. Iida,* and *H. Yui,* College of Science and Technology, Nihon University, Narashinodai 7-24-1, Funabashi-shi, Chiba 274, Japan

Electrochromic color changes and life have been investigated in solid type of cells using different two complex films in erbiumphthalocyanine compound. Crude compounds were extracted into two complexes by soxlet method with toluene and methanol. The film prepared from purified Er-diphthalocyanine complex gave the long-life and/or stable electrochromic color changes. On the contrary, the cell using another complex film showed inferior electrochromic properties.

LUMINESCENCE AND DISPLAY MATERIALS/ENERGY TECHNOLOGY

Optical Imaging: IR Light Sources, Detectors, and Imaging Techniques

1258 **Experimental Methods for Optical Characterization of Materials:** *W. M. Yen,** Dept. of Physics and Astronomy, The University of Georgia, Athens, GA 30602

We present a brief tutorial review of spectroscopic techniques that are commonly utilized to characterize the optical properties of materials that find use in various opto-electronic applications. We discuss conventional methods, but place emphasis on experimental procedures that have evolved recently and that are, for the most part, based on various laser devices. Illustrative examples of these latter measurements are presented. (This work was supported in part by the National Science Foundation under DMR-8704486.)

1259 **Characterization of Infrared Materials and Devices by Modulation Spectroscopy:** *F. H. Pollak,* Physics Dept., Brooklyn College, Brooklyn, NY 11210

The use of modulation spectroscopy, particularly electromodulation, to characterize infrared materials such as HgCdTe (and related semiconductors) is reviewed. Electromodulation yields the sharpest structure, related to the third derivative of the optical constants, and is sensitive to surface (interface) electric fields. Information about crystal quality, process-induced effects, surface (interface) electric fields, etc. (including topographical scans and depth profiling) can be obtained from the details of the lineshape and its response to applied electric fields.

1260 **Metal-GaAs Chemistry: Use of Experiments to Understand Reactions and Their Consequences:** *W. E. Spicer,* N. Newman, Z. Liliental-Weber, E. Weber, J. Pallix,* and *C. Becker,* Stanford Electronics Laboratories, Stanford University, Stanford, CA 94305

Semiconductor metal reactions change electrical properties and location of contacts. PES, TEM, I-V, SALI, and AES develop atomic level understanding. Au on GaAs is discussed in detail. Thermodynamics and kinetics must be consistent. Annealing factors such as ambient pressure and oxide at interface can dominate. Ohmic behavior occurs only at the periphery. Schottky height is related to As excess and antisites. Results are extended to other metals. (This work was supported by DARPA, ONR, AFOSR, and DOE.)

1261 **Photorefractive Tungsten Bronze Materials:** *G. J. Salamo,* Dept. of Physics, University of Arkansas, Fayetteville, AR 72701, *M. J. Miller, W. W. Clark III, G. L. Wood,* and *E. J. Sharp,* Center for Night Vision and Electro-Optics, *R. R. Neurgaonkar,* Rockwell International Science Center, Thousand Oaks, CA 91360

We discuss the photorefractive properties of the tungsten bronze crystal $Sr_{1-x}Ba_xNb_2O_6$ and $Ba_{2-x}Sr_xK_{1-y}Na_yNb_5O_{15}$. In particular, we have characterized six different crystal types and report on such characteristics as phase conjugate reflectivity, response time, spectral response, effective density and sign of the charge carriers, and magnitude and sign of the electro-optic coefficients. In addition, we discuss the unusual crystal lattice flexibility of these materials, which should make possible the architecture of crystals with adjustable photorefractive behavior.

1262 **Nonlinear Optical Materials for Computing and Sensor Protection:** *J. A. Neff,* Defense Advanced Research Projects Agency, Arlington, VA 22209-2308

Recent research results into nonlinear optical materials have raised hopes that the interaction of optical beams with one another may soon become a practical reality and lead to many interesting applications. This paper describes two application areas that promise to benefit significantly from these nonlinear interactions: optical computing and sensor protection.

1263 **Power Combining of Semiconductor Lasers:** *J. Katz,* Jet Propulsion Laboratory, California Institute of Technology, Pasadena, CA 91109

In recent years there has been significant interest in the subject of monolithic phase-locked semiconductor laser arrays. Technical developments in this field are reviewed in the context of the more general subject of power combining of semiconductor lasers. Emphasis is placed on the basic theoretical issues and the trade-offs involved with the various power combining configurations.

1264 **Imaging CCD Focal Planes:** *N. Bluzer,* Westinghouse Advanced Technology Laboratories, Baltimore, MD 21203

Charge coupled devices (CCD's), since their invention in 1969, have become a natural choice for imaging and special signal processing applications. These special benefits are derived because CCD's operate in the charge domain. Operation in a sampled analog charge domain provides CCD's with excellent dynamic range (60 db), high speed and very high packing density. All these characteristics when combined with a special architecture have made possible the construction of CCD imagers in x-ray, visible, and IR spectra. Details of each of these imagers are detector driven. The progress attained to data in each spectrum is reported.

1265 **Progress in Photorefractive Materials for Optical Data Processing:** *G. C. Valley, M. B. Klein, D. Rytz,* and *B. A. Wechsler,* Hughes Research Laboratories, Malibu, CA 90265

Few of the photorefractive materials with large electro-optic coefficients, such as $BaTiO_3$, $KNbO_3$, and the tungsten bronzes, operate at the quantum limit for photorefractive sensitivity. Since quantum-limited materials are needed for applications in optical data processing and spatial light modulation, much recent effort has been devoted to growth and modification of these materials in order to approach this limit. We review this work and the physical limitations on the photorefractive effect.

1266 **Quantum Architecture of Novel Semiconductors:** *A. Zunger,* Solar Energy Research Institute, Golden, CO 80401

The way in which first-principles electronic structure theory of solids has been recently used to predict and characterize novel classes of semiconductors whose bandgaps span a full range: from IR to photovoltaic materials is described. The approach on: (i) a

Self-oscillation in $BaTiO_3$ using a multimode laser

Juan Rodriguez and Gregory Salamo

The effect of temporal coherence on the phenomena of self-oscillation in photorefractive materials is analyzed using multilongitudinal-mode argon-ion and helium–neon lasers. Observations demonstrate that self-oscillation is possible when the mirror–crystal separation is large compared to the laser coherence length. The observations are shown to agree with predictions based on the recurrence in the temporal coherence of a multilongitudinal-mode laser.

I. Introduction

We report on the observation of the effect of temporal coherence on the phenomena of self-oscillation[1] in the photorefractive crystal $BaTiO_3$. In particular, we have observed self-oscillation even when the mirror–crystal separation greatly exceeds the coherence length of the laser pump source. For both multimode argon-ion and helium–neon lasers self-oscillation was observed to reappear at mirror–crystal separations corresponding to recurrences in the temporal coherence of the pump laser. Such recurrences are indeed possible as was first pointed out in a paper by Mandel and Wolf[2] and by many other authors[3,4] since their original publication.

II. Experimental Apparatus and Observations

Using $BaTiO_3$ as a phase-conjugating mirror we have carried out two experiments which demonstrate the effect of temporal coherence on the phenomenon of self-oscillation.

In the first experiment self-oscillation was observed using a multimode He–Ne laser and an optical resonator formed by the conjugate mirror and a normal mirror[3] as shown in Fig. 1. The coherence length of the 5-mW He–Ne laser, as determined using an interferometer, was ~5 cm. However, self-oscillation was observed at distances d of ~2, 38, and 74 cm. In fact, at all three positions, self-oscillation was observed over a range of ~10 cm as would be predicted based on the measured coherence length of the He–Ne laser. No obvious degradation in the quality of the self-oscillation was observed at the three different mirror separations. Our observations clearly indicated a recurrence in the ability of the resonator to sustain self-oscillation as the cavity length was increased. Since the He–Ne laser cavity length was 36 cm, the period of the recurrence was observed to be equal to the He–Ne cavity length.

In the second experiment a self-pumped oscillator was observed using a multimode argon-ion laser[4] as shown in Fig. 2. In this configuration only one pump beam is required. Apparently, the self-generated pumping beams[5] of the single input beam can be used to pump the resonator formed by the phase-conjugate mirror and the normal mirror. The coherence length of the 200-mW argon-ion laser, also determined by an interferometer technique, was ~2.5 cm. As in the first experiment self-oscillation was observed to reappear at special cavity lengths. For the argon laser these lengths were at ~102 and 202 cm. At each position oscillation could be maintained over a range of ~5 cm which was approximately equal to the coherence length of the laser. Since the argon-ion cavity length was 100 cm the recurrences in the observation of self-oscillation occurred at a period corresponding to the argon-ion cavity length. Self-oscillation at a cavity length of ~2 cm could not be attempted due to limitations in the geometry of the apparatus. The observation of self-oscillation was made with and without a lens in the oscillator. The only difference in behavior between the two cases was the higher speed associated with the buildup of oscillation when the lens was in the cavity and the ease with which the same cavity could be aligned. This would be expected since the lens increases the photon flux required to initiate the cavity oscillation and makes the cavity alignment relatively insensitive to the orientation of the normal mirror.

The authors are with University of Arkansas, Physics Department, Fayetteville, Arkansas 72701.

Received 7 June 1986.
0003-6935/87/112260-03$02.00/0.

Bistability and optical switching in a total internal reflection phase conjugator

Juan Rodriguez, Azad Siahmakoun, and Gregory Salamo

We report the observation of bistability in a $BaTiO_3$ total internal reflection phase conjugator. The system makes use of the position of the crystal relative to the input field as the dynamic variable. Switching behavior, induced by intensity changes at the input, is also reported.

The search for an efficient optical transistor[1] has intensified with the discovery of new nonlinear processes in various materials. Among these, photorefractive materials stand out for their large four-wave mixing efficiencies.[2] In this paper we report the observation of bistability[3] and optical switching in a $BaTiO_3$ total internal reflection phase conjugator.[4]

The apparatus is shown in Fig. 1. An argon-ion laser, operating in the lowest fundamental transverse mode at 514.5 nm, is used as a pump source. The pump beam is intersected by a glass plate to monitor the returning phase conjugate (PC) beam on a photodetector. The unfocused beam, polarized in the plane of the paper (extraordinary ray) is then incident on a single domain $BaTiO_3$ crystal, immersed in a cell containing ethylene glycol[5] with the c-axis oriented along the entrance wall of the cell. The sample is mounted on a translator with its translational axis perpendicular to the pump beam. An angle of incidence of 35° is used throughout this work.

Initially the incident pump power is increased to 160 mW and the crystal is positioned at a point along x (shown in Fig. 1) where self-pumping using total internal reflection occurs spontaneously. When the PC beam reaches a steady-state value, the crystal is then slowly (compared to the crystal response time) translated along the negative x direction, maintaining self-pumping throughout the motion. At a given point, the PC beam is finally observed to decay. The crystal is then translated by an additional 0.05 cm (0.02 in.) and this defines the origin O for all the following measurements.

Figure 2 shows the steady-state magnitude of the PC beam as a function of crystal position. Each scan is performed by repeatedly increasing and decreasing the x reading. The data shown represent the average of several independent readings. The error bars are indicative of amplitude fluctuations, likely to originate in laser instabilities caused by optical feedback.

The four-wave mixing interaction geometry using total internal reflection as feedback is illustrated in Fig. 3. It shows two interaction regions connected only on one side by internal reflection from the corner. The absence of feedback on the side imposes two conditions[6] for starting the oscillation. First, the coupling strength γL must exceed a certain threshold value to compensate for a given loop loss. Second, the oscillation is not self-starting and therefore requires a finite seed beam normally provided by fanning[7] of the input beam.

In Fig. 4 the variation of the coupling constant γ with the loop orientation α_2 is plotted for our particular experimental arrangement. This curve shows γ to be optimized for larger angles. Under the assumption that self-pumping seeks the direction of greatest gain, the loop is expected to overlap with the input beam near the entrance point, where both γ and the interaction length L are maximized. This argument is supported by our observations. The coupling strength should therefore increase with the crystal position x.

Based on the above arguments, we offer a physical interpretation of the observed bistable behavior as follows. When the crystal is positioned at the origin point O, the coupling strength assumes its smallest value within the translational range and most likely below threshold. As x is increased past the switch down position x_n, γL is now raised above threshold but

The authors are with University of Arkansas, Physics Department, Fayetteville, Arkansas 72701.

Received 7 June 1986.
0003-6935/87/112263-03$02.00/0.

Optical Soc of America, p 22-23, 1987 (ISBN-10: 0936659513)

The reflectivity R defined as the ratio of output signals obtained at conjugate and probe frequencies is shown in Fig. 1. It is plotted as a function of the pump intensity inside the cavity normalized to the saturation intensity. This saturation intensity is determined together with the interband absorption coefficient α_0 and the maximum Auger recombination rate AN_0^2 by transmission measurements performed in another experiment. The reflectivity is fitted as shown in curves (*a*) and (*b*). The best fit [see curve (*a*)] is obtained by using $\alpha_0 = 21\ cm^{-1}$ and $AN_0^2 = 1.7 \times 10^{11}\ s^{-1}$. No new parameter has been used for this fit. The value of the Auger recombination rate indicates that the free carrier relaxation time is strongly reduced at high intensity. In our experiment a relaxation time of 10 ps is achieved for the largest intensity used, giving rise to a relatively high value for our experimental reflectivity; with such a rapid population relaxation rate the refractive index relaxes faster than the interference pattern moves, and no scrambling of this index modulation occurs. On the other hand, reflectivity calculated without Auger recombination is lower by ~2 orders of magnitude than the experimental values, evidence of the important role of Auger recombination in these semiconductor doped materials [see curve (*b*)].

This finding could be of interest in the case of thin semiconductor slices or multiple-quantum-well structures and may also have practical interest in designing high-speed absorptive nonlinear devices. **(12 min)**

1. R. K. Jain and R. C. Lind, J. Opt. Soc. Am. **73**, 647 (1983).
2. P. Roussignol, D. Ricard, K. C. Rustagi, and C. Flytzanis, Opt. Commun. **55**, 143 (1985).
3. B. Danielzik, K. Nattermann, and D. Von der Linde, Appl. Phys. B **38**, 31 (1985).

MHH2 Phase-modulated holography: a new technique for the sensitive detection of phase and absorption gratings

C. BRAUCHLE, J. PINSL, U. Munich, Institute for Physical Chemistry, D-8000 Munich, F. R. Germany; M. GEHRTZ, IBM Germany, D-6500 Mainz, F.R. Germany.

Holography has developed into a powerful tool for investigation of photochemical reactions in the solid state and has been successfully used in evaluation of a number of new holographic recording materials.[1,2]

In previous holographic techniques, which we refer to as phase-insensitive holography (PIH), one records the diffracted light intensity.[1,2] With PIH, the absorptive and dispersive part of the overall hologram efficiency cannot be separated, and the sign of either part is completely lost. It is easily seen that a separate recording of absorptive and dispersive holograms including their signs can lead to a much deeper understanding of the mechanistics of hologram formation.

In this paper, we propose and demonstrate a new holographic method—phase-modulated holography (PMH)—which is related to but distinctly different from straightforward homodyne detection techniques. In fact, PMH uses homodyne detection and thus shares the sensitivity advantages of this technique. The sensitivity limits of PMH are evaluated and compared with those of conventional PIH, and the conditions are identified under which PMH approaches the fundamental limits. While a 6-order of magnitude improvement of detection sensitivity is demonstrated in the present work, an 8-order of magnitude improvement is shown to be within reach.

As a distinct feature of PMH, not shared by straightforward homodyne detection techniques reported previously, the absorption and phase gratings induced by the photoreactive material can be recorded separately and simultaneously, and their absolute signs with respect to the hologram forming intensity grating can be determined. This unique feature is demonstrated with a new class of holographic material, tertiary nitroso alkanes dissolved in cyanoacrylate polymer films. After a brief overview, we develop the full theoretical framework necessary to understand hologram formation, hologram detection, and sensitivity limitations under phase-modulated conditions, and additionally we propose a dual-beam modification of PMH which can serve for excess noise reduction. **(12 min)**

1. C. Brauchle and D. M. Burland, Angew. Chem. Int. Ed. **22**, 582 (1983) and references therein.
2. Special issue papers in IEEE J. Quantum Electron. **QE-22** (1986).

MHH3 Self-pumped phase conjugation in photorefractive $Ba_{2-x}Sr_xK_{1-y}Na_yNb_5O_{15}$

JUAN RODRIGUEZ, AZAD SIAHMAKOUN, GREGORY SALAMO, U. Arkansas, Physics Department, Fayetteville, AR 72701; MARY J. MILLER, WILLIAM W. CLARK III, GARY L. WOOD, EDWARD J. SHARP, Center for Night Vision and Electro-Optics, Fort Belvoir, VA 22060-5677; RATNAKAR R. NEURGAONKAR, Rockwell International Science Center, Thousand Oaks, CA 91360.

Many different nonlinear phenomena and techniques have been used to produce phase conjugate beams. Until recently, however, only barium titanate[1] ($BaTiO_3$) and cerium-doped strontium barium niobate[2,3] (SBN) have been successfully used as self-pumped phase conjugate mirrors for milliwatt beam powers. Self-pumped phase conjugation, as reported here, is completely self-contained and requires no external mirrors, pumping beams, or applied electric fields.

We report here on the first observation of self-pumping in the new tungsten-bronze family crystal $Ba_{0.5}Sr_{1.5}K_{0.5}Na_{0.5}Nb_5O_{15}$ (BSKNN).[1] The phase conjugate reflectivities measured on a 6-mm cube of BSKNN are comparable with those previously reported for $BaTiO_3$ (Ref. 2) and SBN.[3,4] In addition to the behavior of BSKNN as a self-pumped phase conjugator, we also report the time required for the onset of the phase conjugate beam and asymmetrical self-defocusing (beam fanning).[5] Both of these characteristic times were measured as a function of pump intensity.

The experimental arrangement used for the self-pumped phase conjugate reflectivity measurements (dashed lines) is shown in Fig. 1. The laser output was kept in a single transverse mode, although several longitudinal modes were oscillating. Extraordinary polarized light was used to write gratings, while ordinary polarized light was used for grating erasure. The beam splitter separated the phase conjugate from the input and permitted normalization of the phase conjugate intensity. The pump and phase conjugate beams were monitored with matching photodiodes *P.D.*1 and *P.D.*2, respectively. Self-pumping was observed over an incident angle $\theta = +45°$. In Table I we present the reflectivity measurements at each of four spectral lines from an Ar-ion laser incident on the crystal at an input angle of $+20°$ with respect to the normal. The unfocused beam diameter (e^{-1} point) was ~1.5 mm at the crystal.

The same apparatus used to obtain the phase conjugate reflectivity measurements was used to obtain the phase conjugate formation time. The phase conjugate formation time τ_f, or the time required for the reflectivity to reach e^{-1} of its final value, as a function of intensity, is presented in curve *a* of Fig. 2. The following expression represents the best fit to this response: $\tau_f = 125/I^{-0.5}$, where τ_f is in seconds and I is in W/cm^2.

The experimental arrangement depicted by the solid lines in Fig. 1 was used to determine the beam fanning response time. In this experiment, opening the shutter caused detector *P.D.*1 to trigger a waveform analyzer that monitored and stored the transient response seen by detector *P.D.*3. The response time was chosen as the time for the transmitted beam to reach e^{-1} of the difference between the initial and equilibrium intensities. Curve *b* of Fig. 2 shows this characteristic response time as a function of the input intensity which best fits the expression, $\tau = 1.54/I^{-0.82}$, where τ is in seconds and I is in W/cm^2. **(12 min)**

1. R. R. Neurgaonkar and W. K. Cory, J. Opt. Soc. Am. B **3**, 274 (1986).
2. J. Feinberg, Opt. Lett. **7**, 486 (1982).
3. G. J. Salamo, M. J. Miller, W. W. Clark III, G. L. Wood, and E. J. Sharp, Opt. Commun. **59**, 417 (1986).
4. M. J. Miller, E. J. Sharp, G. L. Wood, W. W. Clark III, G. J. Salamo, and R. R. Neurgaonkar, submitted to Opt. Lett.
5. J. Feinberg, J. Opt. Soc. Am. **72**, 46 (1982).

MHH4 Measurements of stim[illegible]d Brillouin scattering phase conjugate fidelity

PAUL SUNI, JOEL FALK, U. Pittsburgh, Pittsburgh, PA 15261.

Phase conjugation by stimulated Brillioun scattering (SBS) is not a perfect process. The SBS output is not 100% correlated with the input. The degree to which the output deviates from a perfect replica of the input has been investigated extensively, but to date experimental verification of theoretical predictions is meager.

We present here results of conjugate fidelity measurements which record the dependence of the fidelity on the pump power and pump angular divergence. These measurements show that the fidelity decreases linearly with increasing pump power and increases about linearly with the square of pump divergence. These results are in agreement with some theories of SBS phase conjugation.[1,2]

We generate an SBS phase conjugate by pumping a square ethanol-filled metal waveguide with the 532-nm output from a Nd:YAG laser (Fig. 1). A fraction (10%) of the power is split off from this main beam and sent through a phase grating. In some experiments the main beam traverses a diffuser. The grating splits the probe beam into many orders, two of which are sent into the conjugator via a lens. Energy measurements of the multiple beams which appear after the two conjugated probe beams make a second pass through the grating are used to determine conjugate fidelity. Letting r^2 denote the ratio of the 1–0-order SBS reflectivities, the ratios among the three strong beams which exit the grating after the second pass (see Fig. 2) are

$$F_1/F_{-2} = 1/r^2R, \tag{1}$$

$$F_0/F_{-2} = 1 + 1/r^2R^2 + 2/rR \int E_0^*(x)E_1(x)\,d^2x \tag{2}$$

The electric fields written in Eq. (2) are normalized so that $\int |E|^2 d^2x = 1$. The factor R denotes a grating property, the ratio of the 1–0-order diffracted energies which result from a single pass through the phase grating.

Measurement of F_1/F_{-2} thus allows us [Eq. (1)] to calculate r. This in turn lets us determine the field overlap integral in Eq. (2), which is [illegible]

ISAF '86. Proceedings of the Sixth IEEE International Symposium on Applications of Ferroelectrics (Cat. No.86CH2358-0), 51-6, 1986

SBN AS A BROADBAND SELF-PUMPED PHASE CONJUGATE MIRROR

by

Edward J. Sharp, Mary J. Miller, Gary L. Wood,
and William W. Clark, III,
Night Vision and Electro-Optics Center
Fort Belvoir, VA 22060-5677

Gregory J. Salamo
Physics Department
University of Arkansas
Fayetteville, AR 72701

Ratnakar R. Neurgaonkar
Rockwell International Science Center
Thousand Oaks, CA 91360

ABSTRACT

The first observation of self-pumped phase conjugation using total internal reflection in cerium doped strontium barium niobate was described earlier for 442nm radiation [1]. We report here on an expansion of the frequency range from 458nm to 633nm which includes seven argon laser lines and one helium neon laser line. The self-pumped phase conjugate reflectivities for milliwatt beams at near normal incidence to the crystalline c-axis have been measured. Based on these measurements the importance of linear absorption in the operational bandwidth of the phase conjugate mirror is discussed. Applications include low power optical storage devices and optical diodes.

INTRODUCTION

Self-pumped phase conjugation using total internal reflection was first observed in a crystal of $BaTiO_3$ [2] and later in strontium barium niobate (SBN) [1] and barium strontium potassium sodium niobate (BSKNN) [3]. These self-pumped phase conjugate mirrors (SPPCMs) are completely self-contained and require no external mirrors, pumping beams, or applied electric fields. In addition, such devices are self-starting, self-aligning and require only milliwatt incident beams to produce a phase conjugate.

In a SPPCM the phase conjugate beam is produced by four-wave mixing. However, the two pumping beams that are normally required for four-wave mixing are self-generated within the crystal from the incident beam itself via beam fanning [4]. Light that is asymmetrically defocused by way of the photorefractive effect is internally reflected from faces adjacent to an edge of the crystal thereby forming a two-way loop as shown in Figure 1. This retroreflection of light from the incident beam within the crystal produces the pump beams and leads to the self-alignment and self-starting of the phase conjugate mirror.

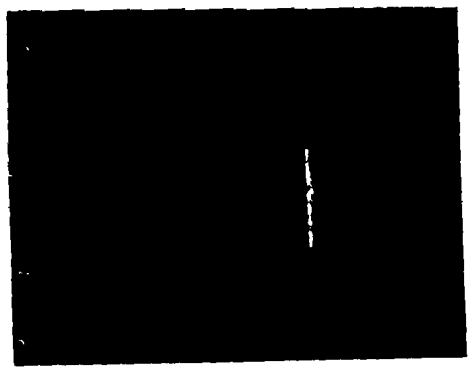

FIGURE 1 Self-pumping corner loop in a 6mm crystal cube of Ce-doped SBN:60.

CH2358-0/86/0000-0051 $1.00

Lifetime of excited atomic states

J. D. Cresser,* A. Z. Tang, G. J. Salamo, and F. T. Chan
Physics Department, University of Arkansas, Fayetteville, Arkansas 72701
(Received 26 December 1984; revised manuscript received 26 July 1985)

In this paper we derive an expression for the lifetime of excited atomic states taking account of contributions due to nonresonant two-photon transitions. Explicit integration of the two-photon emission spectrum is not required. The results are applied to the case of the hydrogen atom.

I. INTRODUCTION

Although two-photon emission in atomic systems is a subject much studied since the original work of Goeppert-Mayer,[1] there still remain certain aspects of this process which have not been satisfactorily dealt with. This is the case in situations in which an atom in an excited state can decay to its ground state by two-photon emission while passing through an intermediate atomic state having an energy higher than the initial state (nonresonant two-photon emission) or through an intermediate state with an energy lower than that of the initial state (resonant two-photon emission). An obvious example of such a situation is that of the two-photon decay of the $3s$ (or $3d$) level of hydrogen in which nonresonant emission is mediated by the higher-lying intermediate np states ($n \geq 4$) and the lower-lying intermediate $2p$ state. The former process, being nonresonant, is very unlikely compared to the latter, but still has interesting potentially observable effects arising from quantum interference between the two different routes by which the atom can arrive in its ground state.[2,3]

A somewhat more basic aspect of this kind of two-photon decay was addressed by Florescu,[3] namely the problem of actually calculating the lifetime of such an excited state. The interest in this problem is related to the fact that for a metastable level (i.e., one for which there is no resonant lower-lying intermediate state) this lifetime can be calculated by simply integrating the two-photon emission spectrum over the frequencies of the emitted photons, taking account of the conservation of energy. Thus, for hydrogen (in atomic units)

$$A^{2E_1}_{n_i l\to 1s} = \int_0^{(E_{n_i}-E_1)/4\pi} A_{n_i l\to 1s}(\nu')\,d\nu' \tag{1a}$$

$$= \int_0^{(E_{n_i}-E_1)/4\pi} \frac{2^{10}\pi^6}{C^6}(\nu')^3(\nu'')^3\frac{1}{2l+1}\sum_m \left|\left| \sum_{n=2} \left[\frac{\langle 1s\,|\,\hat{\epsilon}'\cdot\mathbf{r}\,|\,n\rangle\langle n\,|\,\hat{\epsilon}''\cdot\mathbf{r}\,|\,n_i lm\rangle}{E_n - E_{n_i} + E_{\nu'}} + \frac{\langle 1s\,|\,\hat{\epsilon}''\cdot\mathbf{r}\,|\,n\rangle\langle n\,|\,\hat{\epsilon}'\cdot\mathbf{r}\,|\,n_i lm\rangle}{E_n - E_{n_i} + E_{\nu''}} \right] \right|\right|^2_{\text{ave}} d\nu' , \tag{1b}$$

where ν' and ν'' are the frequencies of the two photons (with unit polarization vectors $\hat{\epsilon}'$ and $\hat{\epsilon}''$, respectively) emitted with

$$\nu' + \nu'' = (E_{n_i} - E_1)/2\pi = \nu_{n_i 1} = \omega_{n_i 1}/2\pi . \tag{2}$$

The sums over n in Eq. (1b), the second-order matrix elements, run over all hydrogen wave functions, including both continuum and bound states, and could be evaluated exactly via the implicit technique[2] or the Coulomb Green's function in momentum space.[3]

In the absence of any resonant intermediate states, e.g., $n_i = 2$, the expressions in Eqs. (1a) and (1b) remain finite. However, if in the sums in Eq. (1b) there appears a resonant intermediate state, e.g., if $n_i = 3$, the corresponding denominators in the summation will vanish. That is, the perturbation theory expression breaks down. In order to perform the integration in Eq. (1) in this case, Florescu[3] adopted a procedure in which the energy of the intermediate state was assigned a complex energy, the imaginary part of this complex energy being the natural linewidth of this level. As shown in Ref. 3, such a procedure applied to, say, the $3s$ and $3d$ levels in hydrogen, yields, after numerically integrating the emission spectrum over frequency, the usually quoted value for the one-photon lifetime of the initially excited state.[4] The conclusion that was drawn was that the contribution to the lifetime of the excited state due to nonresonant two-photon decay is negligibly small, as already mentioned above, and in agreement with intuitive expectations.

The general validity of this procedure is, of course, open to question. In fact, Florescu[5] has raised the point that the lifetimes of both the initial and resonant intermediate states should be properly taken into account, and

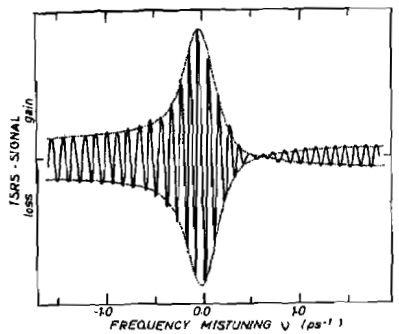

Fig. 4. Experimental frequency scan at zero time delay on diamond. The fringes in this plot are a result of a very useful trick employed to get rid of the dependence of the signal on the optical phases. We performed simultaneously with the frequency scan of the lasers a very slow scan of the time delay between the pump and probe pair. In this way one passes slowly through the maximum and minimum signal strength.

induction regime ($t \gg$ pulsewidth) as has been measured by Laubereau et al. [6]. The detection of this frequency drift, computed in fig. 2, is also possible in a TSRS experiment. It results in a change in the rhythm of the gain and loss pattern underneath the envelope of the energy transfer measured (fig. 2 in ref. [1]). We have observed this change in the frequency but to obtain good qualitative values the system (mirrors, beamsplitters) must have extreme optical phase stability.

An estimate of the strength of the electronic contribution with respect to the isotropic nuclear part can be obtained with the experiment we will describe below. The time delay between the pump and the pr... pair (Δ) is fixed at zero. Now a frequency scan o... of the dye lasers is performed. Monitoring the TS... signal one obtains a result like fig. 4. The height o... peak with respect to the frequency independen... ground is a measure of the strength of the isotrop... component with respect to the electronic contribu... Unfortunately the pulse shapes also influence thi... tio. Combining the measured ratio (10.0) with the... act pulse shapes results in a relation $a/a = 0.55$ pa... Taking the orientation of the diamond into accou... this is in reasonable agreement with earlier CARS m... surements [7].

Acknowledgement

This research has been supported by the Dutch ... foundation for "Fundamenteel Onderzoek der M... terie" (FOM).

References

[1] M. v. Exter and A. Lagendijk, Optics Comm. 56 (19... 191.
[2] J.P. Heritage, Appl. Phys. Lett. 34 (1979) 470.
[3] A. Owyoung, R.W. Hellwarth and N. George, Phys. Re... B5 (1972) 628.
[4] R.W. Hellwarth, Prog. Quant. Electr., Vol. 5 (Pergamon Press 1977) p. 1.
[5] A. Laubereau and W. Kaiser, Rev. Mod. Phys. 50 (... 607.
[6] A. Laubereau, H.R. Telle and G.M. Gale, Appl. Phys. B34 (1984) 23.
[7] M.D. Levenson, C. Flytzanis and N. Bloembergen, ... Rev. B6 (1972) 3962.

STRONTIUM BARIUM NIOBATE AS A SELF-PUMPED PHASE CONJUGATOR

Gregory SALAMO

Physics Department, University of Arkansas, Fayetteville, AR 72701, USA

Mary J. MILLER, William W. CLARK III, Gary L. WOOD and Edward J. SHARP

Night Vision and Electro-Optics Laboratory, Fort Belvoir, VA 22060-5677, USA

Received 11 October 1985; revised manuscript received 3 June 1986

Self-pumping has been observed in strontium barium niobate at 442 nm. An undoped crystal produced up to 60% phase conjugate reflectivity and a cerium doped crystal produced near 30%. A frequency shift in the phase conjugate wave was not observed. We also investigated asymmetrical self-defocusing and observed transmissions through the cerium doped crystal were limited to about 0.1% of the incident radiation for a wide acceptance angle.

Introduction

...report the first observation of self-pumping ...the photorefractive crystal strontium barium ...ate [2] (SBN). In particular, we have observed ...pumping in both doped and undoped SBN sam... 442 nm. For an undoped sample we have mea... phase conjugate reflectivities near 60% while ...cerium doped sample measured reflectivities ...ear 30%. The phase conjugate wave did not ...the frequency shift reported for barium titanate

...addition to its behavior as a self-pumped phase ...ator we also report on the use of asymmetrical ...defocusing [6] in SBN as an optical beam de... ...ier [7]. In particular, we observed transmis... ...through the cerium doped crystal that were ...to about 0.1% of the incident radiation for a ...ceptance angle.

...-pumping

...-wave mixing is used in a self-pumped photo... ...ive material to produce a phase conjugate ...However, the two pumping beams that are nor... ...eeded for four-wave mixing are self-generated via the fanning effects [6]. In particular, light which is fanned forms a two-way loop, as shown in fig. 1, near an edge of the crystal which apparently acts as a corner cube retro-reflector. For this reason, only

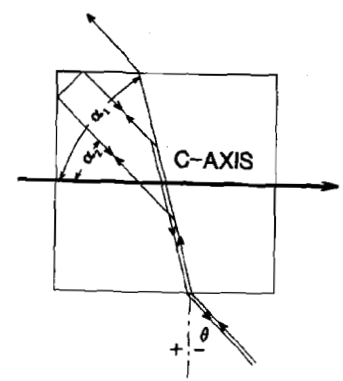

Fig. 1. Sketch of an SBN crystal and input laser beam which undergoes asymmetric self-defocusing or "fanning". The fanned beam is directed toward the crystal face which was held at a negative potential during poling and a "loop" is self-generated, as discussed in detail in ref. [1].

Intensity profiles of short optical pulses via temporally reversed pulses

Steven R. Montgomery, Donald O. Pederson, and Gregory J. Salamo
University of Arkansas, Physics Department, Fayetteville, Arkansas 72701

(Received 11 June 1986; accepted for publication 16 July 1986)

A new technique is reported for determining the intensity profile of optical pulses on a subpicosecond timescale. Several examples are presented in order to demonstrate the capability of the technique.

The development of cw mode-locked dye lasers[1] has produced a source of femtosecond optical pulses which can be used to probe ultrafast phenomena. An ideal means of analyzing the temporal structure of such short optical pulses, however, has not yet been developed. The techniques most commonly used are autocorrelation[2] and the streak camera[3] where only the latter can yield the temporal intensity profile $I(t)$ of the pulses. Streak camera resolution, however, is limited to the picosecond domain. In this letter we report a "self-convolution" technique for determining the intensity profile of optical pulses on a subpicosecond timescale.

Of the aforementioned techniques autocorrelation is the method generally preferred for characterizing the output of cw mode-locked lasers due to the high cost and limited resolution of streak cameras. In the autocorrelation technique a train of optical pulses from the output of a mode-locked laser is split into two pulse trains with a beamsplitter. These two pulse trains are recombined in a nonlinear material such as a second harmonic generating (SHG) crystal considered here as an example. The experimental arrangement, shown in Fig. 1, is very similar to a Michelson interferometer except that a relative delay τ between the optical pulse trains is introduced before the pulse trains are combined in the SHG crystal. The intensity of the frequency doubled output then becomes a function of the relative delay. Experimentally, the variable delay is introduced by simply changing the optical path length of one of the arms of the interferometer.

The intensity of the frequency doubled output of the SHG crystal is proportional to the square of the fundamental intensity.[4] From this it can be shown[5] that the intensity of the second harmonic light is enhanced when the optical pulses from each arm of the interferometer overlap in the SHG crystal. Quantitatively this enhancement is proportional to

$$G(\tau) = \int I(t)I(\tau + t)dt, \tag{1}$$

where $I(t)$ represents the temporal intensity profile of an individual pulse in the pulse train and $G(\tau)$ is called the autocorrelation of $I(t)$. An experimental setup, such as the one described in Fig. 1, to measure $G(\tau)$ is commonly referred to as an autocorrelator. The autocorrelation of a known pulse is illustrated in Fig. 2.

From $G(\tau)$ it is possible to obtain an approximate value of τ_p, the temporal width of an optical pulse in the train, only by first assuming a specific form for $I(t)$. The width of $G(\tau)$ can then be related to τ_p by Eq. (1). The estimated τ_p is then dependent on the choice of functional form of $I(t)$ so that $G(\tau)$ alone yields neither the temporal structure nor τ_p. In fact, the assumed $I(t)$ can often lead to erroneous results.[6] In this letter we demonstrate a new technique, "self-convolution," which yields $I(t)$, and hence "τ_p," directly from the data.

The self-convolution technique described here is similar

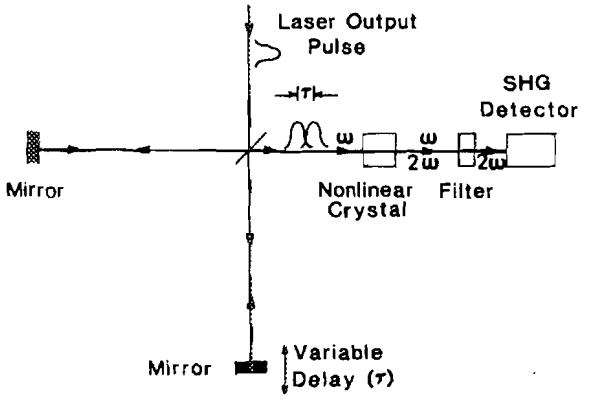

FIG. 1. Interferometric apparatus used for pulse correlation measurements by second harmonic generation. The apparatus is referred to as an "autocorrelator."

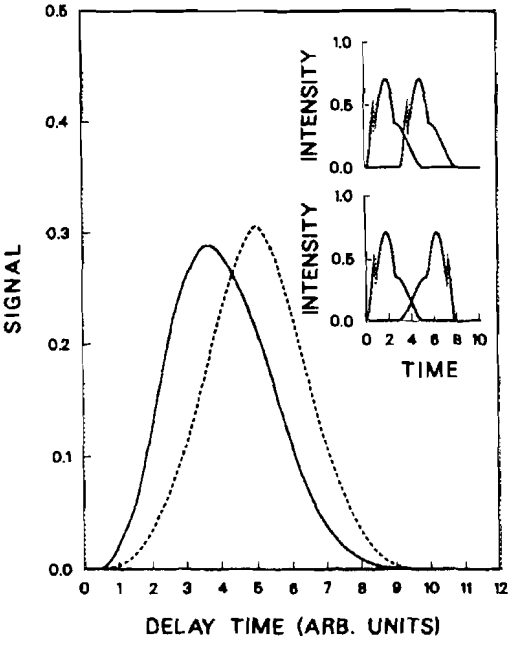

FIG. 2. Dashed autocorrelation curve is produced by the pulse overlap depicted in the upper insert. The solid self-convolution curve is produced by the pulse overlap shown in the lower inset.

 0003-6951/86/370620-02$01.00

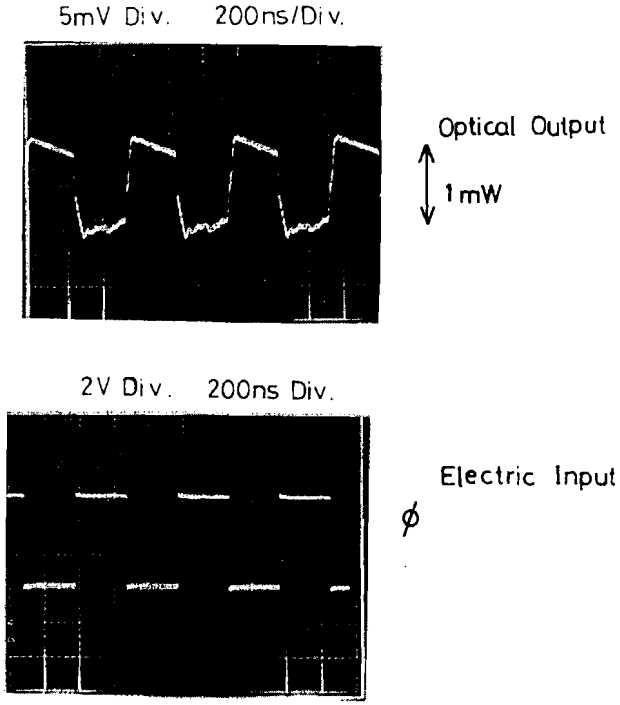

Fig. 2. Optical response to an electrical signal, which is applied to the monolithically integrated circuit.

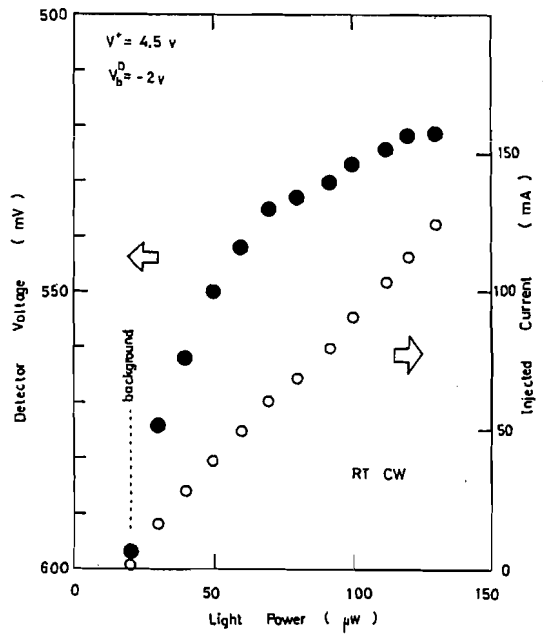

Fig. 3. Detected voltage as a function of the optical output ● and injection current vs optical output ○.

References

1. N. Bar-Chaim, I. Ury, and A. Yariv, IEEE Spectrum 38 (May 1982).
2. H. Matsueda, S. Sasaki, and M. Nakamura, J. Lightwave Technol. LT-1, 261 (1983).

Photoacoustic deflection spectroscopy: a new specie-specific method for combustion diagnostics

A. Rose, G. J. Salamo, and R. Gupta

University of Arkansas, Physics Department, Fayetteville, Arkansas 72701.

Received 15 October 1983.
0003-6935/84/060781-04$02.00/0.

Recently we have shown that photothermal deflection spectroscopy has an excellent potential for developing into a sensitive combustion diagnostic technique for minority species concentration measurements.[1] In this technique a dye laser (pump beam), tuned to an absorption line of the molecule (or atom) of interest, is directed through the combustion region. Most of the optical energy absorbed by the molecules is rapidly converted into heat due to quenching collisions. Heating of the dye laser irradiated region is accompanied by refractive-index gradients due to the spatial profile of the dye laser beam and diffusion of this heat. The refractive-index gradient is probed by observing the deflection of a He–Ne laser (probe) beam. This deflection can be correlated with the concentration of absorbing molecules. Application of this technique to a combustion environment was demonstrated by observing a photothermal signal from NO_2 produced in the combustion of methane and oxygen.[1] In this Letter, by application to OH molecules in a methane–oxygen flame, we show that the pressure change accompanying the heating of the dye laser irradiated region can also be detected by the deflection of the probe beam placed a small distance from the pump beam. This technique, photoacoustic deflection spectroscopy (PADS), can be used as a sensitive technique for minority species and local temperature measurements. If significant concentration gradients are present in the flame, application of photothermal deflection spectroscopy (PTDS) is not straightforward. The PTDS signal in this case may be proportional to the concentration gradients rather than concentration of the absorbing molecules if the pump and probe beams overlap. The problem may be largely alleviated if the pump and probe beams are spatially separated.[1] However, the PTDS signal amplitude decreases very fast with increasing probe–pump beam distance[2] reducing the sensitivity of the technique. In this case (i.e., when significant concentration gradients are present) PADS can be used with advantage because the PADS signal does not decrease with probe–pump beam distance very fast, and its sensitivity for spatially separated beams is much higher than that for PTDS. Moreover PADS also offers a simple way to measure simultaneously local temperature by measurement of the acoustic velocity in the flame. In this respect, PADS is related to Tam's recently developed "Optoacoustic Laser Deflection (OLD)" technique for temperature measurements.[3] A more detailed discussion of OLD and its comparison with PADS will be given later in the Letter.

PADS is similar to conventional photoacoustic spectroscopy (PAS)[4,5] except that the pressure change is detected optically and not by a microphone (or a piezoelectric transducer). PADS has several advantages over PAS while retaining the sensitivity of PAS: (1) The optical detector that measures the deflection of the probe beam can be placed as far away from the flame as necessary without adversely affecting the sensitivity. The SNR depends on the separation between the probe and pump beams inside the flame and not on the position of the detector. This permits application of this technique to hostile environments. (2) The acoustic signal never

Two-photon decay of hydrogenic atoms

J. H. Tung, X. M. Ye, G. J. Salamo, and F. T. Chan
Physics Department, University of Arkansas, Fayetteville, Arkansas 72701
(Received 9 December 1982; revised manuscript received 13 July 1983)

The two-photon decay mode of hydrogenic atoms from an arbitrary state (n_1,l_1,m_1) to an arbitrary state (n_2,l_2,m_2) is studied within the framework of nonrelativistic quantum mechanics. In the dipole approximation, these decay rates, which involve infinite summation over intermediate states, are derived exactly via a general second-order matrix element obtained by Kelsey and Macek and an implicit technique introduced by Dalgarno and Lewis. The results are expressed in terms of hypergeometric functions. For transitions $n_1s \rightarrow n_2s$, our results reduce to those of Klarsfeld whose starting point is the Coulomb Green's function. For transitions to the ground state, an alternative expression involving a simple one-dimensional integral is presented. The decay rate of the $2s$ metastable state of atomic hydrogen is calculated as an illustration of the method. The result, $1/\tau = 8.2284\ \text{sec}^{-1}$, agrees with Klarsfeld. For transitions of $n_1s \rightarrow 1s$ and $n_1d \rightarrow 1s$ $(n_1 \geq 3)$, the transition rates exhibit interesting and unexpected structures. In particular, "zeros" are found in the two-photon emission spectrum indicating that two-photon emission is not possible at certain frequencies. Physically, these "zeros" are the result of destructive interference between the radiating dipole terms associated with the sum over intermediate states. In addition to the emission spectrum the expected coincidence signal between two detectors monitoring the two photons simultaneously emitted during a two-photon transition is calculated as a function of the angle between the detectors. The angular distribution for the $n_1d \rightarrow 1s$ transitions is shown to be significantly different from the $n_1s \rightarrow 1s$ transitions. Finally, a possible experiment is suggested to test the results presented in this paper.

I. INTRODUCTION

The possibility of a two-photon process, which proceeds via intermediate states, was first pointed out by Mayer[1] in 1931. Breit and Teller[2] applied this theory to the case of the $2s \rightarrow 1s$ transition in atomic hydrogen and found that double photon emission is the most probable radiative decay mode, and is therefore the principal cause of the decay mechanism of the interstellar $2s$ hydrogen atoms. They also found that the mean lifetime τ corresponding to this mode of decay can be bracketed by the relation $6.5 < 1/\tau < 8.7\ \text{sec}^{-1}$. Later, more detailed calculations[3,4] were carried out which involved term-by-term numerical evaluation of the infinite summation over intermediate states in the second-order matrix elements responsible for the decay. In particular, Shapiro and Breit[4] found that the decay rate for the metastable $2s$ state of a hydrogenlike atom of atomic number Z, $1/\tau$, is equal to $8.226Z^6\ \text{sec}^{-1}$, which corresponds to a lifetime of 1.9 msec for the case of He^+. However, these conclusions could be modified[5,6] due to the possible existence of a nuclear or electronic dipole moment which would produce a nonzero one-photon decay mode for the metastable hydrogenlike atom. Therefore, a careful study of the properties of this state is useful in the search for new fundamental interactions.

In connection with this interest and in view of experimental success in two-photon-absorption and ionization experiments, a series of theoretical papers[7–20] has appeared on how to perform exactly, within the framework of nonrelativistic quantum mechanics, the infinite sums in the second-order matrix elements responsible for various multiphoton processes. For the decay transition, the numerical result of the two-photon decay rate of metastable hydrogenic atoms, viz., $1/\tau = (8.2283 \pm 0.0001)Z^6\ \text{sec}^{-1}$, obtained by Klarsfeld[14] is believed to be the most accurate one.[6,19] Recent calculations,[21,22] including all relativistic and retardation effects and all combinations of photon multipoles, give a very small correction in the case of low-Z hydrogenlike atoms. In addition, the two-photon decay rates of the singlet and triplet metastable states of heliumlike ions have also been calculated using variation procedures by Drake, Victor, and Dalgarno.[23]

In a recent paper[24] Kelsey and Macek used the implicit technique[7,8] to obtain a simple reformulation of a closed-form expression for a general second-order matrix element for hydrogen. While equivalent expressions have been derived[13,25,26] employing various representations[27–29] of the Coulomb Green's function, the mathematics involved is quite cumbersome. Although the work of Kelsey and Macek is very important and useful, it has not received enough attention. One of the purposes of this paper is to show that the elegant results of Kelsey and Macek and the powerful implicit technique can be employed to study the two-photon decay mode of a hydrogenlike atom from an arbitrary initial state (n_1,l_1,m_1) to an arbitrary final state (n_2,l_2,m_2). As a result, the two-photon transition rate is expressed in terms of repeated parametric differentiations of hypergeometric functions. The results we have obtained are equivalent to those of Gazeau,[19] but the starting points are quite different. Gazeau used powerful group-theoretical techniques whereas we have used simple alge-

LASER-PHOTOACOUSTIC DETECTION OF WATER POLLUTANTS

Gregory J. Salamo
Richard J. Anderson

Physics Department, University of Arkansas
Fayetteville, Arkansas 72701

Research Project Technical Completion Report

Project B-068-ARK

The work upon which this report is based was supported in part by federal funds provided by the U. S. Department of the Interior, as authorized under the Water Research and Development Act of 1978, (P.L. 95-467), through annual cooperative program agreement number 14-34-0001-1206.

Arkansas Water Resources Research Center
University of Arkansas
223 Ozark Hall
Fayetteville, Arkansas 72701

Publication No. 102

March, 1984

Photoacoustic detection of OH molecules in a methane–air flame

A. Rose, J. D. Pyrum, G. J. Salamo, and R. Gupta

Pulsed photoacoustic signals from OH molecules in a methane–air flame have been observed. Quantitative measurements are made and compared with the results of a theoretical model. Very good agreement between theory and experiment is obtained. A detection sensitivity of 250 ppb for OH molecules in a combustion environment has been obtained.

I. Introduction

There is considerable interest in the development of new optical combustion diagnostic techniques for minority species concentration measurements. Following the work of Crosley and collaborators,[1] we have recently shown that photoacoustic spectroscopy has an excellent potential for developing into a very valuable combustion diagnostic technique.[2,3] The technique is nonperturbing, has good temporal resolution, and has excellent sensitivity. In this paper we report on the application of this technique to the measurement of the concentration of OH molecules produced in the combusion of methane and air. The experimental results are used to check a theoretical model of signal generation and propagation in a combustion medium. Very good agreement between the theory and experiment is obtained.

Although the discovery of the photoacoustic effect is quite old,[4] most of the applications of this technique have been developed since the advent of lasers.[5] the photoacoustic effect may be explained simply as follows: Let us say a sample of molecular gas is illuminated by light of such a wavelength that it is absorbed by the gas molecules. The excited molecules can either radiatively decay or lose their energy via collisions. The energy lost in collisions may subsequently appear as rotational-translational energy of the gas molecules. The temperature of the gas rises, or equivalently, for constant volume, the pressure rises. If the light source is pulsed, a pressure pulse may be detected by a microphone. The technique is specie selective since the laser radiation may be tuned to excite a specific molecular or atomic species. Since this technique depends on quenching collisions, the real advantage of this technique lies in the fact that small concentrations of the gases of interest can be detected in the presence of foreign gases at atmospheric pressure. On the other hand, unless special schemes are used, fluorescence spectroscopy in such circumstances is generally less appropriate since most of the excited molecules decay nonradiatively due to quenching collisions with foreign gas molecules. This is primarily why the photoacoustic technique has been so successful for pollution measurements.

Our initial work was done with NO_2 molecules produced in the combustion of methane and air.[2,3] We had chosen NO_2 for that study because of its optical absorption in the visible region. Although that investigation was very successful in proving the excellent potential of this new application of photoacoustic technique, quantitative work proved difficult for the following reasons: (1) NO_2 has a very complex spectrum in the visible region (almost a quasi-continuum); (2) the optical absorption coefficient of NO_2 molecules is small, and the NO_2 density in a methane–air flame is very low; (3) the absorption coefficient of NO_2 at flame temperature is not known and cannot easily be computed or measured. In the investigation reported here we have applied the photoacoustic technique to OH molecules produced in the combustion of methane and air in a flat-flame burner. OH molecules have a high concentration in this flame,[6] and their spectrum is well-resolved (discrete) and well-understood.[7] This has allowed a quantitative investigation of the photoacoustic effect in a flame. Our investigations on several isolated lines of the $A^2\Sigma^+ - X^2\Pi$ band of OH in the vicinity of 3100 Å have proved the validity of a theoretical model.

The authors are with University of Arkansas, Physics Department, Fayetteville, Arkansas 72701.

Received 24 October 1983.
0003-6935/84/101573-07$02.00/0.

Production of $O(^1D)$ and $O(^3P)$ by vacuum ultraviolet photodissociation of molecular oxygen

G. A. Germany, G. J. Salamo, and R. J. Anderson
Department of Physics, University of Arkansas, Fayetteville, Arkansas 72701

(Received 31 January 1983; accepted for publication 29 April 1983)

A pulsed fluorine excimer laser operating at 1576 Å wavelength, 10 ns pulse width, 10 Hz repetition rate, and ~0.2 MW average output power is used to photodissociate ground state molecular oxygen, $O_2(X^3\Sigma_g^-)$. The dissociation products, $O(^1D)$ and $O(^3P)$, are produced with unit quantum efficiency and ~0.4 eV translation energy. Time-resolved techniques are used to monitor the $O(^1D_2)\rightarrow O(^3P_2)$ radiative transition over the O_2 pressure range 10–400 mTorr. The $O(^1D)$–O_2 quenching rate constant is determined to be $(3.7 \pm 0.3)\times 10^{-11}$ cm^3 s^{-1}. The $O(^1D)/O_2$ dissociation fraction is estimated to be 0.4% to ~50% corresponding to $O(^1D)$ densities as high as 3×10^{15} cm^{-3}.

PACS numbers: 79.20.Ds, 33.20.Ni

I. INTRODUCTION

Because of its 1.97 eV of internal energy and 147 s radiative lifetime, the $O(^1D)$ metastable state of atomic oxygen plays an important role in the free radical chemistry of the atmosphere. Therefore, much effort has been devoted to laboratory analysis of $O(^1D)$ gas kinetic[1] and photochemical reaction rates[2] and to the role of the $O(^1D)$ state in intermediate reactions[3] of atmospheric interest. For example, the auroral and airglow characteristics ascribed to the $O_2(b\,^1\Sigma_g^+\rightarrow X^3\Sigma_g^-)$ emissions appear to have their origin in the energy transfer process $O(^1D)+O_2(X^3\Sigma_g^-)\rightarrow O_2(b\,^1\Sigma_g^+)$.[4] Similarly the $O(^3P)$ ground state atom also has received considerable attention in the analysis of the photochemistry of the terrestrial atmosphere.[5] Its production by solar ultraviolet photolysis of O_2, O_3, NO_x, etc., and its role in subsequent gas kinetic collisional processes also make it an important factor in atmospheric models. Thus, laboratory studies of reaction rates for three body collision processes such as $O(^3P)+O_2+M\rightarrow O_3+M$ have received considerable attention from atmospheric scientists.[6] In addition, the possibility of the production of significant densities of electronically excited oxygen atoms by charged particle impact or optical pumping of metastable or ground state atoms introduce yet another factor into the analysis of observed atmospheric emissions.[7]

Unambiguous laboratory analyses of these and other collisional excitation processes require the use of experimental techniques capable of producing a high density, well characterized sample of atomic oxygen. The most popular of these have been dissociation by (i) a rf or microwave discharge,[8] (ii) an oven or furnace,[9] or (iii) photolysis of O_3, NO_x, etc.[10] Each, however, is not without experimental drawbacks. For example, although rf or microwave discharge sources have the capability of producing intense beams of atomic oxygen, their very nature makes the excited state distribution of these atomic samples ambiguous. An oven source, meanwhile, yields an atomic sample which is comprised of nearly 100% ground state atoms at a typical operating temperature of 2300 K. However, its density is a rather low $\sim 10^9$ cm^{-3} and the accompanying background oven radiation is quite intense. On the other hand, although laser photolysis of a gas such as O_3 through the process $O_3+h\nu\rightarrow O(^1D)+O_2(a^1\Delta_g)$ has been used to produce workable densities of metastable oxygen for quenching rate experiments, it requires the presence of a high pressure background O_3 carrier gas such as He or SF_6.

This work describes a different approach to the problem of atomic oxygen production. It reports the details associated with the production and measurement of a high density sample of $O(^3P)$ and $O(^1D)$ states produced by laser photodissociation of O_2 in the absence of a high pressure buffer gas. Although our present research plan is to use this technique to provide target atoms in future low-energy electron impact experiments, it is also suitable for use in a variety of other photochemical, quenching, or reaction rate experiments.

II. EXPERIMENT

A. Technique

Our approach to the production of high density, well characterized samples of atomic oxygen is based upon the previous work of Lee and Slanger[11] and utilizes 1576 Å laser radiation to photodissociate O_2 via the process

$$O_2(X^3\Sigma_g^-)+h\nu\rightarrow O_2(^3\Sigma_u^-)\rightarrow O(^3P)+O(^1D)+\Delta\epsilon,$$

where $\Delta\epsilon = 0.8$ eV is the kinetic energy shared by the dissociation fragments.[12] This process is characterized by several features which make it an especially attractive source of oxygen target atoms for excitation experiments involving charged particles or photons. Among these are that:

(i) every photon absorbed results in a photodissociation event,[13]

(ii) both $O(^3P)$ and $O(^1D)$ are produced in equal quantities and measurement of the $O(^1D_2)\rightarrow O(^3P_2)$ radiative transition at 6300 Å can be used to directly monitor the densities of the atomic states (Fig. 1),

(iii) only $O(^3P)$, $O(^1D)$ and $O_2(X^3\Sigma_g^-)$ exist as initial experimental conditions for subsequent excitation experiments,

(iv) given sufficient laser intensity (either through high laser power, focusing of the laser beam, or multiple laser

 0021-8979/83/084573-05$02.40

Minority species concentration measurements in flames by the photoacoustic technique

K. Tennal, G. J. Salamo, and R. Gupta

The potential of the photoacoustic technique to detect minority species concentrations in combustion environments has been investigated. In particular, we have detected very low concentrations of NO_2 molecules produced in the combustion of methane, oxygen, and nitrogen in a flat-flame burner.

I. Introduction

There is presently a need for the development of combustion diagnostic techniques to measure such parameters as gas concentrations and local temperatures in practical flames.[1-3] These techniques should (1) be nonperturbing to permit *in situ* measurements; (2) have spatial resolution; and (3) have temporal resolution. Optical techniques are best suited for this purpose since they easily satisfy all three criteria. In fact, several optical techniques have already been successfully used for species concentration measurements, e.g., coherent anti-Stokes Raman scattering, spontaneous Raman scattering, and saturated fluorescence. However, there is currently no single technique which is suitable under all circumstances, and all the above techniques can be seen to have relative advantages and disadvantages over each other. In this paper we report on an experiment which indicates the potential of a laser photoacoustic technique to identify and to measure minority species concentrations in a flame. In particular, we have applied this technique to measure low NO_2 concentrations produced by methane–air combustion in a flat-flame burner.

The photoacoustic effect was discovered by Alexander Graham Bell in 1880,[4] but it was largely ignored until recently. With the advent of lasers there has been a resurgence of interest in this technique.[5] Stated simply, the photoacoustic effect consists of the following: a sample (let us say a molecular gas) is illuminated by light of such wavelength that it is absorbed by the gas molecules. The excited molecules can either radiatively decay or lose their energy via collisions. The energy lost in collisions may subsequently appear as translational energy of the gas molecules. The temperature of the gas rises, or equivalently, for constant volume the pressure rises. If the light beam is amplitude modulated at acoustic frequencies, the pressure goes through periodic changes at acoustic frequencies and may be detected by a microphone. If the light source is pulsed, a pressure pulse may be detected. The technique is species selective since the laser radiation may be tuned to excite a specific molecular or atomic species. The real advantage of this technique lies in the fact that small concentrations of the gases of interest can be detected in the presence of foreign gases at atmospheric pressure. Fluorescence spectroscopy in such circumstances is generally inappropriate since most of the excited molecules decay nonradiatively due to quenching collisions with foreign gas molecules. On the other hand, it is precisely under such circumstances that the photoacoustic effect is most effective.

The potential of the application of photoacoustic spectroscopy to flame studies was recently demonstrated by Crosley and collaborators.[6] These authors found that in a flame seeded with Na, if a pulsed dye laser was tuned to the resonance lines of Na, the sound produced by the photoacoustic effect was easily audible to an observer standing within a meter of the burner. They have investigated this effect in some detail and have measured the speed of sound (and thus the temperature) and some quenching rates in the flame. Our own experiments with a flame seeded with sodium have confirmed Crosley's findings.[7]

In this paper we investigate further the photoacoustic effect in a flame with a view to develop this technique into a combustion diagnostic tool. In particular we describe our experiments in which we have measured low concentrations of NO_2 molecules ($\sim 10^{13}$ molecules/cm^3) in a flat-flame burner.

II. Apparatus

Our experimental setup is shown schematically in Fig. 1. Light from a chromatix CMX-4 flashlamp pumped dye laser was used to excite NO_2 molecules in the flame. The laser produces $\sim$1-μsec long pulses with an average energy of $\sim$9 mJ/pulse and with a bandwidth of $\sim$3 cm^{-1}. The burner is a stainless steel flat-flame burner which is operated at atmospheric pressure. We use an oxygen-rich mixture of O_2, CH_4, and N_2 for fuel. The burner is enclosed inside a glass cross. The combustion products are exhausted out of the room through the top of the cross. The laser beam enters and exits through

The authors are with University of Arkansas, Physics Department, Fayettesville, Arkansas 72701.

Received 4 December 1981.
0003-6935/82/122133-08$01.00/0.

5. G. Giordano and G. Matone, "Laser Light Modulation: The Acoustooptical Effect and the Cavity Dumping Technique," LNF-77/32 (1977).
6. W. Del Bianco *et al.*, Phys. Rev. Lett. **47**, 1118 (1981).
7. G. Matone and A. Tranquilli, "Mode-Locking on a Long Cavity to Obtain High Power Laser Pulses," LNF-75/21 (1975).
8. R. Caloi *et al.*, "Mode-Locking on Coupled and Long Laser Cavities. The New Experimental Set-Up for the Ladon Beam," LNF-79/42 (1979).
9. V. Chimenti *et al.*, Finestra rotante sotto vuoto per esperienza Ladon; LNF Int. Memo M-14 (1981).
10. L. Federici *et al.*, Il nuovo setup sperimentale del fascio Ladon, LNF-79/6 (Int), 1979.
11. G. Matone *et al.*, Lect. Notes Phys. **61**, 149 (1976); (Erice Course, Photonuclear Reaction II). Invited contribution to the Europhysic Study Conference on High Power Laser and Scientific Applications, Oxford (1975); Laser Opt. Non Conv. **55**, 3 (1975).

Application of the photothermal deflection technique to combustion diagnostics

A. Rose, J. D. Pyrum, C. Muzny, G. J. Salamo, and R. Gupta

University of Arkansas, Physics Department, Fayetteville, Arkansas 72701.
Received 19 April 1982.
0003-6935/82/152663-03$01.00/0.

There is considerable interest[1,2] in development of combustion diagnostic techniques for minority species concentration measurements which (1) are nonperturbing, (2) have temporal resolution, and (3) have spatial resolution. In this Letter we report on the first application of photothermal deflection spectroscopy[3] to combustion diagnostics. The technique meets all three of the above requirements and has the potential of developing into an excellent combustion diagnostic tool for measurements of very low concentrations of molecules in flames. In particular, we report on preliminary experiments in which we have detected low concentrations of NO_2 produced in the combustion of a monomethylamine-seeded methane–air flame.

Several techniques are presently under extensive investigation for species concentration measurements in flames. Coherent anti-Stokes Raman scattering (CARS) is a very successful technique for majority species concentration measurements.[4] Fluorescence techniques have a high sensitivity; however, for these techniques to be useful combustion diagnostic tools one must either eliminate the effect of or quantitatively account for all quenching collisions. The saturated fluorescence technique[5] has recently received a lot of attention. In this technique the effect of quenching collisions is practically eliminated by making the absorption and stimulated emission rate much higher than the quenching rate by using high laser intensities. Following the work of Crosley,[6] we have recently shown[7] that the photoacoustic technique has a high potential of developing into an excellent technique for measurements of very low concentrations of molecules in combustion environments. Parts per million sensitivity (with a resolution of few microseconds) has been obtained for NO_2 molecules, and parts per billion sensitivity can easily be achieved for strongly absorbing molecules like OH. Achievement of spatial resolution, however, is not very easy in the photoacoustic technique, although these attempts are in progress in our laboratory. Photothermal deflection technique in many ways is similar to the photoacoustic technique but eliminates use of a microphone for signal detection, and both spatial and temporal resolution may easily be achieved.

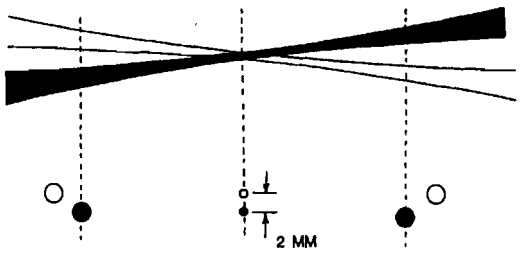

Fig. 1. Pump (dark) and probe laser beams as viewed from above (top part of the figure). The bottom part shows the cross sections of the two beams in three vertical planes.

The photothermal deflection technique has been pioneered by Amer and collaborators.[8] The basic idea behind the technique is quite simple. Two laser beams, a dye laser beam (pump beam) and a He–Ne laser beam (probe beam), intersect in the region where the molecules of interest are to be detected. The pump beam is tuned to an absorption line of the molecules of interest. Laser energy is absorbed by the molecules, who lose most of that energy by quenching collisions with other flame molecules. Most of this energy eventually appears in the heating of the flame gases, thereby changing the refractive index of the medium. The probe beam suffers a deflection due to the refractive-index gradient that is produced, which is detected by a position sensitive optical detector. The amplitude of the signal, among other things, is also proportional to the concentration of the molecules of interest. Spatial resolution is obtained because the intersection of the pump and probe beams localizes the region where the signal is observed. The temporal resolution is obtained by using a pulsed laser.

Application of this technique to a combustion environment produces complications because of the existence of the concentration gradients of the absorbing molecules. In particular, if the pump and probe beams intersect, a deflection of the probe beam may also be produced by the refractive-index gradients due to the concentration gradients of the absorbing molecules. In this case, deflection is proportional to the concentration gradients rather than the concentration of the absorbing molecules. In our experiment the two beams do not intersect but pass close to each other as shown in Fig. 1. The top part of the figure shows how the two beams look when viewed from above. The bottom part shows cross sections of the two beams in vertical planes at three different positions. In other words, the two beams are in two different horizontal planes. The detector is arranged in such a way that it detects only the vertical component of the deflection of the probe beam. Under our experimental arrangement, the vertical deflection of the beam is proportional only to the concentration of the absorbing molecules and not to the concentration gradients.

Figure 2 shows our experimental setup. A stainless steel flat flame burner with methane, oxygen, nitrogen, and 70-ppm monomethylamine is used. The addition of small amounts of monomethylamine increases the concentrations of NO_2 in the flame for ease of detection.[9] The burner, ~6 cm in diameter and operated at atmospheric pressure, produces a faint blue pancake shaped and ~1.5-mm thick flame. Part of the burner head is masked by a stainless steel sheet to give a straight edge to the flame as shown. The straight edge was not essential to this experiment and was there for historical

Radiative-lifetime measurements of the $4p\ ^5P$, $4p\ ^3P$, and $4d\ ^5D^\circ$ multiplets of O I

R. L. Day, R. J. Anderson, and G. J. Salamo

Department of Physics, University of Arkansas, Fayetteville, Arkansas 72701

Received September 21, 1980; revised manuscript received January 22, 1981

Time-resolved spectroscopy is used to observe the $4p\ ^5P \rightarrow 3s\ ^5S^\circ$, $4p\ ^3P \rightarrow 3s\ ^3S^\circ$, and $4d\ ^5D^\circ \rightarrow 3p\ ^5P$ multiplet transitions of the O I spectrum occurring at λ = 3947, 4368, and 6157 Å, respectively. The excited atomic states are produced through dissociative excitation of an O_2 target gas by a pulsed electron beam of ~0.5–2-μsec pulse width and 100-eV incident energy. The mean radiative lifetimes of the $4p\ ^5P$, $4p\ ^3P$, and $4d\ ^5D^\circ$ multiplets are obtained from analysis of the resulting radiative decay over the pressure range ~20–100 mTorr and are reported as 194, 161, and 95 nsec, respectively. The corresponding collisional deactivation cross sections for the multiplets are also obtained from the lifetime-versus-pressure measurements and are reported as 3.2×10^{-15}, 7.7×10^{-15}, and 1.6×10^{-15} cm^2, respectively.

1. INTRODUCTION

Determination of radiative-transition probabilities for strong spectral lines of the atomic-oxygen spectrum is an important problem that has received the attention of numerous investigators. These previous efforts include both theoretical calculations and experimental measurements with a wide variety of research techniques used to obtain values of the radiative-transition probabilities, oscillator strengths, or mean lifetimes. A catalog of the research effort during the period 1914–1977 is available in the National Bureau of Standards (NBS) bibliography by Fuhr *et al.*,[1] whereas Wiese[2] recently published a new survey of the atomic-transition probability literature covering the period 1975–1978. Many of the more recent lifetime measurements have been obtained by using pulsed-electron excitation and delayed-coincidence photon-counting techniques. These methods include the high-frequency-deflection (HFD) technique,[3–5] in which excitation is produced by thousand-electron-volt electron impact of low-density beams of target atoms or molecules, and suppressor grid pulsing, in which excitation is produced by low-energy (e.g., ≤500-eV) electron impact over a range of target-gas pressures, electron-beam energies, and excitation-pulse widths. The present work employs the latter technique to confirm the lifetime measurements of the $4p\ ^5P$, $4p\ ^3P$, and $4d\ ^5D^\circ$ multiplets of O I previously carried out by Bromander *et al.*,[6] using the HFD technique, and to obtain estimates of the O I*–O_2 collisional quenching cross section of these levels.

2. EXPERIMENT

Detailed descriptions of the construction and operation of the present time-resolved apparatus have been given in previous papers[7,8] and will not be repeated here. However, use of a modified electron gun is required in the present work to ensure its extended operation in an O_2 atmosphere. Therefore our experiment employs a new triode electron gun, which uses slotted stainless-steel plates covered with 90%-transmission tungsten mesh as excitation-tube grids and a 0.1-cm × 2-cm iridium-coated tungsten ribbon as a directly heated cathode. The cathode, operating at ~6 A and 10 V, produces a sheet electron beam of ~5-mA/cm^2 current density at 100-V accelerating voltage. A positive square-wave voltage pulse applied to the negatively biased grid of the electron gun produces a pulsed electron beam of 0.5–2-μsec pulse width, 200-kHz repetition rate, and ≤5-nsec cutoff time. The electron beam passes through a field-free collision region positioned along and adjacent to the monochromator entrance slit, is collected in a deep Faraday cup, and is monitored by a sampling oscilloscope. Standard delayed-coincidence photon-counting techniques are used to detect the resulting collisional radiation.

Intensity-versus-wavelength scans of the O I spectrum, produced by dissociative excitation of the O_2 target gas, are used to identify the observed spectral lines. For example, Fig. 1 displays the wavelength scan used to identify the $4p\ ^5P \rightarrow 3s\ ^5S^\circ$ transition occurring at λ = 3947 Å. The scan, obtained at a spectral resolution $\Delta\lambda = \pm 3$ Å, represents the worst-case situation with respect to overlap of unwanted spectral lines observed in the present work. The λ = 3947-Å line experiences line blending to shorter wavelengths because of the presence of the λ = 3945-Å line of the O II spectrum. However, the fraction of its integrated intensity that is observed within the λ = 3947-Å bandpass is only about 6% of the total integrated intensity of the λ = 3947-Å line under observation. In addition, although the lifetimes of the two transitions are well separated (~46 versus 191 nsec), a short-lived decay mode corresponding to the λ = 3945-Å transition is not observed in the present data. Therefore the λ = 3947-Å line is spectrally resolved for the purposes of the present experiment.

Time-resolved measurements of the radiative decay, after the cessation of the electron beam, are obtained with the center of the monochromator bandpass, $\Delta\lambda \leq 3$ Å, set at the wavelength corresponding to peak line intensity. The relative

0030-3941/81/070851-05$00.50

models are used for the laser bandwidth. Exact solutions are found for a model "autoionizing" continuum. The Torrey-type polynomials governing the decay of the single bound state are derived. An explicit formula for the spectrum of the excited electrons is given for both low and high laser intensities.
*Research supported by the US Department of Energy.

DB 4 Coherent Resonant Propagation of Two Optical Pulses.* B. SOBOLEWSKA** and J.H. EBERLY, Univ. of Rochester-- The coherent propagation of two optical pulses, a pumping pulse and an amplified resonant-Raman-type pulse, in a three level medium is studied theoretically. The pulses are much shorter than the homogeneous atomic phase memory time. The relevant system of Maxwell-Bloch equations is considered under the assumption that the two pulses do not overlap significantly in time during their spatial propagation. The analog of a pendulum equation, well-known for single pulse propagation, has been derived. A kind of "area theorem", in the form of two coupled differential equations, has also been found. The difference in behaviour of pulses longer and shorter than the inhomogeneous lifetime is pointed out.
*Research partially supported by the US Office of Naval Research
**Fulbright-Hays Scholar, 1980.

DB 5 Simultons: Theory of Simultaneous Propagation of Short Different-Wavelength Optical Pulses.* M.J. KONOPNICKI, Air Force Weapons Laboratory. P.D. DRUMMOND and J.H. EBERLY, Univ. of Rochester--Propagation of short different-wavelength optical pulses in many-level absorbers has been studied. New analytic solutions to the appropriate Maxwell-Bloch equations were found. The solutions represent simultaneous (equal velocity) different-wavelength optical solitons, so called simultons. In order for simulton propagation to occur, both the pulses and the medium have to be initially prepared in a manner determined by medium's physical parameters. The analytic findings are extended by applying numerical methods reported elsewhere.[1]

*Work supported by DOE contract numbers EY-76-F-03-118 and W-7405-Eng-48.

[1]M.J. Konopnicki and J.H. Eberly, Proc. of 10th Annual Modeling and Simulation Conference, eds. W.G. Vogt and M.H. Mickle (ISA, Pittsburgh, 1979), p. 1199.

DB 6 Four-dimensional Simulation of Multiple-Laser Pulse Propagation.* P.D. DRUMMOND and J.H. EBERLY, Physics Dept., U. of Rochester.--We discuss the simultaneous propagation of several laser pulses, each of which is nearly resonant with one of the successive dipole transitions in an N-level medium. Both transverse diffraction effects and Gaussian inhomogeneous broadening are included. The Maxwell-Bloch equations are integrated numerically with a computer program that includes coherent pulse-atom interactions as well as spontaneous emission, collisional dephasing, optical pumping and ionisation. Recently discovered SU(N) symmetry relations provide a straightforward way of estimating the overall error in computing the N-level atomic time-development for each space-point and each frequency that is integrated. Also, a check of the program is provided by comparison with recently discovered analytic results for N-level "simulton" pulse propagation, with plane waves. New results are reported for the transverse effects in Gaussian cross-section pulses that are near-resonant with two successive transitions in a three-level medium.

*Research supported by the US Department of Energy and the US Office of Naval Research.

DB 7 Experimental Observation of Self-Induced Transparency Using a Train of Optical Pulses.* G. J. SALAMO and P. N. BREAUX, UNIVERSITY OF ARKANSAS.--Coherent propagation of pulse trains through a two-level atomic absorber has been discussed previously by other authors. Their studies are based on the self-induced transparency (SIT) equations with the assumption of zero atomic relaxation. Recently, the effects of relaxation on pulse-train propagation have been analyzed. It has been predicted that after the entire absorber has relaxed to a time-repetitive equilibrium with the field, strong pulse reshaping is still present and, in fact, the characteristic features of single-pulse SIT are still observable with modest absorption lengths. These effects at equilibrium persist even when relaxation is so weak that its effect during a single pulse is negligible. Surprisingly, the absorber is still neither dephased nor saturated after an arbitrary number of pulses. In this paper, we report the experimental observation of pulse-breakup and pulse-peaking in support of the recent theoretical predictions.

*Supported by the Research Corporation.

DB 8 Pulsed Phase Conjugation Due to a Tensor Refractive Index Grating in Sodium Vapor.* S.N. JARIC, L.K. LAM and R.W. HELLWARTH, Univ. of So. Calif.--We observe the scattering of a light beam at frequency w from a refractive index grating formed by beating two other beams, also at w, near the one-photon D-line resonances in sodium vapor. There are two components of comparable intensity but different spectra. The first 'scalar' component, studied previously by Wandzura,[1] and Humphrey, et al.,[2] arises from a grating of excited sodium atoms. Here we examine a second 'tensor' component which arises from oriented but not optically pumped ground-state atoms, and is present even when the two grating-forming beams are orthogonally polarized (and hence can produce no grating of excited atoms). We observe, as we expected, that the scattering by this 'tensor' grating occurs mainly at the D_1 line when the grating is formed by nitrogen-laser-pumped dye-laser pulses. We present a simple theoretical account of the observed effects.

*Work supported by the AFOSR grant No. 79-0098 and Lawrence Livermore Subcontract No. 7509105.
1. S.M. Wandzura, Optics Letters, 4, 208 (1979).
2. L.M. Humphrey, J.P. Gordon, and P.F. Liao, Optics Letters, 5 (1980).

DB 9
LASER LINESHAPE EFFECTS IN RESONANCE FLUORESCENCE, A. T. Georges and S. N. Dixit, Department of Physics, University of Southern California, Los Angeles, CA 90007.

The effects of different laser lineshapes on the intensity and spectrum of resonance fluorescence from a two-level atom are investigated. The laser model considered is that of an ideal single-mode laser operating high above threshold, having a constant amplitude and undergoing phase-frequency fluctuations analogous to Brownian motion. As the correlation time of the frequency fluctuations increases from zero to infinity, the laser lineshape changes from Lorentzian to Gaussian in a continuous fashion. It is shown that for intermediate and strong fields, the average intensity of fluorescence in the case of a resonant, broadband, Lorentzian lineshape is higher than that in the case of a Gaussian lineshape with the same bandwidth and total power. This is in contrast to the weak field case where the higher peak power of the Gaussian lineshape makes it more effective than the Lorentzian lineshape. Several other new results on the dependence of the spectrum and the two-time intensity correlation on the laser lineshape are presented.

Power spectrum of light scattered by a two-level atom in the presence of a pulse-train driving field

Mark A. Newbold and Gregory J. Salamo
Department of Physics, University of Arkansas, Fayetteville, Arkansas 72701
(Received 31 January 1980)

The power spectrum of the light scattered by a two-level atom in the presence of a coherent continuous-pulse-train driving field is analyzed. Separate expressions for the coherent and incoherent components of the spectrum are obtained. The coherent part of the spectrum consists of a series of spikes (delta functions) which are displaced from the optical carrier by multiples of the pulse repetition frequency. The incoherent spectrum can have fixed peaks at these same frequencies plus sidebands equally spaced on opposite sides of these fixed peaks. That is, the spectrum consists of a series of triplets. The special case of a two-mode driving field is treated numerically and graphs of spectra are presented.

I. INTRODUCTION

The spectrum of light scattered from a strongly driven two-level atom has received much attention recently.[1] The experiments of Wu, Grove, and Ezekiel[2] support the predictions of the theory presented by Mollow.[3] In Mollow's work it is assumed that the atom is driven by a perfectly monochromatic optical field. It is the purpose of the present paper to extend Mollow's work to the case of a pulse-train driving field such as that produced by a mode-locked cw dye laser. As in the Mollow theory, it is assumed that the atom has come to equilibrium with the driving field through radiation damping.

II. THE THEORETICAL MODEL

Following Ref. 3, we consider a single atom fixed at the coordinate origin and driven by a near-resonant classical[4] optical field. The atom fluoresces through its interaction with a bath of quantum field oscillators. It is assumed that only two atomic levels are involved in the interaction: $|0\rangle$ and $|1\rangle$, having energies 0 and $\hbar\omega_0$, respectively. The following atomic operators may be defined at $t=0$ in the Heisenberg picture:

$$a(0) = |0\rangle\langle 1| \tag{1a}$$

and

$$a^\dagger(0) = |1\rangle\langle 0| . \tag{1b}$$

The electric field operator may be decomposed into its positive and negative frequency parts:

$$\vec{\mathbf{E}}(\vec{\mathbf{r}},t) = (1/\sqrt{2})[\vec{\mathbf{E}}^{(+)}(\vec{\mathbf{r}},t) + \vec{\mathbf{E}}^{(-)}(\vec{\mathbf{r}},t)], \tag{2}$$

where

$$\vec{\mathbf{E}}^{(+)}(\vec{\mathbf{r}},t) = \epsilon(\vec{\mathbf{r}},t)\hat{e}_0 + i\sum_{\vec{k},s}(\hbar\omega_{\vec{k}}/V)^{1/2}\hat{e}_{\vec{k},s}b_{\vec{k},s}(t)e^{i\vec{k}\cdot\vec{r}} \tag{3}$$

and $\vec{\mathbf{E}}^{(-)}(\vec{\mathbf{r}},t)$ is given by the adjoint of (3). Here $b_{\vec{k},s}$ is the annihilation operator for the quantized-field mode with wave vector $\vec{k}$ and polarization index $s(=1,2)$, $\omega_{\vec{k}}$ is its frequency, $\hat{e}_{\vec{k},s}$ is its polarization vector, and V is the quantization volume; $\epsilon(\vec{\mathbf{r}},t)$ represents the positive frequency part of the classical electric field, with polarization vector $\hat{e}_0$. Near resonance, the dipole interaction Hamiltonian may be approximated by

$$H_I(t) = -(1/\sqrt{2})[a^\dagger(t)\vec{\mu}\cdot\vec{\mathbf{E}}^{(+)}(0,t) + a(t)\vec{\mu}^*\cdot\vec{\mathbf{E}}^{(-)}(0,t)], \tag{4}$$

where $\vec{\mu} \equiv \langle 1|\vec{\mathbf{d}}|0\rangle$, with $\vec{\mathbf{d}}$ being the atomic-dipole-moment operator (at $t=0$ in the Heisenberg picture). We write, for the positive frequency part of the classical driving field,

$$\epsilon(0,t) = [\epsilon_1(t) - i\epsilon_2(t)]\hbar e^{-i\omega t}/\sqrt{2}(\vec{\mu}\cdot\hat{e}_0), \tag{5}$$

where ω is the optical carrier frequency, $\epsilon_1(t)$ and $\epsilon_2(t)$ are real quantities representing the field envelope at the position of the atom, and the time-independent factors have been inserted for later convenience. In Ref. 3 (Eq. 3.16), the classical driving field was assumed to be perfectly monochromatic (ϵ_1 and ϵ_2 constant). In the present paper, we generalize this work by assuming that the driving field is that of a pulse train. Thus ϵ_1 and ϵ_2 are assumed to be repetitive with period τ_r:

$$\epsilon_1(t+\tau_r) = \epsilon_1(t), \tag{6a}$$

$$\epsilon_2(t+\tau_r) = \epsilon_2(t). \tag{6b}$$

As discussed in Ref. 3, the positive-frequency part of the scattered field is given approximately by

$$\vec{\mathbf{E}}^{(+)}(\vec{\mathbf{r}},t) = \vec{\phi}(\vec{\mathbf{r}})a(t-r/c) + \vec{\mathbf{E}}_F^{(+)}(\vec{\mathbf{r}},t), \tag{7}$$

where

$$\vec{\phi}(\vec{\mathbf{r}}) \equiv (\omega_0^2/2\sqrt{2}\pi c^2 r^3)\vec{\mathbf{r}}\times(\vec{\mu}\times\vec{\mathbf{r}}) \tag{8}$$

and $\vec{\mathbf{E}}_F(\vec{\mathbf{r}},t)$ is the "freely-propagating part" of the electric-field operator—a linear combination of

Physica 100A (1980) 212–214 © *North-Holland Publishing Co.*

COMMENT ON "PROPAGATION OF ULTRASHORT LIGHT PULSES IN A RESONANT MEDIUM"

MARK A. NEWBOLD and GREGORY J. SALAMO

Department of Physics, University of Arkansas, Fayetteville, Arkansas 72701, USA

Received 3 May 1979

Previous conclusions on the propagation of ultrashort light pulses in a resonant medium are found to be in error. There is no physical basis for rejecting the nd u and dn u solutions.

In a recent paper in this journal[1]) and elsewhere[2]), Harney has presented an analysis and extension of Mishkin's[3]) treatment of ultrashort optical pulse train propagation in a resonant two-level medium. His major conclusion was that the dn u and nd u Jacobi elliptic analytic solutions to the coupled Maxwell–Bloch equations are unphysical. We wish to point out that this conclusion is in error.

Following Mishkin[3]), Harney writes solutions for the pulse envelope E in the following form

$$E = E_0 e(u) \qquad \text{with } u = \frac{1}{\tau}(t - z/V), \tag{1}$$

where $e(u)$ is a Jacobi elliptic function of modulus k, τ is a characteristic time and V is the pulse velocity. The four forms Harney considers are given by

$$e(u) = \begin{cases} \mathrm{cn}(u) & \text{with } E_0 = 2k/\tau \\ \mathrm{dn}(u) & \text{with } E_0 = 2/\tau \\ \mathrm{sd}(u) & \text{with } E_0 = 2k(1-k^2)^{1/2}/\tau \\ \mathrm{nd}(u) & \text{with } E_0 = 2(1-k^2)^{1/2}/\tau. \end{cases} \tag{2}$$

The component of the atomic Bloch vector representing the inversion is given by

$$\eta = \eta_0 + \tfrac{1}{2} E_0 \tau A e^2(u), \tag{3}$$

where η_0 and A are determined by the requirement that the length of the Bloch vector is unity.

Mishkin and Harney identify η_0 of eq. (3) as the "initial population inversion density"[1]) of the atomic system. Harney uses this interpretation as a

basis for rejecting the dn u and nd u forms, noting that for these forms, $\eta_0 < -1$ whereas physically the inversion should be ≥ -1. We want to point out that the identification of η_0 as an "initial inversion" is untenable in the case of the dn u and nd u. This incorrect interpretation was apparently suggested by the form of eq. (3), in which it appears that η takes on the value η_0 when the field $e(u)$ is zero. The error lies in the fact that for the dn u and nd u forms with $k^2 < 1$, the field never goes to zero. Thus at no time in the cycle does the inversion η take on an unphysical value, and there is no basis for discarding the dn u and nd u forms as unphysical.

As Harney pointed out, the solutions obtained with the sd u and nd u are identical to those obtained with the cn u and dn u, respectively, except for a translation of the time origin. Thus the full range of physically allowable solutions is given by

$$E = \frac{2k}{\tau}\,\mathrm{cn}(u - u_0; k) = \frac{2k}{\tau}(1-k^2)^{1/2}\,\mathrm{sd}(u - u_0 + K(k); k) \tag{4}$$

and

$$E = \frac{2}{\tau}\,\mathrm{dn}(u - u_0; k) = \frac{2}{\tau}(1-k^2)^{1/2}\,\mathrm{nd}(u - u_0 + K(k); k), \tag{5}$$

where u_0 is arbitrary. $K(k)$ is the complete elliptic integral of the first kind. In an effort to make these identities clear he discusses the experimental distinguishability of the sd u form from the equivalent cn u and the nd u form from the dn u. In this discussion, he compares the pulse energy and pulse area of the equivalent forms to argue that they are indistinguishable. However, his graphs of "energy" vs k appear to support the opposite viewpoint. In fact, he states that the cycle energy goes to infinity as $k \to 1$ for the sd u and nd u but remains finite for the cn u and dn u. The problem is that the quantity graphed (in fig. 1 of ref. 1) is the energy divided by E_0. E_0 has a different explicit k-dependence for each different form [Eqs. (2)]. Thus these curves do not correctly show the dependence of energy on k unless it is assumed that E_0 is held constant by making τ vary with k. However, τ is then a different function of k in each of the four forms [Eqs. (2)] and there is no basis for comparison of his four curves. We note that for the same k and τ, the energy of the sd u is of course the same as that of the corresponding cn u and the energy of the nd u is the same as that of the dn u.

[5]M. Broyer, J. Vigué, and J. C. Lehmann, J. Phys. (Paris) 39, 591 (1978); R. L. Cook and F. C. De Lucia, Am. J. Phys. 39, 1433 (1971).
[6]C. H. Townes and A. L. Schawlow, *Microwave Spectroscopy* (McGraw-Hill, New York, 1955).
[7]M. S. Child, Can. J. Phys. 53, 1838 (1975).
[8]E. P. Gordeev, S. Ya. Umansky, and A. I. Voronin, Chem. Phys. Lett. 23, 524 (1973).
[9]E. Luc-Koenig, C. Morillon, and J. Verges, Physica (Utrecht) 70, 175 (1973); V. Jaccarino, J. G. King, R. A. Satten, and H. H. Stroke, Phys. Rev. 94, 1798 (1954).
[10]J. Wei and J. Tellinghuisen, J. Mol. Spectrosc. 50, 317 (1974); J. Tellinghuisen, private communication.
[11]J. Brooke Koffend, S. Goldstein, R. Bacis, R. W. Field, and S. Ezekiel, Phys. Rev. Lett. 41, 1040 (1978).

Effects of Relaxation on Coherent Continuous-Pulse-Train Propagation

Mark A. Newbold and Gregory J. Salamo
Department of Physics, University of Arkansas, Fayetteville, Arkansas 72701
(Received 29 January 1979)

We have analyzed the effects of relaxation on coherent pulse-train propagation through a two-level absorber. It is shown that after the entire absorber has relaxed to a time-repetitive equilibrium with the field, the characteristic features of single-pulse self-induced transparency are still predicted.

Coherent propagation of pulse trains through a two-level atomic absorber has been discussed previously by other authors.[1-4] Their studies are based on the self-induced transparency (SIT)[5] equations with the assumption of zero atomic relaxation. In the present paper, the effects of relaxation on pulse-train propagation are analyzed. It is shown that after the entire abosrber has relaxed to a time-repetitive equilibrium with the field, strong pulse reshaping is still present and, in fact, the characteristic features of single-pulse SIT are still observable with modest absorption lengths. These effects at equilibrium persist even when relaxation is so weak that its effect during a single pulse is negligible. Surprisingly, the absorber is still neither dephased nor saturated after an arbitrary number of pulses. Therefore SIT phenomena should be observable on the continuous, high-repetition-rate trains of pulses which have recently become available with mode-locked cw dye lasers. Furthermore, shape-preserving pulse-train propagation, such as that described in the earlier studies, may be observable. In the earlier studies, analytic pulse-train solutions to the SIT equations were found but no mechanism was proposed for the atomic variables to attain the necessary special initial state. It is shown here that with weak relaxation present, the atomic variables relax to correct values to allow shape-preserving propagation of the analytic pulse-train envelopes. An analytic expression for the atomic Bloch vector is given in this limit.

For a $\Delta m = 0$ electric dipole transition, we assume a linearly polarized plane-wave electromagnetic field[6]

$$\vec{E}(t,z) = \mathcal{E}\hat{e}(\hbar/d)\cos(\omega t + \varphi),$$

where t is retarded time (laboratory time $- z/c$); $\mathcal{E}(t,z)$ and $\varphi(t,z)$ are slowly varying envelope functions; d is the magnitude of the transition dipole moment; $\hat{e}$ is a constant unit vector; z is propagation distance. We assume that this field is interacting with a two-level absorber described by the Bloch vector $\vec{p} = (u,v,w)$. The reshaping of the envelope functions is given by the reduced Maxwell equations[7]:

$$\partial\mathcal{E}/\partial z = [\alpha/2\pi g(0)]\langle v(t,z,\Delta\omega)\rangle_{\Delta\omega}, \tag{1a}$$

$$\mathcal{E}(\partial\varphi/\partial z) = -[\alpha/2\pi g(0)]\langle u(t,z,\Delta\omega)\rangle_{\Delta\omega}, \tag{1b}$$

The angular brackets denote averaging [weighted by the atomic line shape $g(\Delta\omega)$] over $\Delta\omega$, the off-resonance parameter for the atoms [$\Delta\omega$ = (atomic resonance frequency)$-$(field-carrier frequency)]; α is the Beer's-law (weak monochromatic field) absorption constant. The time development of the Bloch vector $\vec{p} = (u,v,w)$ is given by the Bloch equations:

$$\dot{u} = -(\Delta\omega - \dot{\varphi})v - (T_2')^{-1}u, \tag{2a}$$

$$\dot{v} = (\Delta\omega - \dot{\varphi})u + \mathcal{E}w - (T_2')^{-1}v, \tag{2b}$$

$$\dot{w} = -\mathcal{E}v - (T_1)^{-1}(w+1), \tag{2c}$$

where the dot denotes $\partial/\partial t$. The terms involving T_1 and T_2' allow the atom to relax to its ground state when $\mathcal{E} = 0$. A Bloch vector of length less

Physics for architects

Gregory J. Salamo, John A. Brewer, and James A. Berry
Physics Department, University of Arkansas, Fayetteville, Arkansas 72701
(Received 28 February, 1978; accepted 30 June 1978)

We describe a program which was prompted by and designed to satisfy the modern needs of architects who will be confronted more and more with the constraints imposed by the principles of physics, particularly those relating to energy. The program is designed to make clear, through lectures and laboratory investigations, the relationship between concepts in physics and practice in architecture. It is designed to help the student of architecture recognize that the behavior of a structure is as much a part of his creativity as the structure itself. Experiments range from individual labortory experiments to group around-the-campus experiments.

I. INTRODUCTION

About 2½ years ago, the physics department at the University of Arkansas initiated a new program called Physics for Architects.[1] This program was prompted by and designed to satisfy the modern needs of architects who will be confronted more and more with constraints imposed by physical principles, particularly those relating to energy conservation. In this paper we describe the program and report initial results which, judging from student and peer evaluations, has been very successful in relating physical principles in a clear and interesting way to architecture.

The unifying theme of this new program is the relationship between the principles of physics and the practice of building and operating structures for man's use. It is actually easy to develop this theme since the relationships between the principles of physics and those of architecture are enormously large. For example, every architectural student has a strong appreciation for knowledge of the structural, thermal, acoustical, electrical, and optical behavior of structures. Each of these areas can be developed in a logical way using very fundamental and traditional concepts of physics. In this sense, our program differs from traditional physics courses only by its goal and the examples chosen to demonstrate the application of a physics concept.

In addition to these rather clear relationships between physics and architecture there are also several more subtle points which are worth making. For example, it is not too difficult to show that artistic creativity will very often follow developments in our scientific understanding of nature. The laserium and similar art shows with light are current examples of this idea. Gothic architecture is a good example demonstrating how our "understanding of the times" pervades the "art of the times." The period during and shortly after the time of Newton, the so called "age of reason" is another good example of how a *change in scientific outlook on nature* is followed by a similar change in the arts. Not only is this parallel expected but there are several precedents as well. For this reason, a student of architecture with knowledge of our current concept of nature will have an increased opportunity to be creative in his architectural design.

Another interesting point worth making is the relationship between the "technology of the times" and current practices in architecture. This relationship can be made clear through the use of laboratory equipment which the student of architecture can choose to continue to use during his practice as an architect. For example, state of the art acoustical equipment can be used to measure noise levels, reverberation times, etc., during laboratory investigations with the idea that such exposure will encourage the potential architect to continue to use similar equipment in the future. This approach can be complemented in the lecture by emphasizing that order of magnitude calculations are often easy to perform and can be extremely helpful in designing new types of structures. Together, the laboratory and lecture can develop the attitude that the student can be quantitative in almost any aspect of architectural design *as well as make a measurement* on the performance of a structure in order to test the accuracy of design.

This brings us to another interesting and subtle point which is that phyiscs is a very deductive type of science and deductive reasoning is particularly important to designing an energy conservative home as well as one that utilizes the sun in an effective and efficient manner. Therefore, the *experience in deductive reasoning* can be an educational advantage to the student of architecture, particularly if it is emphasized and made clear in the Physics for Architects program.

To affect the attitude of the developing architect at an early stage is indeed a valuable contribution. Today's architect, perhaps more than ever before, needs to approach his practice with the attitude that a structure which functions properly, is energy efficient, and as self-sufficient as possible, has an artistic beauty all its own. In essence, he is creator not only of the structure but of its behavior as well. For the architect, physics is simply a quantitative but intuitive study of the behavior of materials and structures under various types of loads. Having the knowledge of how materials and structures behave under loads and the ability to predict their behavior in new situations, the architect has a tool which will aid him in the development of his creative ability to design beautiful and correct structures.

II. STRUCTURE OF THE PROGRAM

In Physics for Architects, students participate in 3 h of lecture and 2 h of laboratory investigations each week during the 1-yr (fall and spring semesters) program. In the lecture students are introduced to concepts in physics with particular examples relating to architecture. During the laboratory investigations, the concepts discussed in lecture become visible and the relationship between a principle of physics and an application in architecture is reinforced. The lecture points out that many concepts, such as acoustical

 0002-9505/79/010024-05$00.50

in H_2 and its isotopes. By proper design our multi-pass cell approach allows the 16 μm output to be scaled to significantly higher energy levels. Recent experimental results will be presented. (25 min.)

1. R. L. Byer, "A 16 μm Source for Laser Enrichment," IEEE J. Quantum Electron. QE-12, 732–733 (1976).
2. R. L. Byer and W. R. Trutna," 16 μm Generation by CO_2 Pumped Rotational Raman Scattering in H_2," (unpublished).

Contributed Papers

WI2. Recombination Lasers in CO_2 Laser-Produced Plasmas of Cd and Pb. W. T. SILFVAST, L. H. SZETO, AND O. R. WOOD, II, *Bell Telephone Laboratories, Holmdel, N. J. 07733.* —Laser oscillation in PbI and CdI has been produced in 1-cm-long laser-produced plasmas by vaporizing Pb and Cd with a focused CO_2 TEA laser. The population inversions are produced by recombination from the single ion to highly excited states in the neutral species of these elements. A low pressure background gas is used to retard the plasma expansion and enhance the electron cooling rate. Laser transitions occur at 1.31 μm in Pb and at 1.39, 1.43, and 1.64 μm in Cd between levels above and below energy gaps in the highly excited states of these atoms. These gaps serve as bottlenecks to accumulate recombining electrons in the upper laser levels. Scaling to higher ionization stages would access similar gaps at much shorter wavelengths. (13 min.)

WI3. High Power D_2O Submillimeter Laser Using Tunable Narrow Linewidth Optical Pumping.* P. WOSKOBOINIKOW, H. C. PRADDAUDE, W. J. MULLIGAN, D. R. COHN, AND B. LAX, *Francis Bitter National Magnet Laboratory, M.I.T., 170 Albany St., Cambridge, Mass. 02139.* Submillimeter (SMM) wave output energy pulses of 120 mJ in 100 ns have been achieved with an optically pumped D_2O vapor laser oscillator. About two thirds of this energy comes from the 385 μm stimulated Raman transition for which we have demonstrated the existence of narrow linewidth (≤10 MHz full width at half-maximum) cavity modes and a 1 GHz tunability. The remaining SMM energy was due to D_2O lasing at the 359 μm cascade transition and at the 239 μm ground-state transition. Conversion efficiency of the 9.26 μm $R(22)$ tunable CO_2 laser pump energy to the 385 μm D_2O laser energy as high as 0.4% has been achieved. The key to this development of tunable SMM laser emissions with high power, high efficiency, and narrow linewidth has been the development of a high power, single mode, tunable CO_2 TEA pump laser. This CO_2 laser consisted of a grating and etalon tuned CO_2 oscillator followed by an amplifier chain which produced 25 J, 100 ns, single mode pulses with a tunability of ±1 GHz around the CO_2 9 $R(22)$ line center. The optimum CO_2 laser pump frequency does not coincide with the D_2O absorption line center because of the stimulated Raman mechanism of the SMM transition. We believe that the use of tunable, single mode pump lasers will greatly improve the efficiency and spectral characteristics of other optically pumped high power SMM lasers. Some of the measurements reported here were made possible by the novel use of a surface acoustical wave (SAW) dispersive filter which allowed us to determine the mode structure of the D_2O laser oscillator in real time. (13 min.)

WI4. Synchronous Generation of Independently Tunable Ultrashort Pulses by Double Mode-Locking of the cw Dye Laser. BOURKOFF, J. R. WHINNERY, AND A. DIENES,* *Electronics Research Laboratory, University of California, Berkeley, Calif. 720.* The production of subpicosecond pulses by the technique double mode-locking has been recently discussed.[1] Although the eviously reported configuration had the unique feature of keeping e physical cavity lengths identical for each of the two wavelengths, is was not necessarily an optimum arrangement. By replacing the ut filter by a Brewster prism and adding an additional output irror, we are now able to adjust the relative cavity lengths to obtain inimum pulse durations and also to control the amount of output upling at each wavelength. In addition, by rotating each of the two utput mirrors, it is now possible to independently tune the two trains f pulses over a wide range. By rotating only the Brewster prism, we can spectrally tune the two pulse trains while maintaining a fixed wavelength separation between them. Finally, since the generation of the shorter wavelength pulses are responsible for the production of pulses at the longer wavelength, the two pulse trains are synchronized with respect to each other. (13 min.)

* Department of Electrical Engineering, University of California, Davis.

[1] E. Bourkoff, J. R. Whinnery, and A. Dienes, "Parametric Study of Double Mode Locking of the cw Dye Laser," Proceedings of the OSA Topical Meeting on Picosecond Phenomena, Hilton Head, South Carolina, May, 1978 (unpublished).

WI5. Variation and Control of Pulse Width and Repetition Rate from a Passively Mode-Locked cw Dye Laser. JAMES A. BERRY AND GREGORY J. SALAMO, *Physics Dept., University of Arkansas, Fayetteville, Ark. 72701* In this paper we report the observation of pulse width and repetition rate control of pulses from a passively mode locked cw dye laser. Our laser cavity follows the Ippen and Shank design and is 2.4 m long. This corresponds to a round trip time or pulse repetition time of 16 ns. Using a series of etalons to control the longitudinal mode structure of the laser cavity we have systematically varied the repetition rate and pulse width of the output mode-locked pulses. The repetition rate was increased from one pulse every 16 ns to one pulse every 4 ns and detection of further increases in the repetition rate was limited by the response time of our detection system. The pulse width was varied from 2 to 0.2 ns and detection of shorter pulses was again limited by our detection system. In all cases the pulses were nearly bandwidth limited. Results indicate that "multiple pulsing" found to occur in cw mode-locked dye lasers is due to periodic missing longitudinal oscillating modes. (13 min.)

WI6. High-Repetition-Rate Thin Picosecond Dye Laser.* GARY HAYWARD AND A. E. SIEGMAN, *Edward L. Ginzton Laboratory, Stanford University, Stanford, Calif. 94305.* A high efficiency low pump-energy picosecond thin dye laser has been demonstrated operating in the range of 560 to 580 nm. Mirror spacings of 10–300 μm with ultrashort cavity transit times allow quasi-cw operation with pump pulses of 5 ps or less. The laser converts the frequency doubled 60 ps output pulses of a 100 pps Q switched and mode locked Nd:YAG laser into either single axial mode or broadband output pulses over the emission spectrum of rhodamine 6G. Thresholds for this laser is on the order of 20 nJ, and internal energy conversion efficiencies of 18% are obtained without optimization for pump energies of 1 mJ. Operating parameters of the device agree well with a simple model of mode buildup within the laser, predicting the spatial and spectral mode characteristics. This analysis should allow design of an optimized and fully stabilized thin dye laser with single mode linewidth of 0.1 nm or less. This laser is simple in construction and of immediate utility in double pulse picosecond spectroscopy when high repetition-rate tunable pulses at two different wavelengths are required with a fixed temporal separation. (13 min.)

* Work supported by the National Institute of Health.

WI7. Variable Width Pulses from a Mode-Locked TEA-CO_2 Hybrid Laser. P. BERNARD AND P. A. BÉLANGER, *Physics Dept., Université Laval, Cité Universitaire, Ste-Foy, Québec, G1K 7P4, Canada* For many applications, it is often desirable to produce smooth pulses with reliable and predictable width and amplitude. For CO_2 lasers and for pulses in the nanoseconds region active and passive mode-locking techniques are usually used for this purpose. As for mode-locking of a TEA-CO_2 laser by intracavity loss modulation, we found that the insertion of a very thin large section in the cavity increases the stability and reliability of the pulses. Note that this section need not be lasing. This scheme also relaxes the usually stringent operational conditions of the modulator. Smooth pulses with full width at half intensity variable anywhere from 1 to 10 ns can thus be easily produced. (13 min.)

WI8. Investigation of TEA-CO_2 Laser Mode-Locking by an Intracavity. M. PICHÉ AND P. A. BÉLANGER, *Dept. de Physique*